Evaluating the potential to extract high-resolution paleoclimate information from the near-shore New Zealand molluscan species *Austrovenus stutchburyi*

Jessica J. Orsman

A thesis submitted for the partial fulfilment for the degree of Master of Science with Honours in Geology, Victoria University of Wellington, March 2011

TABLE OF CONTENTS **Page no.**

ABSTRACT

Li, B, Mg, Al, Mn, Cu, Zn, As, Sr, Ba and U/Ca ratios were measured by laser ablation inductively coupled plasma mass spectrometry for 11 modern *Austrovenus stutchburyi* clams to assess the potential of this molluscan species as a proxy for paleo-ocean temperature and environmental change. *A. stutchburyi* is an intertidal, infaunal, bivalve, widespread in New Zealand coastal regions and throughout the Quaternary-Pliocene sedimentary rock record. Five individuals from Ligar Bay and Estuary (South Island, New Zealand) were analysed to evaluate the variability between individuals calcifying in similar environmental conditions. A further six individuals were sampled from a range of latitudes (38˚ to 40˚) in the North Island, New Zealand to evaluate variability between individuals from different environments.

A strong positive correlation between growth rate and Mg, Al, Mn, Sr, Ba and U/Ca ratios was observed, and a marked negative correlation was found between the same trace element/Ca ratios and ontogenetic age as growth rates slow during the molluscs' life. Thus, biological effects are the primary influence on trace element incorporation in *A. stutchburyi*. No clear seasonal variations were observed in the Mg and Sr/Ca ratio profiles through *A. stutchburyi* shells representing time periods of several years. Furthermore, for two shells for which chronologies could be reliably constructed, there were no significant correlations between Mg and Sr/Ca ratios and sea surface temperature. When Mg/Ca ratios were normalised to Sr/Ca ratios in order to eliminate the growth rate effect on trace element incorporation into the mollusc shells, some of the remaining variations appeared to visually correlate positively with sea surface temperature in several sections of a shell. However, a quantitative correlation did not confirm this (r^2 = 0.012). It is likely that neither Mg nor Sr incorporation into *A. stutchburyi* shell are primarily thermodynamically controlled.

Several coincident Ba/Ca peaks in two of the Ligar Bay shells are most likely caused by environmental processes such as short periods of phytoplankton blooms or elevated seawater Ba/Ca from river flooding. Mn/Ca and U/Ca variations in *A. stutchburyi* from different coastal sites with different sediment characteristics appeared to be linked to the redox conditions prevailing at an open ocean sand-dominated environment (Ligar Bay) versus tidal mud flat environments (e.g. Miranda). Thus, while *A. stutchburyi* is unlikely to be a useful archive for past coastal ocean temperatures, it holds considerable promise for tracking past changes in coastal ocean productivity and river run-off, as well as sediment redox conditions.

LIST OF FIGURES **Page**

LIST OF TABLES **Page**

ACKNOWLEDGEMENTS

Thank you to my supervisors for their time and support, Joel Baker and David Kennedy. Joel, thank you for sharing your brilliant scientific expertise, and encouraging me to do the project in the first place. I have been really grateful for your quick turn-around on my drafts over the last two months, it enabled me to finish this thesis in time for Law School. Dave, throughout the project your enthusiasm, prompt feedback and advice (even from across the Tasman) was greatly appreciated – thanks! Thank you also to Gavin Dunbar and Lionel Carter for additional advice and input in the project.

Thank you to those who provided technical support, particularly Monica Handler and Marc-Alban Millet in the geochemistry lab, and Stewart Bush for helping with sample preparation. Thank you to Gigi for help on the fieldwork – I suspect we wouldn't have remembered to collect any sediment without you there!

I have been lucky to have wonderful officemates throughout postgrad – Netty, Julene, John, Kylie, George C., Aidan, Katy and Simon. Thanks for the many, many chats, encouragement, and more recently for putting up with me in the final writing stages, including borderline OCD door shutting.

Thank you to all my friends, both in geology and the real world, including: Morgan, Surrey, Andy, George D, Sophie, Chelsea, Alexa, Nicole, Chris M, Matt and Anne. Special thanks to Ramona White for the data-processing problem-solving and for baking me the most awesome chocolate slice, and to Louise Clark for listening to the painstaking details of this project as it unfolded, and nevertheless always being a positive influence. Also to Sarah Martin, for being a great friend to share the Masters experience with! Thank you for the innumerable coffees, lunch breaks, productive and unproductive chats, and being a source of always rational advice.

Finally, to my family: Penny, Roger, Chris D, Grandma, Granddad, Nana, Alice, Bonnie, Min and Pierro – thank you for your support! Dad, thank you for supporting me at University – I'm really lucky to have that. Rose, thanks for being the better sister - I will always admire your optimistic outlook on life and feel blessed to have you in mine. Mum, I can't possibly thank you enough. You don't even like science but you've listened for endless hours to me talk about the ins and outs, and ups and downs of this thesis, and genuinely cared.

CHAPTER 1.0
THE POTENTIAL OF MOLLUSCS AS PALEOENVIRONMENTAL PROXIES

1.1 General introduction and thesis objectives

Geochemical records extracted from marine biogenic carbonates, particularly foraminifera and corals, have provided a wealth of paleoceanographic and paleoclimatic information (Katz et al., 2010), including ocean temperature (Elderfield and Ganssen, 2000; Lear et al., 2000; Sadekov et al., 2009), salinity (Schmidt et al., 2004; Arbuszewski et al., 2010) and ice volume, primary production and tracing terrigenous influx of elements (McCulloch et al., 2003; Sinclair and McCulloch, 2004; Klinkhammer et al., 2009). Molluscan species also offer the possibility of high-resolution, sub-seasonal records of paleo-ocean conditions in coastal environments, especially when coupled with the interpretation of shell growth patterns (sclerochronology) (Richardson, 2001).

Mg/Ca and Sr/Ca ratios in molluscan shells have been correlated to temperature in some cases (Dodd, 1965; Klein et al., 1996; Vander Putten et al., 2000; Elliot et al., 2009), but in most other cases the geochemistry has been linked to physiological factors such as calcification (growth) or metabolic rate (Klein et al., 1996; Lorrain et al., 2005; Gillikin et al., 2005; Carré et al., 2006; Takesue et al., 2008). Nevertheless, more molluscan species need to be analysed to test their potential as paleoenvironmental proxies. Further, the incorporation of other trace elements may provide other important environmental information. In particular, Ba/Ca and Mn/Ca ratios in molluscs have been linked to seawater concentrations, phytoplankton blooms, and sediment run-off (Vander Putten et al., 2000; Lazareth, 2003; Freitas et al., 2006; Gillikin et al., 2006; Gillikin et al., 2008); and the incorporation of heavy metals (Pb, Zn, Cu As) have been

used to study levels of contaminants (Purchase and Fergusson 1985; Richardson, 2001). Thus, trace elements in molluscan shells have the potential to be useful tracers of ocean and estuarine chemistry or conditions, as well as biomarkers for pollution (Freitas et al., 2006).

The key objectives of this thesis were to investigate the mechanisms controlling trace element incorporation into the shell of the New Zealand clam *Austrovenus stutchburyi* and identify potential paleo-temperature or environmental indicators. *A. stutchburyi* was chosen because of its abundance in New Zealand at a range of latitudes and preservation in the fossil record. Trace element ratios (Li/Ca, B/Ca, Mg/Ca, Al/Ca, Mn/Ca, Cu/Ca, Zn/Ca, As/Ca, Sr/Ca, Ba/Ca and U/Ca) were determined using laser ablation-inductively coupled plasma-mass spectrometry (LA-ICP-MS) in modern specimens of *A. stutchburyi*. Eleven shells from eight locations were analysed to evaluate the variability of shell element chemistry between individuals, including individuals from the same site and environmental conditions (Vander Putten et al., 2000). Sediment samples from each collection location were also analysed by X-ray fluorescence to compare shell major element/Ca ratios to those which occur in the clams' habitat.

1.2 Extracting paleoenvironmental information from molluscs

Arguably one of the most important developments in the paleoclimate field, and for geology, in the 20th century was the discovery of a thermodynamic fractionation of oxygen isotopes (^{18}O and ^{16}O) in the calcium carbonate shell of marine organisms, which are precipitated at near isotopic equilibrium with seawater (Urey, 1947; Epstein, 1953). This relationship has enabled numerous records of paleoceanographic and paleoclimatic conditions to be made from the $\delta^{18}O$ values of foraminiferal microfossils (Emiliani, 1955; Erez and Honjo, 1981; Deuser and Ross, 1989; Mortyn and Charles, 2003); but with one significant complication: shell $\delta^{18}O$ values are a product of the

seawater $\delta^{18}O$ composition, which is influenced by salinity and continental ice volume, as well as seawater temperature (Lea et al., 2003). Over the past 10-20 years, trace element analyses in foraminifera have been at the forefront of solving "Urey's problem". In particular, species-specific calibration of the thermodynamic incorporation of Mg^{2+} into calcite shell have provided records of ocean temperature, isolated from the ice volume effect (Lea et al., 2000; Lear et al., 2000; Cleroux et al., 2008).

Yet while Mg/Ca foraminifera analyses provide excellent paleo-temperature records - extending as far back as the early Cenozoic (e.g. Hollis et al., 2009), the temporal resolution of paleo-ocean temperatures that foraminifera can provide is restricted to the time-span of the microfossil's life and, more critically, also the temporal resolution of the sedimentary rock record. Thermodynamically controlled trace element incorporation in corals (Sr/Ca and U/Ca), offers sub-seasonal resolution (Cohen and McConnaughey, 2003), but the geographic location of coralline records is limited to the tropical regions. In addition, the aragonite skeletons of coral appear to be sensitive to diagenetic and vital effects, which means their records tend not to be well preserved in the paleo-record (Lea et al., 2003).

However, molluscs potentially have several advantages for reconstructing paleoclimate. They are geographically widespread, occurring in all types of shallow marine environments. The sequential manner in which shells are precipitated, with discrete increments of growth marked by growth patterns, potentially allows a high-resolution (seasonal to sub-tidal) record of the environment to be reconstructed over the life span of the mollusc (years to centuries) (Richardson, 2001; Freitas et al., 2006). Oxygen isotope analyses that have been conducted on a number of molluscan species have proved the success of integrating geochemistry and sclerochronology (Schöne et al., 2004; Schöne et al., 2007; Schöne, 2009; Klein et al., 1996; Goodwin, 2003); however,

the same difficulty of deconvolving the ambient temperature signal from the seawater $\delta^{18}O$ signal is encountered.

Developing trace element-temperature calibrations for molluscan species would create a powerful tool for determining paleo-ocean temperatures that could resolve crucial paleoclimate questions. The requirement for seasonal climate data is commonly recognised; as emphasis is being placed on the role of seasonal changes in driving global climate change (Schöne, 2010). For example, modelling permanent ice cover in the northern and southern hemispheres is dependent on seasonal temperature data (Crowley et al., 1986). In New Zealand, a molluscan paleo-ocean temperature proxy that could provide seasonally and annually resolved past ocean temperature data would allow assessment of the effect of the El Niño Southern Oscillation (ENSO), which an important present-day control on NZ's annual climate and on NZ in past climatic regimes. Furthermore, the near-shore record of ocean and estuarine temperatures has the potential to resolve (past and future) geographically muted or magnified local responses to broad global warming or cooling events.

However, to date, very few successful calibrations utilising Sr/Ca and Mg/Ca shell ratios have been reported for molluscs (Dodd, 1965; Klein et al., 1996; Table 1.1-1.2). This could be due to the limited number of molluscan species that have been studied, and so arguably the potential of molluscan paleo-ocean temperature proxies is not yet fulfilled (Freitas et al., 2006). Reported results have shown it is likely that there are species-specific biological or physiological influences on trace element incorporation, in addition to the ambient environmental factors of interest (Freitas et al., 2006). These factors, such as calcification rate, appear to be a major complication in the use of trace elements in molluscs; however they may not affect all species. Therefore, carrying out investigations on species that have not yet been studied is still important, and will add to

the limited, but growing knowledge base on the potential of molluscs as archives of paleo-ocean temperatures.

Finally, in addition to potential Mg/Ca and Sr/Ca paleothermometry applications, the discovery of non-thermodynamic relationships for the incorporation of other elements (e.g. Ba, Mn, Cu, Zn, As, Pb) could provide useful proxies for reconstructing paleo-ocean chemistry, including terrigenous input of elements and ocean residence times, and also of anthropogenic contamination of coastal sites (Freitas et al., 2006; Vander Putten, 2000; Lazareth; 2003; Purchase and Fergusson 1986).

1.3 Biomineralization

Biomineralization is the process by which molluscs precipitate their shell, which includes the mineral $CaCO_3$. Shell formation involves both cellular and physiochemical processes (Skinner and Jahren, 2007). The periostracum on a bivalve is a thin organic layer, which covers the shell (Figure 1.1). Enclosed within the two calcareous valves is the mantle – the primary organ of all molluscs. (Wilbur and Saleuddin, 1983).

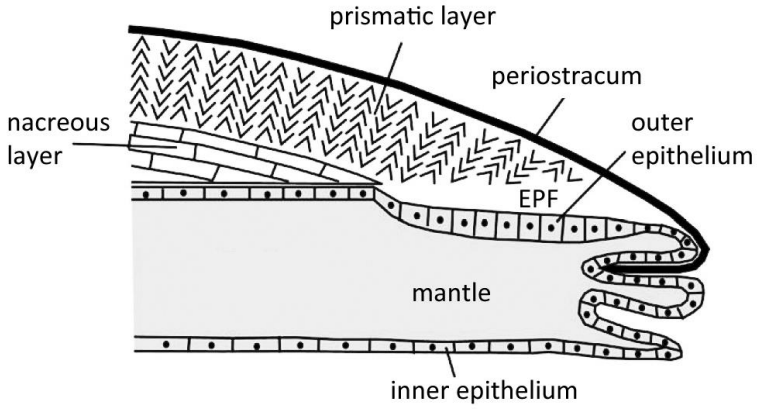

Figure 1.1 Schematic bivalve radial section showing the shell edge and mantle, and location of the extra-pallial fluid (EPF). Figure taken from Carré et al. (2006).

Crystallisation is controlled by the mantle, and occurs within the extra-pallial space (EPS) located between the mantle epithelium and the inner shell surface. The EPS is lined with the extra-pallial fluid (EPF), which contains both the inorganic and organic sources of the shell. These include Ca^{2+} and HCO_3^- ions, which react to produce the mineral component of the shell ($CaCO_3$), and travel from the external environment to the EPS via intracellular and/or intercellular routes (Watabe and Kingsley 1989). Some HCO_3^- is also sourced from reactions within the EPF between H_2O and CO_2 – a metabolic product. (Figure 1.2) Ca^{2+} and other elements that are eventually incorporated in the shell structure may enter the body tissue or hemolymph (blood) of the organism at several different locations including the gills, mantle surface and gut (Wilbur and Saleuddin, 1983; Jodrey, 1953; Horiguchi, 1958; van der Borght and Van Puymbroeck, 1966). Enzymes play a significant role in intracellular transport by enabling the elements to diffuse through the body and mantle epithelium – a process often referred to as 'metabolic pumping' (Klein et al., 1996). One such enzyme, Ca^{2+} - ATPase, is concurrently responsible for removing H^+ from the EPF, which is necessary for crystallisation. Notably, ion flow is bi-directional at the cellular boundaries; therefore, when there is a shortage of Ca^{2+} in the external environment, the element may be lost from the EPF causing decreased calcification rate, and vice versa (Wilbur and Saleuddin, 1983). On the basis of calcification rate variation, Carré et al. (2006) have also proposed a third transport mechanism for Ca^{2+} via calcium channels on epithelial cell membranes. When there is a super-saturation of $CaCO_3$ in the EPF, and ion clusters of a critical size form, crystallisation occurs. The organic material secreted by the mantle epithelium into the EPS, primarily proteins, binds the $CaCO_3$ crystals in an intra-crystalline matrix thereby forming the shell (Wilbur and Saleuddin, 1983).

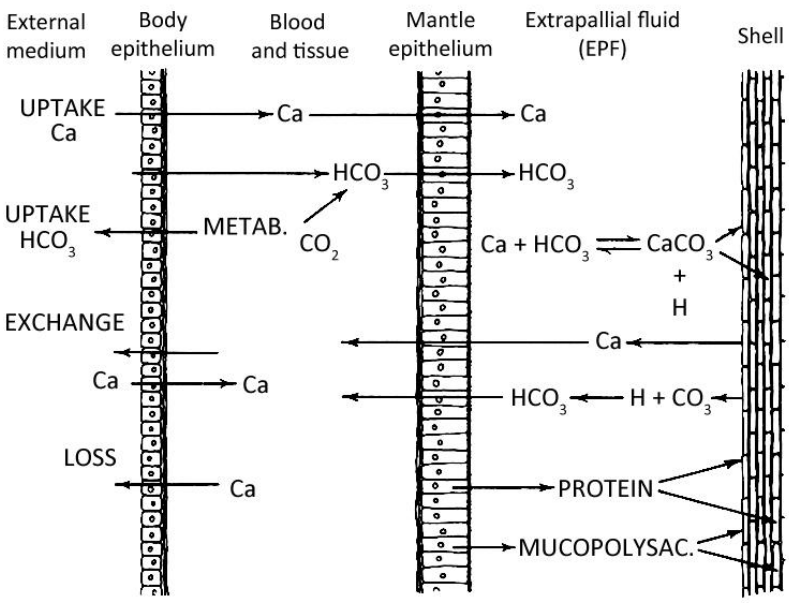

Figure 1.2 Ion exchange in the molluscan mineralizing system. Figure taken from Wilbur and Saleuddin (1983).

1.4 Trace element incorporation

Trace elements are incorporated into the mineral component of the shell when other cations substitute for the divalent Ca^{2+} cation in the $CaCO_3$ lattice. Laboratory studies on inorganic $CaCO_3$ show that differences in molecular structure between calcite and aragonite mean that particular cations are incorporated preferentially in the polymorphs of calcium carbonate. In calcite, where each Ca^{2+} ion is in 6-fold coordination with oxygen ions from CO_3^- groups, Mg^{2+} is dominant (Figure 1.3). On the other hand, the 9-fold coordination of Ca^{2+} ions in the aragonite structure allows larger cations to substitute for Ca^{2+} (Figure 1.4). In particular Sr is more readily incorporated into aragonitic $CaCO_3$ (Skinner and Jahren 2007). Therefore, trace element concentrations in bivalves might be expected to vary depending on the polymorph present. However, it is likely that a range of internal (biological) and external factors control the incorporation of trace elements, including calcification rate, ambient temperature and metabolic processes.

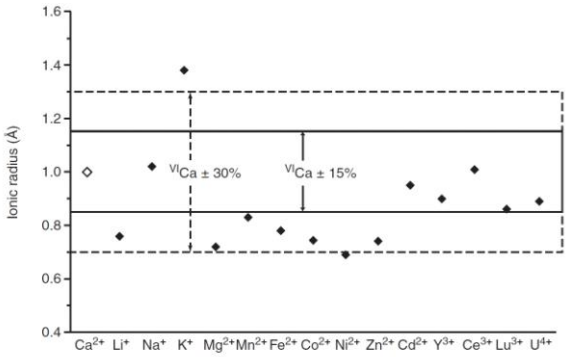

Figure 1.3 Plot of the possible ‘‘best fit’’ (±15%) and next best fit (30%) of cations that could take the place of Ca in sixfold coordination in the calcite structure. Figure taken from Skinner and Jahren (2003).

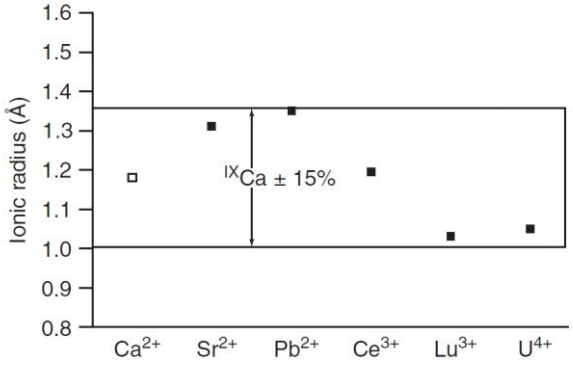

Figure 1.4 Plot of the ‘‘best fit’’ (±15%) of cations that could take the place of Ca in ninefold coordination in the aragonite structure. Figure taken from Skinner and Jahren (2003).

The following sections describe what has been discovered to date about the incorporation of certain trace elements into molluscan shells, in particular bivalves, with emphasis on the consequential use of those trace elements (TE) as proxies for (paleo-) environmental information

1.4.1 Mg/Ca and Sr/Ca in molluscs: proxies for sea surface temperature?

The residence times of Ca^{2+}, Mg^{2+} and Sr^{2+} in the ocean are 1 Myr, 13 Myr and 5 Myr, respectively, compared to an ocean mixing interval of 1000 yr (Broecker and Peng, 1982), and thus seawater Mg/Ca and Sr/Ca ratios are conservative over timescales shorter than those periods. Both Mg/Ca and Sr/Ca ratios are proposed as temperature proxies in biogenic carbonates for this reason, because they do not vary with seawater

salinity, and because of the thermodynamic dependence of their incorporation in calcite and aragonite. Inorganic experiments on Mg/Ca reveal a positive temperature reliance on incorporation into calcite (Mucci, 1987), and an inverse reliance on incorporation into aragonite (Gaetani and Cohen, 2004). For Sr/Ca, incorporation in aragonite is inversely related to temperature (Kinsman and Holland, 1969; Dietzel et al., 2004), while incorporation in calcite is strongly linked to precipitation rate (Lorens, 1981; Morse and Bender, 1990; Tesoriero and Pankow, 1996).

Klein et al. (1996) reported that Mg/Ca shell ratios in the calcitic shell of the mussel *Mytilus trossulus* (formerly *edulis*) positively correlated to recorded SSTs taken periodically over a one year period ($r^2 = 0.74$). However, earlier, Dodd (1965) found only a weak, positive correlation between Mg/Ca in calcite and temperature for *Mytilus edulis* and *Mytilus californianus*, and in fact suggested that the increase in Mg/Ca concentration with temperature was related to shell size and thus growth rate, which increases during higher temperatures for the species (Fox and Coe, 1943; Dodd, 1964). Growth (or calcification) rate has been found to positively correlate with Mg/Ca ratios in *Mesodesma donacium* and *Chione subrugosa* (Carré et al., 2006). When Vander Putten et al. (2000) analysed *M. edulis* shells they found a significant correlation between Mg/Ca and temperature only during spring time, inferring a possible seasonal physiological effect. It was suggested this effect may be due to seasonal variations in the calcite crystal properties, which could be influenced by the surrounding organic matrix and changes to its composition, or the organic matrix may increase and decrease the absorption of trace elements from the mineral component into the matrix (Morse and Mucci, 1984, Vander Putten et al., 2000). Similarly, Takesue and van Geen (2004) reported that temperature influenced Mg/Ca ratios to some degree in *Protothaca staminea* bivalves with aragonite shells. In one increment of the shell a correlation coefficient of 0.71 was observed, but this was not consistent across the other sections.

In any case, when the calibration with the best correlation was applied to Holocene *P. staminea* fossils temperatures were considerably underestimated because of a diagenetic decrease in Mg/Ca ratios.

Evidence of thermodynamic incorporation of Sr^{2+} into molluscan shell has also proved elusive. Following laboratory studies of the mussel *Mytilus trossulus*, Lorens and Bender (1980) found Sr/Ca increased linearly in response to increases in Sr/Ca in the water they lived in. Dodd (1965) reported a difference between the aragonitic and calcitic sections in *M. edulis* and *M. californianus* shells, whereby Sr/Ca positively correlates to temperature in calcite, but shows a negative correlation in aragonite. However, subsequent studies have not revealed a temperature dependence on incorporation of Sr (Vander Putten, 2000). Rather, as for Mg/Ca, shell growth rate has been proposed as a primary cause of Sr/Ca variations in molluscan shells. Significant correlation between growth rate and Sr/Ca ratios has been reported for a number of species: the mussel *M. edulis* (Vander Putten et al., 2000); the calcitic bivalve *Pecten maximus* (Lorrain et al., 2005); and the aragonitic bivalves *P. staminea* (Takesue and van Geen, 2004), *Saxidomus giganteus* (Gillikin et al., 2005), *M. donacium*, *C. subrugosa* (Carré et al., 2006) and *Arctica islandica* (Schöne, 2011). In many cases growth rate-Sr/Ca (and Mg/Ca) trends are also associated with ontogenetic trends; equating to a decrease or increase in TE/Ca ratios with the ontogenetic age of the mollusc (Takesue and van Geen 2004; Gillikin et al., 2005; Carre et al., 2006; Schöne, 2011). The trends are related, as for all molluscan species growth rate decreases as the organism grows older (Schöne, 2008).

Conversely, Klein et al. (1996) found that growth rate in *M. trossulus* had minimal influence on Mg/Ca and Sr/Ca shell concentrations, although the sample numbers used were potentially too few (only 26 data points per shell). Rather, Klein et al. (1996)

hypothesised that Sr/Ca ratios vary with the mollusc's metabolic efficiency in diffusing Ca^{2+} ions through the mantle epithelium to the EPF (Purton et al., 1999). Accordingly, low Sr/Ca ratios observed in *M. Trossulus* calcite occurred when Ca^{2+} ions were pumped into the EPF at a higher rate, as a result of intra-cellular (metabolic) transport of ions (favouring Ca^{2+}) exceeding inter-cellular transport of ions (non-preferential) (Wheeler, 1992). This is seen as a decrease in Sr/Ca ratios from the ventral margin of the shell - where mantle metabolic rate is lower, towards the shell's lateral margin, where intra-cellular transport dominates (Rosenberg and Hughes, 1991), meaning higher metabolic rate and lower Sr/Ca ratios.

Overall, there is no conclusive evidence that Mg or Sr incorporation in calcitic or aragonitic mollusc shells is under thermodynamic control so as to make either of these useful proxies for deriving paleo-ocean temperatures. Where the incorporation of these elements in shells appears to be related to temperature, it is more likely that this is an indirect effect. Temperature may influence the biological and physiological processes responsible for mineralization, specifically growth rate, metabolic pumping, and crystallographic properties of $CaCO_3^-$, which appear to be the dominant control on Mg and Sr incorporation. Unravelling these physiological signals for a species may allow Sr/Ca and Mg/Ca records to be potential proxies for SST (Schöne, 2008; Schöne, 2011).

An additional question remains about the possible correlation between Mg/Ca shell chemistry and Sr incorporation. It is proposed that when Mg^{2+} substitutes for Ca^{2+} in the crystal lattice, a distortion is created in the lattice because of the smaller ionic radius of Mg^{2+} thus creating more space in adjacent areas of the lattice for substitution by a larger ion, such as Sr^{2+} (Mucci and Morse, 1983; Goldsmith et al., 1961; Vander Putten et al.; 2000).

Table 1.1 Summary of key studies of Mg incorporation in molluscan shells. For each study, the species, location of individuals studied, polymorph of $CaCO_3$ and result for the incorporation of Mg are reported.

Study	Species	Location	Proxy	Result
Dodd (1965)	*Mytilus edulis* *Mytilus californianus*	Pacific Coast from Washington to southern California	Mg/Ca calcite	Weak positive correlation with temperature – likely related to changes in growth rate
Klein et al. (1996)	*Mytilus trossulus*	Strait of Georgia, British Columbia	Mg/Ca calcite	Positive correlation with temperature
Vander Putten et al. (2000)	*Mytilus edulis*	The Netherlands	Mg/Ca calcite	Positive correlation between with temperature only during spring
Carré et al. (2006)	*Mesodesma donacium* *Chione subrugosa*	Peruvian Coast	Mg/Ca aragonite	Positive correlation with calcification rate
Takesue and van Geen (2004)	*Protothaca staminea*	Humboldt Bay, northern California	Mg/Ca aragonite	Positive correlation with temperature in one growth increment. Diagenetic decrease in Mg/Ca in fossils of the species
Schöne et al. (2011)	*Arctica islandica*	Iceland	Mg/Ca aragonite	Strong negative correlation with growth rate, positive correlation with ontogenetic age Growth rate-detrended ratios inversely correlated to SST
Elliot et al. (2009)	*Tridacna gigas*	San Francisco Bay, California	Mg/Ca Aragonite	SST causes seasonal Mg/Ca variations, but ratios cannot be quantitatively linked to SST Positive correlation with ontogenetic age

Table 1.2 Summary of key studies of Sr incorporation in molluscan shells. For each study, the species, location of individuals studied, polymorph of $CaCO_3$ and result for the incorporation of Sr are reported.

Study	Species	Location	Proxy	Result
Dodd (1965)	*Mytilus edulis* *Mytilus californianus*	Pacific Coast from Washington to southern California	Sr/Ca calcite	Positive correlation with temperature
			Sr/Ca aragonite	Negative correlation with temperature
Lorens and Bender (1980)	*Mytilus trossulus*	Grown in laboratory	Sr/Ca calcite	Linear increase in Sr/Ca with water Sr/Ca ratios
Klein et al. (1996)	*Mytilus trossulus*	Strait of Georgia, British Columbia	Sr/Ca aragonite	Ratios vary with metabolic efficiency of Ca^{2+} pumping
Vander Putten et al. (2000)	*Mytilus edulis*	The Netherlands	Sr/Ca calcite	Positive correlation with calcification rate
Lorrain et al. (2005)	*Pecten maximus*	Bay of Brest, France	Sr/Ca calcite	Positive correlation with calcification rate
Takesue and van Geen (2004)	*Protothaca staminea*	Humboldt Bay, northern California	Sr/Ca aragonite	Positive correlation with calcification rate
Gillikin et al. (2005)	*Saxidomus giganteus*	Washington and Alaska	Sr/Ca aragonite	Positive correlation with calcification rate
Carré et al. (2006)	*Mesodesma donacium* *Chione subrugosa*	Peruvian Coast	Sr/Ca aragonite	Positive correlation with calcification rate
Elliot et al. (2009)	*Tridacna gigas*	San Francisco Bay, California	Sr/Ca aragonite	SST growth rates and metabolic rates do NOT control Sr/Ca ratios
Schöne et al (2011)	*Arctica islandica*	Iceland	Sr/Ca aragonite	Strong negative correlation with growth rate, positive correlation with ontogenetic age
				Age-detrended ratios inversely correlated to SST

1.4.2 Ba/Ca and Mn/Ca: Indicators of primary productivity, salinity and redox?

The residence time of Ba in the ocean is only 0.01 Myr (Paytan et al., 2007), and therefore the concentration of Ba in seawater depends strongly on local influences over short timescales. In particular, it is well known that high primary productivity increases seawater Ba levels (Goldberg and Arrhenius, 1958; Chow and Goldberg, 1960; Dehairs et al., 1980; Dehairs et al., 1987; Bishop, 1988). Sediment run-off greatly affects the Ba concentration of seawater in coastal locations, especially those sites vulnerable to flood plumes. High resolution analyses of aragonitic coral skeletons from the Great Barrier Reef have shown that Ba/Ca variations provide a record of storm events, as well as quantifying erosion relating to land use change in eastern Queensland, and information on the terrigenous sources of Ba (McCulloch et al., 2003; Sinclair and McCulloch, 2004).

Analyses of Ba/Ca ratios in bivalves to date have revealed low background concentrations interspersed with periodic peaks of elevated Ba/Ca (Vander Putten et al., 2000; Stecher et al., 1996; Gillikin et al., 2006; Lazareth et al., 2003; Gillikin et al., 2008). Vander Putten et al. (2000) suggested that the peaks observed in *Mytilus edulis* shells were due to phytoplankton blooms, based on the their coincidence with observed spring-time blooms and peaks in chlorophyll. However, it was noted that the Ba/Ca-chlorophyll correlation was not year long, limiting shell Ba/Ca as a proxy for primary productivity. Likewise, Stecher et al. (1996) attributed Ba/Ca peaks in *Mercenaria mercenaria* and *Spisula solidissima* to local diatom blooms increasing levels of particulate Ba, which were then ingested by the bivalves. Gillikin et al. (2008) found that synchronous Ba/Ca peaks in two *Saxidomus giganteus* bivalves and four *Pecten maximus* scallops were not fully explained by phytoplankton blooms. Although these Ba/Ca peaks occurred near peaks in the chlorophyll record, there was a month long

delay between the Ba/Ca peaks forming and the 'crash' of the phytoplankton bloom. Additionally, the amplitude of chlorophyll and Ba/Ca peaks were not correlated. Another potential cause of the Ba/Ca peaks in *P. maximus* postulated by Gillikin et al. (2008) was the effect of the scallop's reproductive cycle on Ba/Ca incorporation– as peaks coincided with times when the scallops were not spawning.

Gillikin et al. (2006) used field and laboratory experiments to examine the Ba/Ca ratios observed in *M. edulis* excluding the Ba/Ca peaks (the "background" signal). These authors found that background Ba/Ca shell ratios were directly related to, and thus could be used as a proxy for the Ba/Ca ratios of the seawater in which the shells crystallised. This is consistent with some previous studies on corals that showed bulk chemistry Ba/Ca ratios were related to seawater Ba/Ca ratios (Bowen, 1956; Harris and Almy, 1964; Livingston and Thompson, 1971), and an earlier study by Torres et al. (2001) that found a correlation between Ba/Ca ratios in clam shells and seawater Ba/Ca. Gillikin et al. (2006) argued that in estuarine mussels the shell Ba/Ca-seawater proxy could be extended to provide a relative record of salinity, because of estuarine-specific relationships between salinity and seawater Ba/Ca (Gillikin et al., 2006; Coffey et al., 1997). However, for *S. giganteus* bivalves, Gillikin et al. (2008) conceded that ontogenetic decrease in background Ba/Ca ratios complicated the use of that particular species for a salinity proxy. *A. stutchburyi* clams, also filter feeders, were collected for this study from a mixture of estuarine and open ocean sites; thus the Ba/Ca ratios measured in their shells could shed light on Ba incorporation, and the potential of the proxies discussed above.

Like barium, manganese also has a very short ocean residence time - 760 yr (Savenko, 2008). It is sourced in dissolved form (Mn^{2+}) from riverine input of terrigenous sediment, and once in the ocean is oxidised to Mn^{4+}. In anoxic conditions, Mn^{2+} can be

recycled through reduction, and there are high amounts of Mn found in ocean floor sediment. There is evidence to suggest that the concentration of particulate Mn in seawater is associated with primary productivity due to algae taking up dissolved Mn, and certain phytoplankton catalysing the oxidation of Mn to form insoluble Mn oxides (Morris, 1971; Sunda and Huntsman, 1985; Vander Putten, 2000). Several records of Mn/Ca in bivalves have shown correlated peaks with Ba/Ca, and have likewise been correlated to chlorophyll concentrations (Vander Putten et al., 2000; Lazareth et al., 2003). Freitas et al. (2006), however, found that variations of Mn/Ca in *P. maximus* bivalves in Menai Strait were more closely related to hydrographical conditions, specifically changes in temperature and redox conditions, which affected the seawater dissolved Mn^{2+}. These authors suggested, therefore, that the bivalve was a potential proxy for seawater Mn^{2+}.

As is the case for Ba/Ca ratios, the Mn/Ca ratios in molluscan shells, and their potential use as a proxy, are likely to vary for a given species depending on the environment the mollusc lives in, and the local influences on Mn seawater concentration. Differences observed between individuals of a species grown in the same conditions suggest that Mn/Ca and Ba/Ca are also biologically influenced, which would require further research to disentangle from the environmental influence (Freitas et al., 2006). Calcification (growth rate) is likely to be one such influence; Carré et al. (2006) found this physiological process accounted for 54% of Mn/Ca ratio variations and 44% of Ba/Ca ratio variations in *M. donacium* shells.

1.4.3 As, Zn, Cu & Pb: Tracers of pollution?

Purchase and Fergusson (1986) analysed Pb concentrations in the shell of *A. stutchburyi* living on the Heathcoate River, Christchurch, where anthropogenic pollution of Pb had previously been linked to a nearby battery factory and traffic. It was found that Pb

concentrations varied across sections of shells; with higher concentrations in the sections close to the umbo (that grew when the clam was young), suggesting incorporation of Pb into the shell may depend on age (or possibly changes in growth rate dependent on seasonality and age). If this effect is confirmed in *A. stutchburyi* in this study for other heavy trace metals (Zn, As, Cu), it would complicate the use of the clams as pollutant indicators, because ontogenetic, or growth related variations in heavy metal concentration could be mistaken for environmental ones. In other bivalves, variations in concentrations of Cu, Zn and Cd have been linked to pollution (Richardson, 2001).

1.5 Sclerochronology: Bivalve microstructure & growth information

Growth information is of vital importance in interpreting molluscan geochemical records for several reasons. First, when growth lines on a species are known to represent certain increments of time a timescale can be assigned to the section of shell. This process is termed sclerochronology. Second, understanding the growth characteristics in the species under study is crucial. Growth may influence the incorporation of trace elements (e.g. for Sr/Ca ratios as described above), and furthermore it is important to identify any periods of growth cessation so that potential interruptions in the geochemical record can be identified. For example, it has been found that the *Arctica islandica* clam does not deposit any shell for two months when it is spawning, and the interpretation of environmental information recorded in its shell must take into account this gap (Schöne et al., 2005).

1.5.1 Shell microstructure

Bivalve shells are divided into two, or sometimes three, calcified layers, and one thin, organic outer layer called the periostracum (Figure 1.1). The calcified layers are largely comprised of a microstructure of $CaCO_3$ crystals with a particular orientation, shape and

size. There are seven possible microstructure types, some of which are associated exclusively with either aragonite or calcite, and others which are found in both these polymorphs of calcium carbonate (Carter, 1980; Gregoire, 1972). Each species has a unique configuration of microstructures and polymorphs, and more than one microstructure has been found in a particular layer. Within the mineral layers of the shell there are also two organic components present: an intra-crystalline organic matrix, which binds the $CaCO_3$ crystals; and an extra-crystalline organic layer, which separates individual increments of crystal growth. The latter organic layer forms during times when the organism's valves are closed and an increase in acidity of the EPF dissolves the previously deposited organic matrix and $CaCO_3$. (Panella, 1975; Palmer, 1995; Takesue and van Geen, 2004).

1.5.1 A. stutchburyi microstructure

A. stutchburyi shells are comprised of three calcified layers: an outer layer with a crossed-lamellar microstructure; an inner layer of homogeneous (irregularly shaped and arranged) crystals; and an inner layer with complex cross lamellar or homogeneous structure. (Jones, 1979; Figure 1.5). The geochemical analyses completed in this study transverse the outer crossed-lamellar layer, which is made of elongate, aragonite crystals (Kobayashi and Samata, 2006; Purchase and Fergusson, 1986).

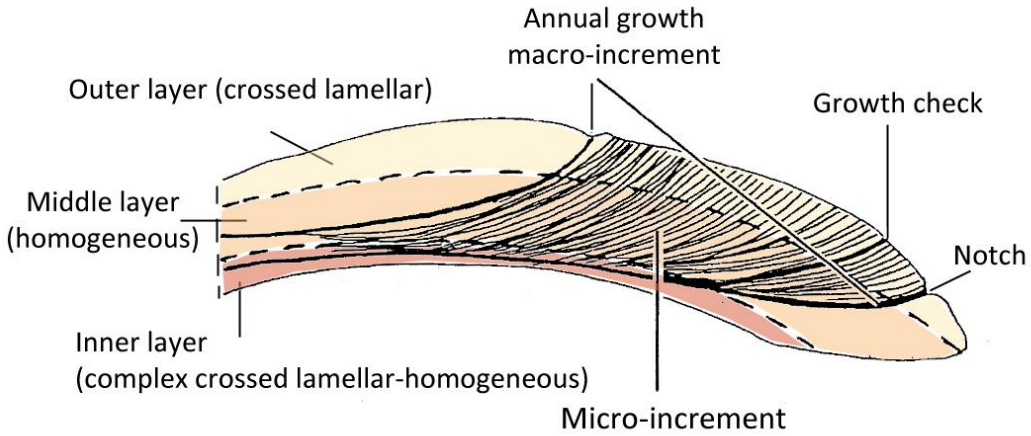

Figure 1.5 Schematic cross-section of *A. stutchburyi* shell showing growth patterns (micro- and macro- increments) and zones of different shell microstructure (crossed-lamellar, homogeneous and complex crossed-lamellar). Figure modified from McKinnon, 1996).

1.5.3 Growth increments

Growth increments are discrete sections of shell, identifiable by extra-crystalline organic layers, and represent a defined period of growth. There are commonly two types of increments found in bivalves: macro-increments - sometimes referred to as growth-bands or rings; and micro-increments - sometimes termed growth-lines (Figure 1.5). Here, the terminology macro- and micro-increment will be used. Macro-increments are defined by two thick, dark bands, which result from a slowdown of shell growth, or complete stop in carbonate deposition. In many species, it has been shown that these are an annual phenomenon, and form seasonally during periods of no deposition. However, similar bands may also be formed in response to an abrupt termination of growth caused by environmental or physiological stress, such as storms or spawning (Schöne, 2008). Annual bands, and thus macro-increments, can be distinguished from stress bands in some bivalves because they are often accompanied by a notch at the shell surface, whereas stress bands often do not extend all the way through the section of shell as shell growth abruptly commences. (Panella, 1975; Takesue and van Geen, 2004; McKinnon, 1996; Clark, 1979).

Micro-increments are defined by fine layers of extra-crystalline organic material, deposited, as discussed above, when valves are closed. In many sub-tidal and intertidal species the increments are related to the cycle of the tides – as valves close and shell growth slows or stops when shells are not immersed during low tide (Kanazawa and Sato, 2008; Takesue and van Geen, 2004; Carré et al., 2005; Carré et al., 2006). However, there is commonly not a one-to-one correlation between low tide events and micro-increments, with seasonality, as well as spring tide and neap tide cycling influencing the size and number of increments formed in a lunar day (McKinnon, 1996; Evans, 1972; Richardson et al., 1990; Takesue and van Geen, 2004).

1.5.4 Growth increments in A. stutchburyi

McKinnon (1996) carried out an extensive study on the growth characteristics of *A. stutchburyi* growing at Port Chalmers in Dunedin. The study confirmed the results of an earlier experiment by Coutts (1974) that macro-increments in the clams have an annual period, with the bands forming during the winter months. In some specimens, stress bands were also observed, which form in the summer months during spawning. Annual bands could be distinguished from stress bands in the manner described above; the annual bands being associated with a notch or depression at the shell surface, and the stress bands commonly being incomplete through the shell (McKinnon, 1996).

Micro-increments in *A. stutchburyi* have a tidal influence that is modulated by other changes in growth rate. McKinnon (1996) found a one-to-one correlation between the number of low tides and the number of micro-increments laid down during the peak growing season only (January and February). However, it appears during the remainder of the year that fewer micro-increments form than there are low tides, and that in June and July only a very small number, or no micro-increments are produced. This is consistent with other studies where low growth rate for an extended period of time produced an increment of shell without distinguishable micro-rings (Jones 1980).

There is also a cyclical variation between *A. stutchburyi* increments added in spring tides, and neap tides, which vary four times during a lunar cycle. During spring tides, when shells are immersed for longer periods of time, the micro-increments are wider; with two strong boundaries separating each increment, and a thin boundary, barely visible, in the centre of each increment as well (Figure 1.6). Conversely, during neap tides the micro-increments are narrower and are defined by only two strong organic boundaries (McKinnon, 1996).

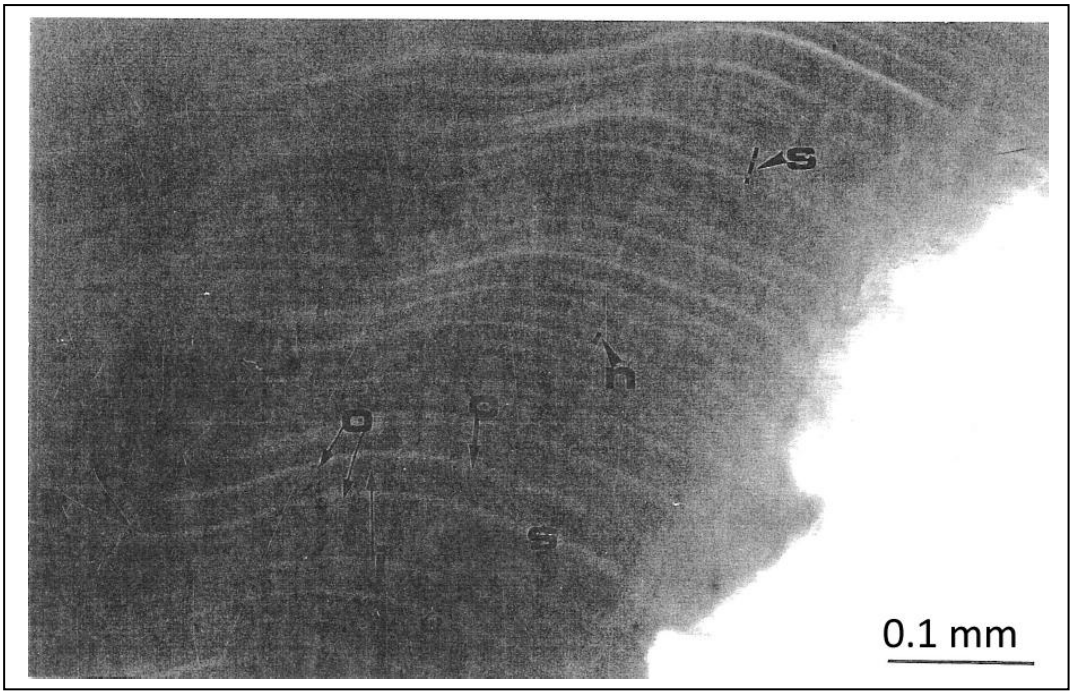

Figure 1.6 Photograph showing the difference between spring tide micro-increments (S), which have strong outer organic boundaries (O) and weak inner boundaries (C). Neap tide micro-increments are narrower (N) Taken from (McKinnon 1996).

The fact that micro-increments on *A. stutchburyi* do not form with every low tide and that they are not formed at all during much of the winter has significant ramifications for geochemical studies utilising the clam. It means that geochemical records taken across a section in the shell may be incomplete, with an underestimation of the winter signal.

1.5.5 Factors affecting A. stutchburyi growth

Besides tidal influence on growth, there are other factors driving growth rate that explain why micro-increments do not perfectly correlate with the number of low tides. Temperature, associated with latitudinal location, is the predominant environmental influence known to affect shell growth rates (Green, 1973; Richardson et al., 1980; Fox and Coe, 1943; Dodd, 1964). Other environmental conditions, such as storms, increases in silty sediment (Appledoorn, 1983), variations in salinity (Marsden, 2004), and

availability of food, have all been shown to cause a slow down or cessation in growth in particular species. In addition, biological factors also have an impact on growth rate; it is common that growth rate slows during spawning and also with ontogenetic maturity or age (Hall, 1974; Jones, 1978).

McKinnon (1996) demonstrated that in *A. stutchburyi*, the cessation of growth coincides with the winter months, when temperatures are lowest. Comparing growth rate measurements with recorded sea surface temperatures for the whole year also revealed a strong correlation between the two parameters ($r^2 = 0.624$). The hours of light in each day (i.e. day length) were also shown to correlate to growth rate. Marsden (2004) has shown that *A. stutchburyi* are very sensitive to salinity dilution, which together with low phytoplankton availability, reduces growth and condition of the clams. McKinnon (1996) found that the stress band seen in some individuals in summer responded to the clams' spawning activity during this time. Finally, a growth-rate model developed by McKinnon (1996) shows that *A. stutchburyi* growth rate slows exponentially with age (Figure 1.7).

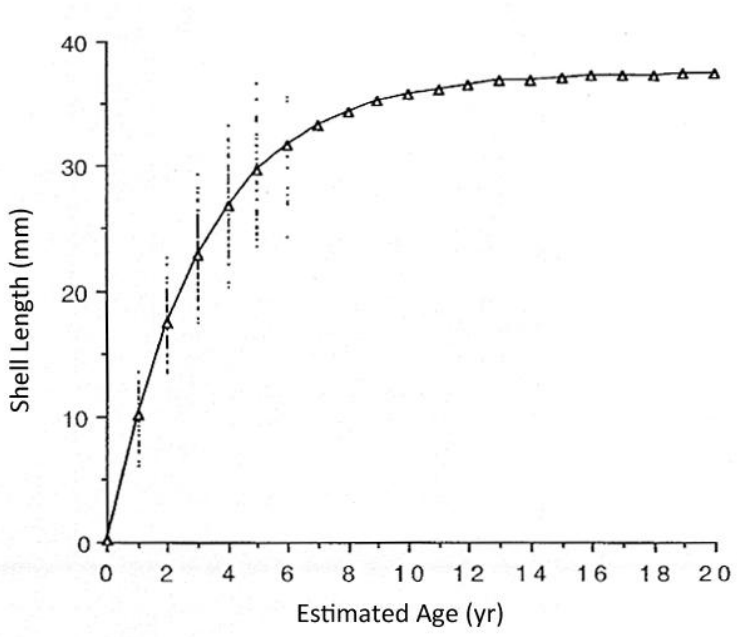

Figure 1.7 Growth rate and age model for *A. stutchburyi*. Figure taken from McKinnon (1996).

1.6 Thesis Structure

Chapter One: Introduction outlines the incorporation of trace elements in molluscs and their potential as environmental proxies; and the thesis objectives.

Chapter Two: Materials and Methods introduces the study species; field sites where samples were collected; sample preparation; sample analyses; how data were processed; and discusses analytical uncertainties.

Chapter Three: Results presents the trace element records for each shell analysed plotted against distance sectioned; correlation matrix between particular trace element/Ca ratios; average shell TE/Ca ratios; and sediment trace element values.

Chapter Four: Discussion

1. ***A. stutchburyi* sclerochronology:** Describes the methods used to produce a chronology for two of the shell sections analysed and discusses the limitations and methods in using sclerochronology.
2. **Trace element incorporation:** Reports growth rate results, and shows this is the primary influence on TE incorporation. Individual influences on incorporation are discussed for Mg/Ca, Sr/Ca, Mn/Ca, Ba/Ca, U/Ca, As/Ca, Zn/Ca and Cu/Ca in light of temporal variation in order to evaluate the suitability of using trace elements in *A. stutchburyi* as paleoenvironmental proxies.
3. **Comparison with other molluscan studies:** Places the results and interpretations for *A. stutchburyi* in context with previous mollusc TE/Ca studies.
4. **Evaluation of A. stutchburyi:** Discusses the usefulness and limitations of using *A. stutchburyi* clams as paleoenvironment indicators.

Chapter Five: Conclusions outlines the key conclusions reached in the study, and makes suggestions for further study.

CHAPTER 2.0 MATERIALS AND METHODS

2.1 Study species: *A. stutchburyi*

Austrovenus stutchburyi (Wood, 1828), commonly referred to as the New Zealand cockle, is a clam from the family *Veneridae*. The species is a shallow-burrowing (20-40 mm beneath the sediment surface), filter-feeder that is found in soft mud to fine-grained sand in sheltered beaches, tidal flats and estuaries, with larger specimens usually found in coarser-grained sediment. (Beu, 2006; Powell, 1979; Jones, 1983; New Zealand Ministry of Fisheries, 2010). *A. stutchburyi* is an intertidal bivalve, with an endogenous tidal rhythm of shell gaping and siphon extension (Beentjes & Williams, 1986). Therefore, the clam's habitat is generally limited by the lowest neap-tide mark, and the highest spring-tide mark (Beu, 2006; Dobinson et al., 1989), although Larcombe (1971) has reported animals higher in the intertidal zone that are submerged for only 3.5 hr in a day. Salinity, phytoplankton availability, and temperature have a strong control on growth rate and survival, as described in the previous chapter. *A. stutchburyi* typically live for 10 yr, and for older specimens it is thought that little shell extension occurs after 10 yr (McKinnon, 1996).

The species is widespread in the North and South Islands of New Zealand, as well as Stewart and the Chatham Islands. Population densities can be very high – as many as 4500 *A. stutchburyi* per square metre have been recorded (New Zealand Ministry of Fisheries, 2010). Preserved *A. stutchburyi* shells are commonly present in large numbers throughout the New Zealand fossil record, dating as far back as the late Pliocene (Beu, 2006). The species has been used to date shoreline progression from the end of the last glacial period through the Holocene (Heap & Nichol, 1997; Kennedy, 2008), and shells found in Maori middens deposits have been dated for archaeological

studies (Higham and Hogg, 1997). Its abundance at a range of latitudes and preservation in the fossil record make *A. stutchburyi* a prime molluscan species candidate for paleoenvironment studies.

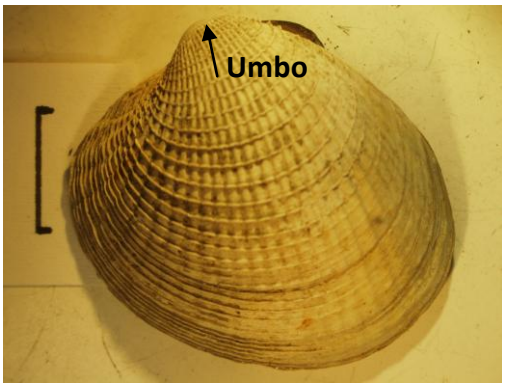

Figure 2.1 Photograph showing one valve of *A. stutchburyi* collected at Manakau Harbour. Scale bar is 1cm long.

2.2 Sampling Locations

A. stutchburyi and sediment samples were collected from eight sites - one in the South Island and seven in the North Island (Table 2.1 and Figure 2.2). The locations were spread over a range of latitudes and a variety of coastal settings: estuarine (Kawhia); tidal mud-flats (Miranda, Bay of Islands, Manakau); and an open ocean beach (Ligar Bay). Therefore, variability in ocean temperature, and between mixed and closed seawater conditions, may have potentially been recorded in the shell chemistry. Also, the locations encompassed a range of geographic settings – specifically land usage and population density.

One shell per location was analysed by LA-ICP-MS, with the exception of Ligar Bay where four shells were analysed. In addition, one shell was analysed from the Ligar Estuary - an estuary adjoining Ligar Bay. In this way, the geochemical variability between individuals experiencing the same environmental conditions could be compared (between the Ligar Bay samples), and the difference between estuarine and open sea individuals living in similar conditions (Ligar Bay and Ligar Estuary) could be

assessed. Samples from these latter two locations were collected at the same time in April 2008, while samples from the remaining sites were collected over a week in January 2009.

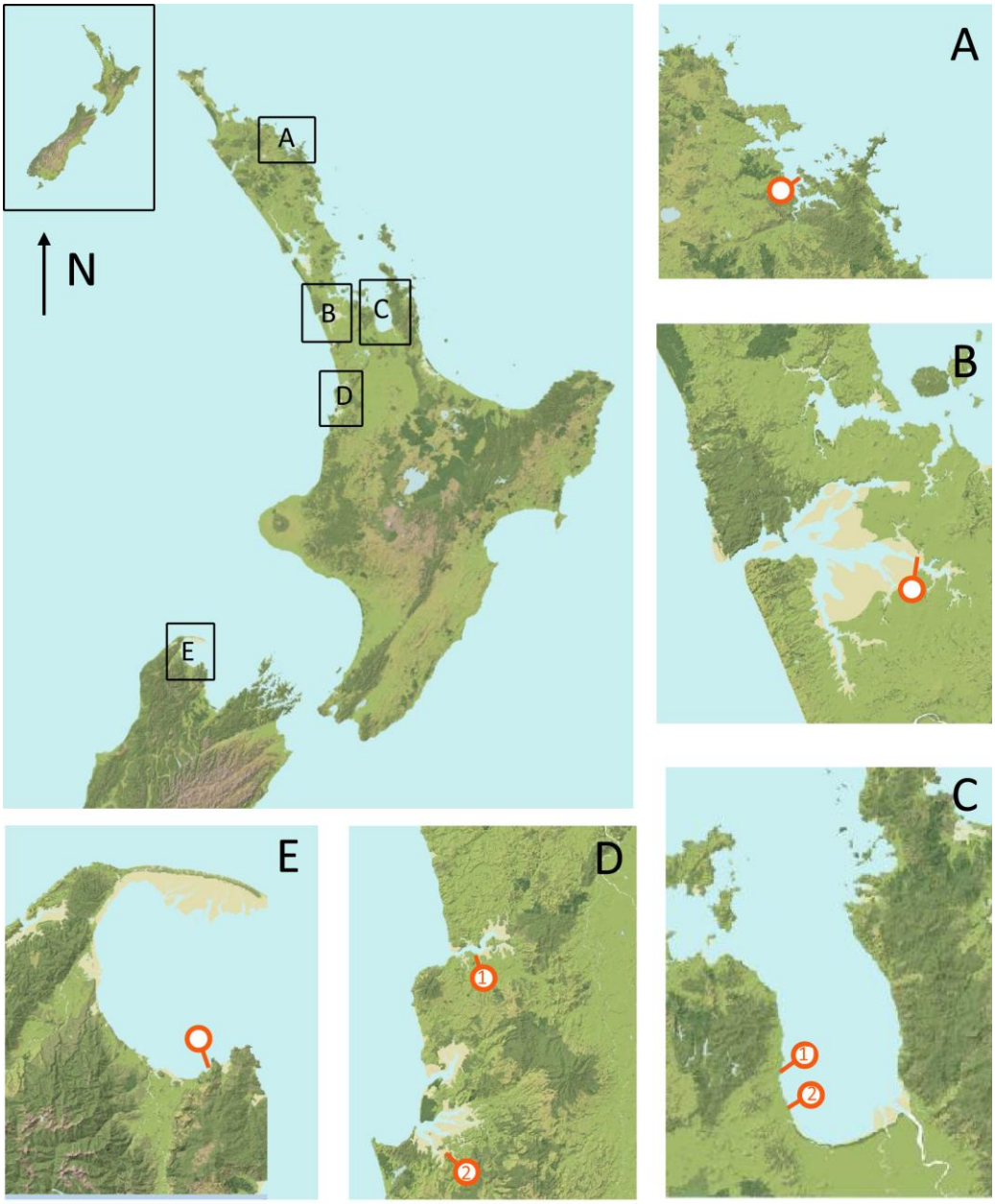

Figure 2.2 Map of sample locations of where *A. stutchburyi* were collected from in New Zealand, and small maps showing individual locations indicated by orange circles. **A** Pomare Bay, Bay of Islands; **B** Manakau Harbour; **C** Firth of Thames **1** Kaiaua **2** Miranda; **D 1** Raglan **2** Kawhia; **E** Ligar Bay and Ligar Estuary. Maps modified from GeographX map of New Zealand.

Table 2.1 Summary of field locations where *A. stutchburyi* were sampled from. Site name, date sampled, latitude and longitude of the sample location, the coastal setting and catchment setting are reported.

Site	Date Sampled	Latitude/longitude	Coastal setting	Catchment setting
Ligar Bay	1 April 2008	40°49'22.47"S, 172°54'15.12"E	Open ocean, beach with medium-coarse sand	Granite; Oligocene-Miocene limestone
Ligar Estuary	1 April 2008	40°49'22.47"S, 172°54'15.12"E	Estuarine	Granite; Oligocene-Miocene limestone
Kawhia	20 Jan 2009	38° 2'48.39"S, 174°49'53.75"E	Estuarine, mud flats	Oligocene limestone; Early Quaternary andesite; Jurassic greywacke
Raglan	21 Jan 2009	37°47'45.22"S, 174°52'13.63"E	Mud flat within harbour entrance, mud-fine grained sand	Oligocene limestone; Early Quaternary andesite
Miranda	22 Jan 2009	37° 8'55.20"S, 175°18'37.81"E	Tidal mud-flats	Quaternary post-glacial alluvium; Quaternary swamp deposits and peat; Jurassic greywacke; Miocene andesite
Kaiaua	22 Jan 2009	37° 6'43.25"S, 175°17'52.90"E	Beach with mud-fine sand, including broken shell fragments	Quaternary post-glacial alluvium; Quaternary swamp deposits and peat; Jurassic greywacke; Miocene andesite
Manakau	22 Jan 2009	37° 2'33.50"S, 174°51'21.92"E	Tidal mud flats within harbour	Quaternary basalt; Miocene limestone; Quaternary postglacial alluvium
Pomare	25 Jan 2009	35°16'0.34"S, 174° 7'39.83"E	Embayed estuarine mud flat	Triassic-Jurassic greywacke

2.3 Sample Collection

Sample collection was carried out at low tide, when most *A. stutchburyi* were not fully submerged. The clams were found buried at a shallow (< 20 mm) depth in the sediment, and could often be identified by a clump of green algae attached to the shell umbo, protruding from the sediment surface. Approximately 20-30 live clams were collected at each location, along with one surface sediment sample (down to ~50 mm depth), taken from the low tide mark.

Once collected *A. stutchburyi* were killed by submerging them in freshwater. During this stage organic tissue fell out of the open valves. Shells were subsequently cleaned in water with a toothbrush to remove sediment and residual organic material, air dried, and stored in sample bags prior to more detailed preparation in the laboratory. Sediment was likewise stored in sample bags.

2.4 Sample preparation

2.4.1 A. stutchburyi shells

In the laboratory, the shells were re-cleaned and dried in the oven for approximately 48 hr at 40°C. Once dry, the dimensions of shells, with both valves connected were measured. Subsequently, valves of each shell were separated, weighed, and labeled ‘a’ or ‘b’ for the left-side valve and right-side valve respectively, relative to the downward direction of the umbo (Fig 2.1).

Samples were then selected for analysis based on the growth patterns visible on the external shell surface. In particular for the Ligar Bay samples, shells were chosen with an apparent range of growth rates, represented by the distance between macro-bands. Left or right valves were chosen at random. Selected shell valves were cut by with diamond saw following the direction of maximum growth (Figure 2.3). The shell

cross-sections were subsequently set in epoxy resin in full circle mounts, along with a fragment of NIST-610 glass (Figure 2.4). Once dry, mounts were polished on a 200 µm lap to expose the shell and NIST-610 surface to be ablated on the LA-ICP-MS.

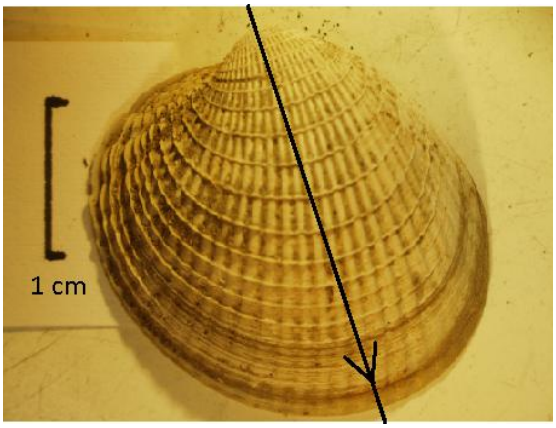

Figure 2.3 *A. stutchburyi* shell, line and the arrow indicates the maximum direction of growth, down which shells were sectioned with a diamond saw.

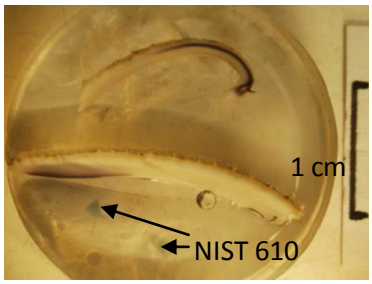

Figure 2.4 A section of *A. stutchburyi* shell mounted in epoxy, with NIST-610 fragments in bottom left section of the mount.

2.4.2 Sediment

Before sediment was sent for X-ray fluorescence (XRF) analysis, it was washed to remove soluble salts precipitated from seawater (principally Na and Mg) and dried in an ultra-clean laboratory. For each sample, preparation was as follows: 5 g of sediment was put into a separate glass beaker, with 40 mL of ultraclean (>18.2 MΩ) water. Samples were then sonicated for 25 min, and subsequently transferred into centrifuge tubes. The dispersed sediment was centrifuged at 2000 rpm for 10-30 min until all particulate material was concentrated at the bottom of the tube. Liquid was then removed by pipette. This process was repeated for each sample until sediment would not separate from the liquid after centrifuge. Each sediment sample was transferred back into a glass beaker, covered, and dried in an oven at 50°C for one week. The samples were then stored in the same beakers until sent for XRF major element analysis at SpectroChem Ltd.

2.5 Sample analysis

2.5.1 A. stutchburyi shells – LA-ICP-MS trace element analysis

Analyses of the sectioned *A. stutchburyi* shells were performed using a New Wave 193 nm laser ablation system coupled to an Agilent 7500CS ICP-MS system at Victoria University of Wellington. A transect of ablation points, at 100 µm and in some cases 50 µm spacing, was made across each shell section through the outer crossed lamellar layer, from the ventral margin edge of the shell, towards the umbo (Fig 2.5). These transects passed through the crossed lamellar layer of the shell, 100-300 µm beneath the periostracum layer. Care was taken to maintain a consistent distance between ablation points and the periostracum, to minimise trace element/Ca (TE/Ca) variation caused by trace element changes with depth through the shell.

Figure 2.5 Cross section of Ligar Bay 1B, showing approximate path of LA-ICP-MS transect (white lines).

Table 2.2 LA-ICP-MS operating parameters

Laser Ablation	
Laser ablation system	New Wave 193 nm (deep UV) solid state
Ablation mode	Static spot analyses
Depth ablated/pulse	~0.1 µm
ICP-MS	
ICP-MS system	Agilent 7500CS
Acquisition mode	Peak hopping
Detection mode	Pulse counting
Tuning	
Tuning standard	NIST 610
Ablation mode	Rastering (2 µm/s) beneath a 35 µm spot
Monitored isotopes	^{7}Li, ^{11}B, ^{24}Mg, ^{27}Al, ^{55}Mn, ^{63}Cu, ^{66}Zn, ^{75}As, ^{86}Sr, ^{88}Sr, ^{138}Ba, ^{238}U
Carrier gas (Ar)	0.85 L/min
Ablation gas (He)	80-90%
RF Power	1500 W
RF Matching	1.72 V
Repetition rate	5 Hz
Laser Power	55%
Standards and calibration	
Calibration standard	NIST-SRM610
Ablation mode	35 µm spot
Repetition rate	5 Hz
Laser power	55%
Background acquisition	60 s
Sample data acquisition	60 s
Washout time	90 s
Measured Isotopes	^{7}Li, ^{11}B, ^{24}Mg, ^{27}Al, ^{55}Mn, ^{63}Cu, ^{66}Zn, ^{75}As, ^{86}Sr, ^{88}Sr, ^{138}Ba, ^{238}U
***A. stutchburyi* method**	
Repetition rate	5 Hz
Ablation mode	30 µm spot
Laser power	50%
Background acquisition	60 s
Sample data acquisition	60 s
Washout time	90 s
Measured Isotopes	^{7}Li, ^{11}B, ^{24}Mg, ^{27}Al, ^{55}Mn, ^{63}Cu, ^{66}Zn, ^{75}As, ^{86}Sr, ^{88}Sr, ^{138}Ba, ^{238}U

NIST-610 glass in each mount was ablated to tune the LA-ICP-MS before each run, and was also measured before and after each run, and after every 5-10 ablation points in the shell throughout a run, as an external standard. Data processing was as follows: 1. Raw elemental counts for each ablation were averaged as well as background elemental counts measured prior to each ablation. 2. The background count averages were subtracted from the ablation element averages. 3. The background-subtracted elemental counts were ratioed to Ca. 4. The elemental/Ca ratios were then normalised using NIST-610 values published by the National Institute of Standards and Technology, which corrected for machine drift and elemental fractionation. 5. Finally, atomic trace element/Ca ratios were converted into units of mmol/mol.

2.5.2 Sediment – X-ray fluorescence major element analysis

Major element analyses were carried out on each sediment sample at SpectraChem Analytical Laboratory in Lower Hutt, Wellington. XRF spectrometry was carried out on 1 g samples fused to make borate glass discs producing data for major element oxides (SiO_2, Al_2O_3, Fe_2O_3, CaO, MgO, SO_3, K_2O, Na_2O, MnO, TiO_2 and P_2O_5).

2.6 Analytical uncertainty in LA-ICP-MS analyses

Analytical uncertainty on the LA-ICP-MS analyses was monitored in two ways. Firstly, during tuning the percent relative standard deviation (RSD) for all elements were calculated. For each analysis carried out, all elements had RSD percentages ranging between 2-8%. Secondly, for the Kaiaua, Pomare and Manakua *A. stutchburyi* shells, LA-ICP-MS horizontal transects (parallel to the maximum direction of growth) were repeated on separate days. In these repeats, laser ablation points were made adjacent to the original laser ablation points, in the direction of maximum growth (i.e. new laser ablation points were made in between existing laser ablation points). Graphical comparison of the original and repeat runs for the Kaiaua shell (Figure 2.6) show

excellent reproducibility for Mg/Ca, Mn/Ca, Ba/Ca and U/Ca ratios; moderate reproducibility for B/Ca and As/Ca ratios; and relatively poor reproducibility for Al/Ca, Li/Ca, Cu/Ca and Zn/Ca ratios. The results for the Kaiaua shell are representative of the Pomare and Mankau shells.

Differences in the average TE/Ca ratios between original and repeat laser-ablation runs were calculated for all three shells (Table 2.3). The percentage of variation between average TE/Ca ratios, in respect of the average TE/Ca ratios for those shells, is also reported. It should be noted that some of the variation between the adjacent points is due to real horizontal variation in shell chemistry; so that analytical variance is likely overestimated. These results agree with the visual comparisons (on the next page) – the differences between repeat and original average TE/Ca ratios account for small percentages of average Mg/Ca, Mn/Ca, U/Ca and Ba/Ca shell ratios, but larger percentages of average Al/Ca and Zn/Ca shell ratios. Overall, the comparison of runs completed on completely separate days, demonstrates reproducibility especially for Mg/Ca, Mn/Ca, U/Ca and Mn/Ca.

Table 2.3 The difference in average TE/Ca ratios between original and repeat transects in Kaiaua, Pomare and Manakau shells. Average TE/Ca ratios for each shell. The percentage of the average TE/Ca ratios the difference between averages represent (difference between averages ÷ average TE/Ca x 100) highlighted in grey.

Shell		Li/Ca	B/Ca	Mg/Ca	Al/Ca	Mn/Ca	Cu/Ca	Zn/Ca	As/Ca	Ba/Ca	U/Ca
Kaiaua	Average shell	0.0085	0.074	0.76	0.0023	0.11	0.0014	0.00076	0.0011	0.0068	0.00031
	Difference	0.0013	0.0043	0.00057	0.00089	0.0023	0.00012	0.00042	0.00012	0.00015	0.000016
	Percentage	15	5.8	0.075	39	2	8.7	55	11	2.2	5.3
Pomare	Average shell	0.0083	0.062	1.04	0.0058	0.028	0.0018	0.00052	0.0017	0.0052	0.00022
	Difference	0.00037	0.0011	0.017	0.0017	0.00016	0.00016	0.00027	0.00016	0.000025	0.0000052
	Percentage	4.4	1.7	1.6	29	0.55	9	51	9.4	0.49	2.4
Manakau	Average shell	0.0079	0.085	0.97	0.0025	0.15	0.001	0.00049	0.00056	0.0048	3.20E-04
	Difference	0.00093	0.00058	0.012	0.0042	0.012	0.000041	0.000019	0.000047	0.0001	0.000024
	Percentage	12	0.69	1.2	173	8.3	4.1	4	8.4	2.1	7.6

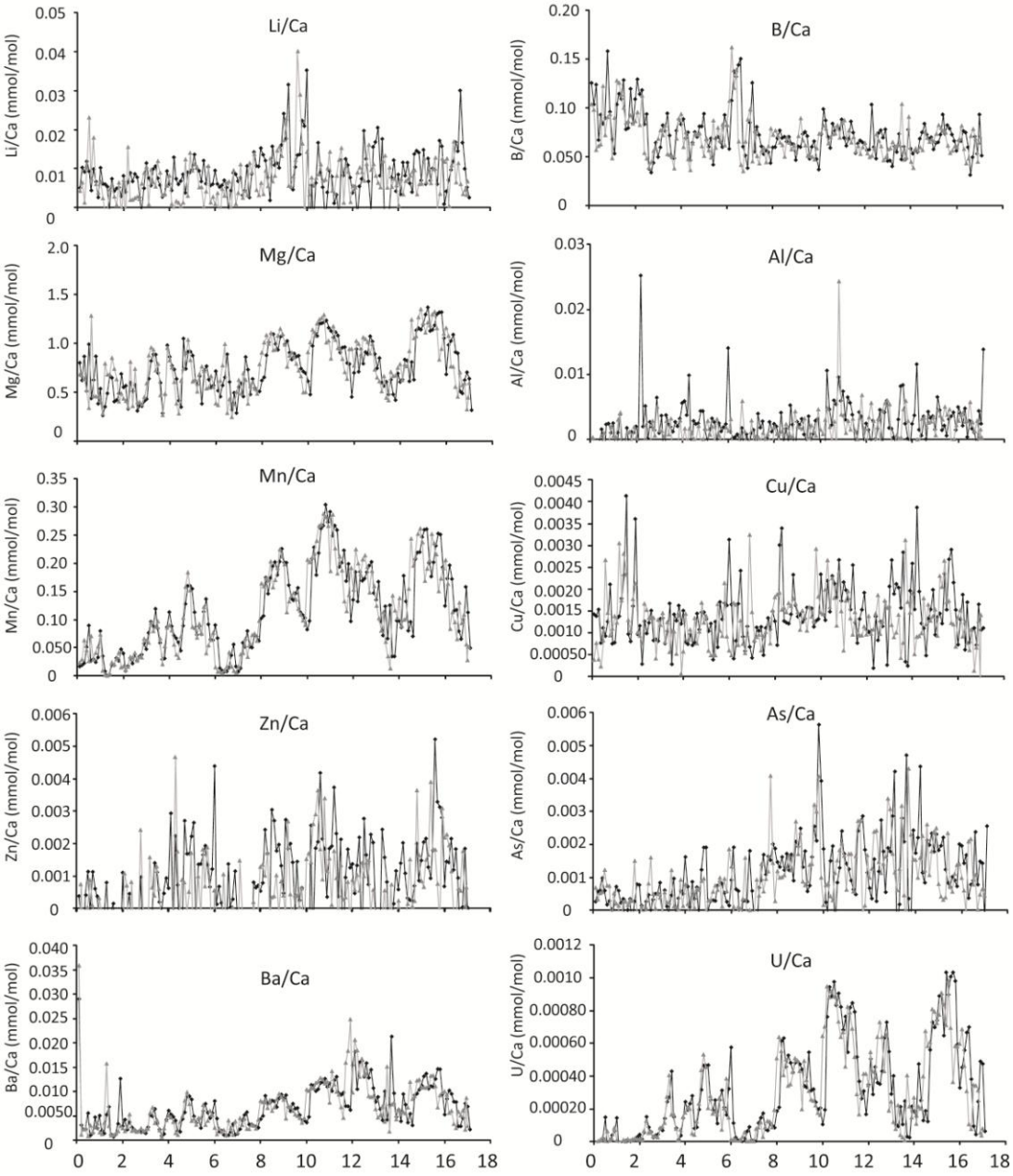

Figure 2.6 TE/Ca ratios for the Kaiaua original and repeat transects, plotted against distance from the ventral margin in mm (horizontal axis). Black lines and markers are the original run. Grey lines and markers are the repeat run.

3.0 RESULTS

3.1 *A. stutchburyi* trace element chemistry

3.1.1 Transects through the shell

Before making transects across the shell surface, parallel to maximum growth direction, in *A. stutchburyi* shells, heterogeneity vertically along a growth band through the shells was assessed. This was done by making four transects that followed growth lines in the Ligar Estaury, Ligar Bay 6B and Raglan shells. These passed through the outer crossed-lamellar layer of shell, and (in some cases) into the middle homogeneous layer (see figure 3.1 below).

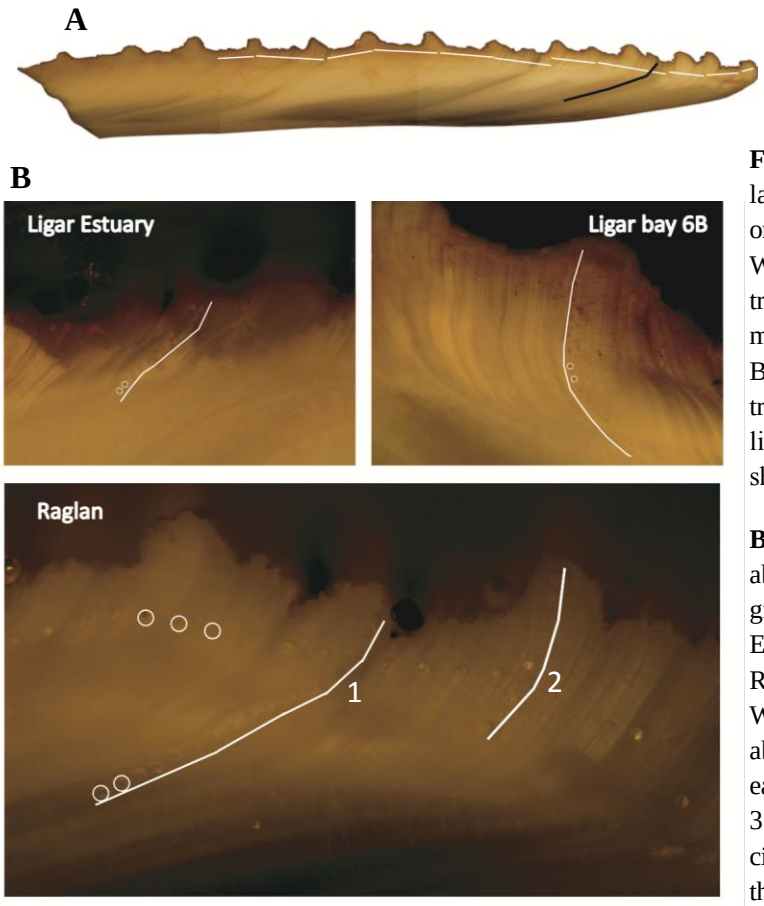

Figure 3.1 A. Example of laser ablation transects made on *A. stutchburyi* shells. White lines represent transects made parallel to maximum growth direction. Black line represents transects parallel to growth lines (a 'transect through shell').

B. Photographs of laser-ablation transects down growth lines in Ligar Estuary, Ligar Bay 6B and Raglan *A. stutchburyi* shells. White lines show the laser ablation transects. Scale: each laser-ablation point is 35 µm in diameter (white circles highlight some of these points).

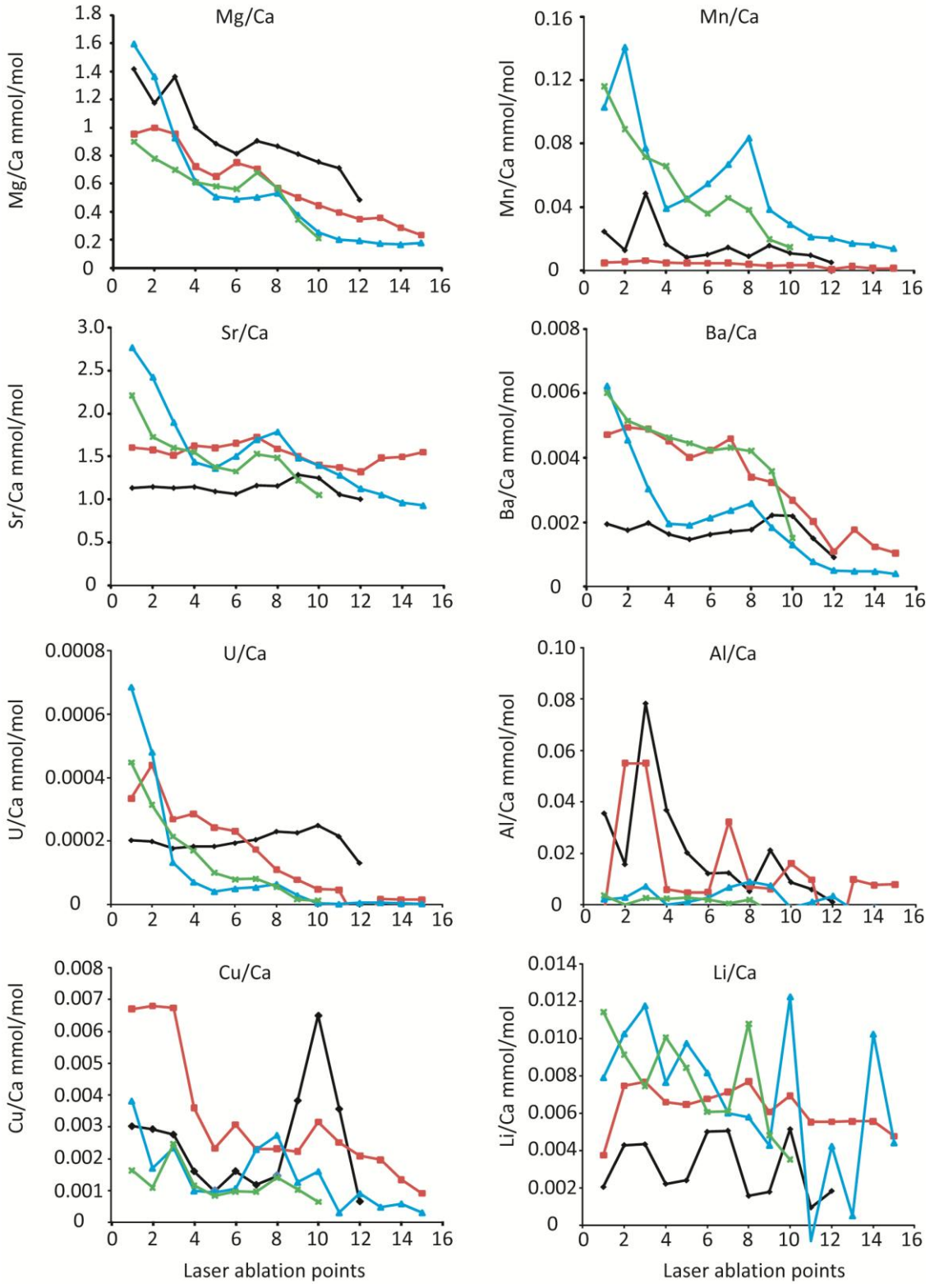

Figure 3.2 Mg/Ca, Mn/Ca, Sr/Ca, U/Ca, Ba/Ca Al/Ca, Cu/Ca and Li/Ca cross-section transects. Combined graphs of four cross-sections through three shells. Point '1' on the horizontal axis is the first laser ablation point – at the top of the growth line, point '16' is the laser point furthest through the shell. Laser ablation points were 35 µm and at approximately 50 µm spacing.

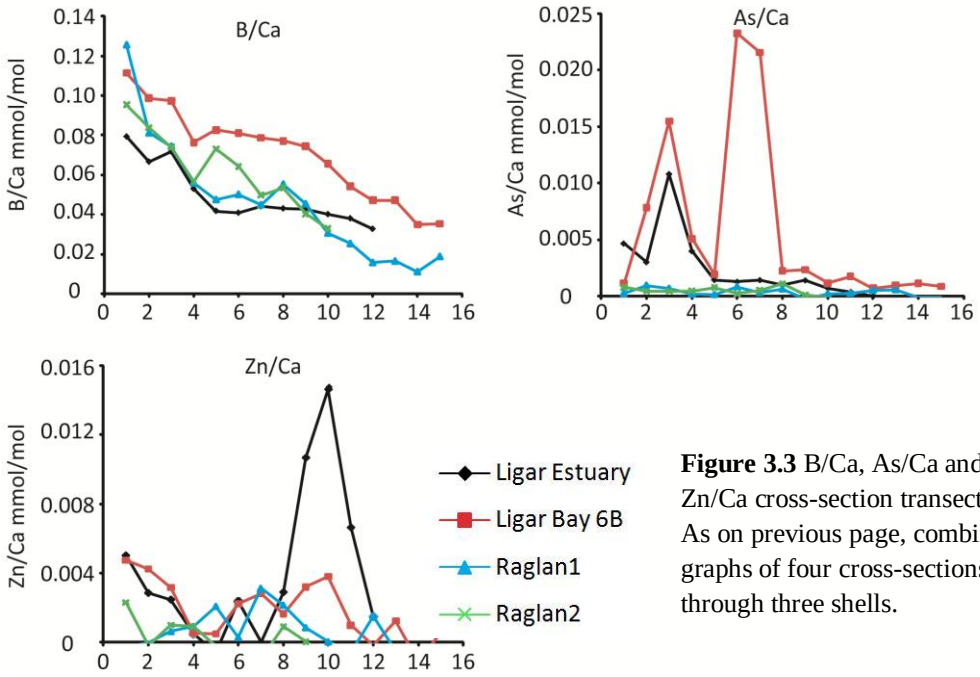

Figure 3.3 B/Ca, As/Ca and Zn/Ca cross-section transects. As on previous page, combined graphs of four cross-sections through three shells.

The most dominant trend in the data from the transects through the shell was the progressive decrease in TE/Ca ratios down the growth lines (i.e. with increased depth into the shell). A linear decrease with a high degree of correlation was observed for Mg/Ca, Mn/Ca, Ba/Ca and B/Ca ratios. Over 450 µm distance down a growth line the decrease of Mg/Ca ratios varied between 1.4-0.6 mmol/mol; for Mn/Ca ratios between 0.11-0.038 mmol/mol, for B/Ca ratios between 0.097-0.04 mmol/mol; for Ba/Ca between 0.0049-0.0020 mmol/mol; for Sr/Ca ratios between 1.4-1.2 mmol/mol; and for U/Ca ratios between 0.00070-0.00034 mmol/mol. There were exceptions: Mn/Ca in Ligar Estuary had one anomalous Mn/Ca peak; Sr/Ca ratios showed a linear decrease in the Raglan shell cross sections, but in the Ligar Bay 6B and Ligar Estuary cross sections Sr/Ca ratios remained constant. Similarly, U/Ca ratios decreased linearly in all cross-sections except for the Ligar Estuary shell. Other TE/Ca ratios (Li/Ca, Al/Ca, Cu/Ca and As/Ca) generally showed an overall decrease through the shell, but were punctuated by large variations between points. This likely due to the larger analytical uncertainty involved in measuring these low concentration elements (Chapter 2).

For the TE/Ca ratios that did follow a linear trend, the rate of decrease was comparable between the two cross sections taken down different growth lines on the same shell from Raglan - with Mg/Ca, Sr/Ca, Ba/Ca, U/Ca Mn/Ca and B/Ca ratios having similar gradients (e.g. -0.59 and -0.86 for Mg/Ca). However, in these Raglan cross-sections the TE/Ca ratios were not individually comparable – the first cross section decreased from typically higher TE/Ca ratios (e.g. Mg/Ca, Fig 3.2), most likely as the cross sections were made through growth lines at different distances horizontally on the shell. Between shells the rate of decrease appeared to vary significantly, as the gradients were quite different (see Figures 3.2 and 3.3). There was strong co-variation between Mg/Ca, Sr/Ca, Ba/Ca, U/Ca, Mn/Ca and B/Ca ratios in each shell cross-section. In particular, in the first Raglan cross-section, there is a peak in each of these TE/Ca ratios at point eight against the general decrease in ratios, which also coincides with major peak in Al/Ca.

3.1.2 Trace element/Ca transects

A series of TE/Ca ratios for each of the eleven shell samples were measured by LA-ICP-MS transects across the shells, beginning at the ventral margin of each shell and running towards the umbo (white lines on Figure 3.1). The distance of each transect varied, comprising between 160 and 406 individual laser ablation measurements to allow for comparison between shells of varying age. Transect data was plotted against distance from the ventral margin (in mm). This means that in the dataset plotted in Figures 3.4-3.25, chronological time runs right to left, and ontogenetic age of the clam is progressively younger from left to right, and progressively older from right to left.

3.1.2.1 Key trends and differences between the Ligar Bay and Ligar Estuary shells

Mg/Ca

The range in Mg/Ca ratios between the Ligar Bay shells was significant. The Ligar Bay 4B and Ligar Bay 6B Mg/Ca records were both within a narrow and low range, with ratios between 0.28-2.6 mmol/mol and 0.14-2.2 mmol/mol respectively (Figure 3.4). The Ligar Estuary shell contained the widest range (0.21 -1.99 mmol/mol), followed by Ligar Bay 3B (0.42-4.0 mmol/mol). The difference between the highest Ligar Bay 3B ratio and the highest Ligar Bay 6B ratio equated to 1.9 mmol/mol. Ligar 1B had a comparable range to the Ligar Estuary shell, with Mg/Ca ratios varying between 0.4-3.9 mmol/mol. The ratio variations throughout the individual records were also quite different. The Ligar Bay 1B and Ligar Estuary records contained large variations that formed peak-trough patterns (up to 2.5 mmol/mol from peak to trough), compared to the relatively flat Mg/Ca record, with small variations (0.5-1.0 mmol/mol) from the Ligar Bay 4B shell. None of the records appeared to follow the same form, or contain the same variations, as any of the others.

Sr/Ca

Sr/Ca ratio ranges were similar in the Ligar Bay and Ligar Estuary shells, with the Ligar Bay 6B shell having the widest range of ratios between 1.0-3.5 mmol/mol (Figure 3.5). Ligar Bay 1B had Sr/Ca ratios between 1.0-3.0 mmol/mol, whereas Ligar Bay 4B ranged between 1.0-3.2 mmol/mol, Ligar Bay 3B had Sr/Ca ratios ranging between 0.98-2.6 mmol/mol, and Ligar Estuary ranged between 1.3-3.2 mmol/mol (although Sr/Ca ratios were only available for the oldest half of the shell). The magnitude of the Sr/Ca ratio variations throughout the records were also quite comparable between the individuals, with the highest variations in all shells being up to 1.5 mmol/mol, except

for Ligar 3B, which had variations mostly < 0.5 mmol/mol. There were no specific variations that could be correlated between records.

Mn/Ca

All four Ligar Bay Mn/Ca records contained ratios within a similar range: Ligar Bay 1B had ratios between 0.00-0.011 mmol/mol; Ligar Bay 3B between 0.00-0.010 mmol/mol; Ligar Bay 6B between 0.00-0.011 mmol/mol; and Ligar Bay 4B had ratios in the narrowest range, between 0.00-0.007 mmol/mol (Figure 3.6). However, Mn/Ca ratios in the Ligar Estuary record were up to an order of magnitude higher than the Ligar Bay records, falling in a very wide range between 0.00-0.57 mmol/mol. The Ligar Estuary record contained 7 sharp Mn/Ca peaks (between 0.086-0.37 mmol/mol). Although of a lower magnitude, there were at least 3 sharp peaks (between 0.0043-0.011 mmol/mol) that interrupted the Ligar Bay 1B record, and 2 peaks (between 0.0048-0.011 mmol/mol) in the Ligar Bay 6B record.

Ba/Ca

Ba/Ca ratios were comparable for the Ligar Estuary (0.0007-0.0084 mmol/mol) and Ligar 6B (0.0004-0.012 mmol/mol) shells (Figure 3.7). Ligar Bay 1B Ba/Ca ratios fell within a slightly wider range of 0.0005-0.017 mmol/mol. Most noticeably, the range in ratios for the Ligar Bay 3B and Ligar Bay 4B Ba/Ca records was an order of magnitude higher than for the other Ligar Bays records, with Ba/Ca ratios between 0.0003-0.039 mmol/mol and 0.0004-0.046 mmol/mol respectively. Within these two records there were matching 3-point peaks in Ba/Ca of similar amplitude - the highest ratio in the peaks being 0.046 mmol/mol and 0.039 mmol/mol for Ligar Bay 4B and Ligar Bay 3B, respectively (marked by red circles on Figure 3.7). However, in the Ligar Bay 4B shell the 3-point peak began at 11 mm from the ventral margin, and was stretched out over a longer section of shell, to 15 mm from the ventral margin. It is also possible that a

small peak found at 3 mm distance from the ventral margin in the Ligar Bay 4B shell, could be correlated to a similar peak found at 2 mm from the ventral margin in the Ligar Bay 3B Ba/Ca record (marked with red circles on Figured 3.7). Peaks (>0.008 mmol/mol) in the other Ligar Bay and Estuary Ba/Ca records (marked with green circles on Figured 3.7) could potentially be correlated to the same event, but as they are not clearly related (in amplitude or shape), these need to be put on the same timescale to test this.

U/Ca

There was a clear distinction between Ligar Bay 3B and Ligar Bay 4B, which had U/Ca ratios between 0.0000-0.0004 mmol/mol and 0.0000-0.0005 mmol/mol, respectively, and Ligar Bay 6B and Ligar Estuary, which had ratios almost twice as high, between 0.0000-0.0008 mmol/mol and 0.0000-0.0008 mmol/mol, respectively (Figure 3.8). The latter two U/Ca records contained much greater variations in ratios (up to 0.0008 mmol/mol), whereas the former two records had small variations (<0.0002 mmol/mol). No U/Ca record was available for Ligar Bay 1B because U was not analysed in this shell.

Cu/Ca

The Cu/Ca records were within similar ranges, except for Ligar Bay 4B, which had ratios an order of magnitude lower than the other three shells (varying between 0.0001-0.0021 mmol/mol). Ligar Bay 3B contained the highest Cu/Ca ratios, with a sharp peak of 0.060 mmol/mol in the middle of the record (Figure 3.9). Peaks were also observed in the Ligar Bay 6B and Ligar Estuary shells, and these were 0.02 mmol/mol and ~0.04 mmol/mol in size respectively.

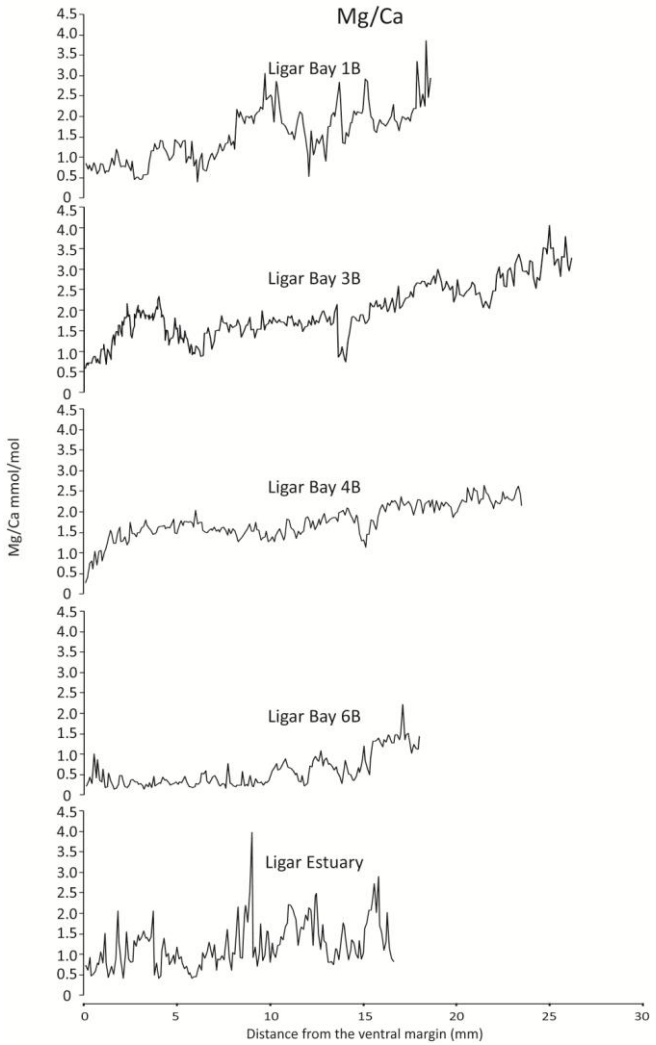

Figure 3.4 (Left) Mg/Ca ratios measured across transects in *A. stutchburyi* shells. from Ligar Bay and Ligar Estuary .

Figure 3.5 (Right) Sr/Ca ratios measured across transects in *A. stutchburyi* shells. from Ligar Bay and Ligar Estuary.

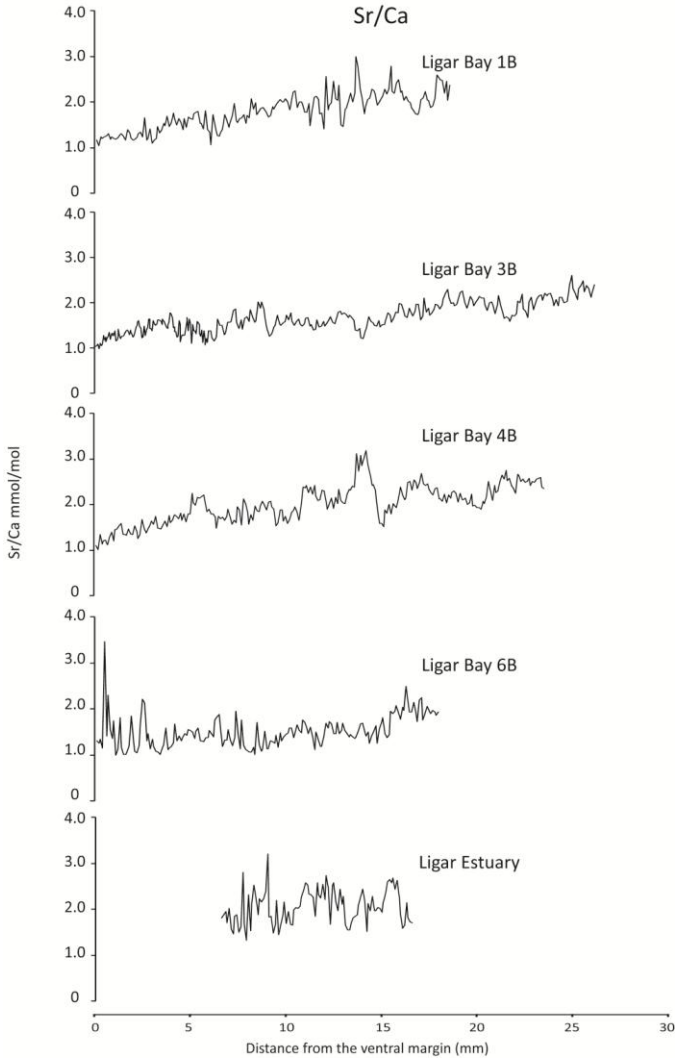

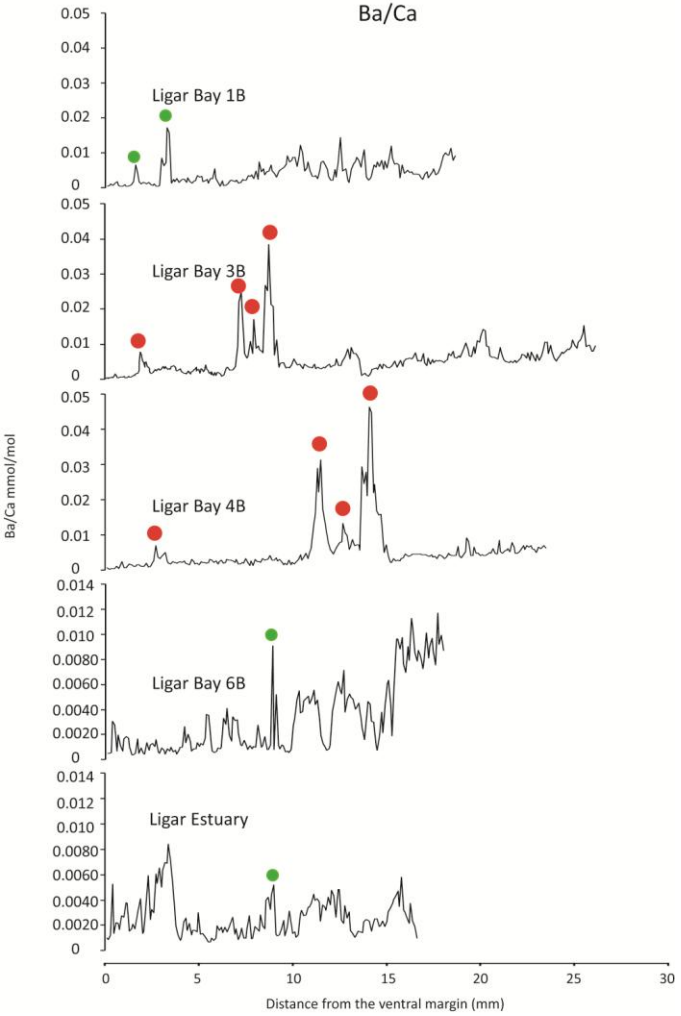

Figure 3.7 (Left) Ba/Ca ratios measured across transects in *A. stutchburyi* shells from Ligar Bay and Ligar Estuary. Red and green dots show Ba/Ca peaks referred to in text.

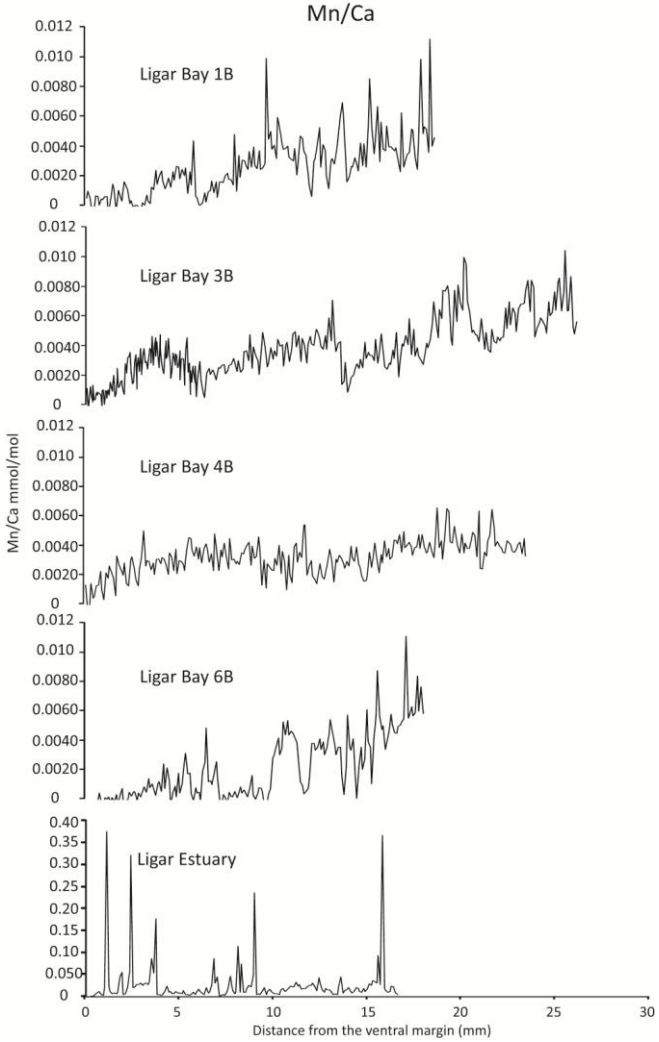

Figure 3.6 (Right) Mn/Ca ratios measured across transects in *A. stutchburyi* shells from Ligar Bay and Ligar Esuary.

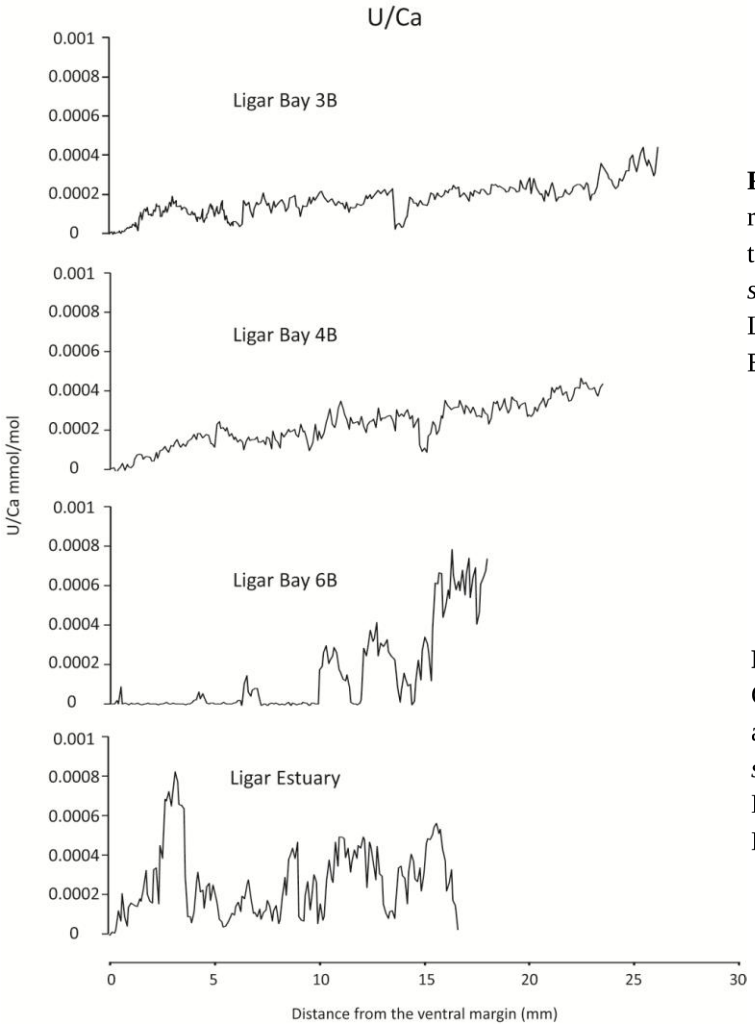

Figure 3.8 (Left) U/Ca ratios measured across transects in *A. stutchburyi* shells from Ligar Bay and Ligar Estuary.

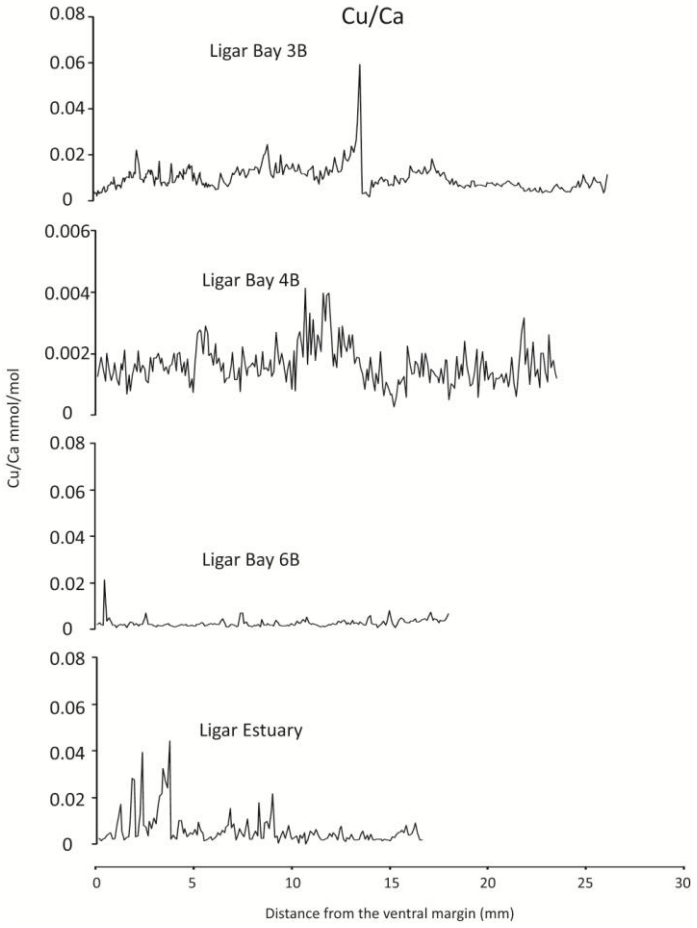

Figure 3.9 (Right) Cu/Ca ratios measured across transects in *A. stutchburyi* shells from Ligar Bay and Ligar Estuary.

Zn/Ca

Ligar Bay 3B and Ligar Bay 4B had similar Zn/Ca records, with ratios ranging between 0.000-0.011 mmol/mol for each shell, and only small variations (<0.008 mmol/mol). The Ligar Bay 1B, Ligar Bay 6B and Ligar Estuary records all had a higher range of ratios, between 0.000-0.026 mmol/mol, 0.000-0.019 mmol/mol, and 0.000-0.020 mmol/mol, respectively (Figure 3.10). There were greater variations in these records (>0.01 mmol/mol), especially throughout the Ligar Estuary record, and the latter halves of the Ligar Bay 1B and Ligar Bay 6B records.

As/Ca

Ligar Bay 3B, Ligar Bay 4B and Ligar Estuary As/Ca records had ratios within a similar range, between 0.000-0.021 mmol/mol, 0.000-0.015 mmol/mol and 0.000-0.048 mmol/mol, respectively (Figure 3.11). The Ligar Bay 6B record would have been in a similar range but for three large peaks in As/Ca; the highest of these was at 14 mm from the ventral margin and was 0.055 mmol/mol. One noticeable feature for three of the Ligar Bay shells – 3B, 4B and 6B – was the decrease in ratios in the latter stage of all three of these clams' lives (starting between 5-10 mm from the ventral margin until 0 mm). This is not an analytical effect as full transects of the three individual shells were analysed in the same analytical session, but each shell on different days, over several months.

Li/Ca

The Li/Ca records for Ligar Bay 3B, Ligar Bay 4B and Ligar Estuary had ratios within similar ranges; between 0.00-0.027 mmol/mol, 0.00-0.041 mmol/mol and 0.00-0.040

mmol/mol, respectively (Figure 3.12). There were no clear temporal trends in any of the records. Li was not measured in the Ligar Bay 1B and Ligar Bay 6B shells.

B/Ca

The Ligar Bay 3B and Ligar Bay 4B B/Ca records were both within relatively narrow ranges (B/Ca between 0.053-0.13 mmol/mol and 0.033-0.11 mmol/mol, respectively) compared to the Ligar Estuary record, which ranged between 0.053-0.32 mmol/mol (Figure 3.13). The latter record also contained a number of sharp increases – up to 0.21 mmol/mol at a time. There also appeared to be no clear temporal trends in any of the records. B was not measured in the Ligar Bay 1B and Ligar Bay 6B shells.

Al/Ca

The Ligar Estuary Al/Ca record contained a number a sharp peaks (up to 0.41 mmol/mol) throughout it (Figure 3.14). The latter half of the Ligar Bay 1B record also contained these peaks, with a similar peak of 0.41 mmol/mol at 14.7 mm from the ventral margin. The records of the remaining shells predominantly consisted of smaller variations (<0.05 mmol/mol), although in the Ligar Bay 3B and Ligar Bay 6B shells there were greater variations and higher ratios in the oldest sections of their records (i.e. the sections furthest away from the ventral margin).

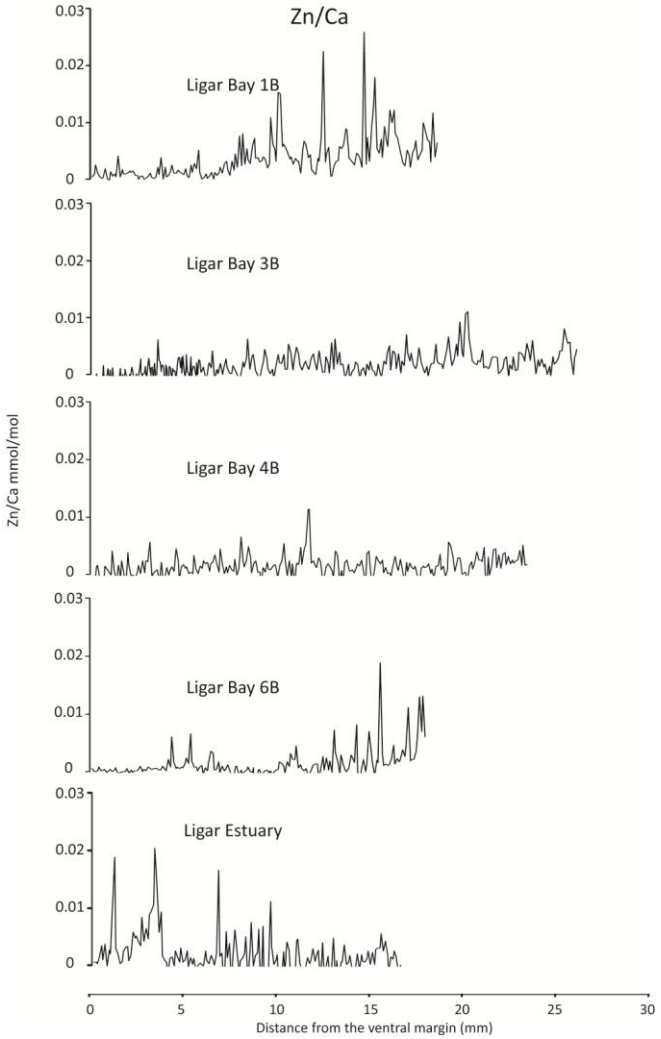

Figure 3.10 (Left) Zn/Ca ratios measured across transects in *A. stutchburyi* shells from Ligar Bay and Ligar Estuary.

Figure 3.11 (Right) As/Ca ratios measured across transects in *A. stutchburyi* shells from Ligar Bay and Ligar Estuary.

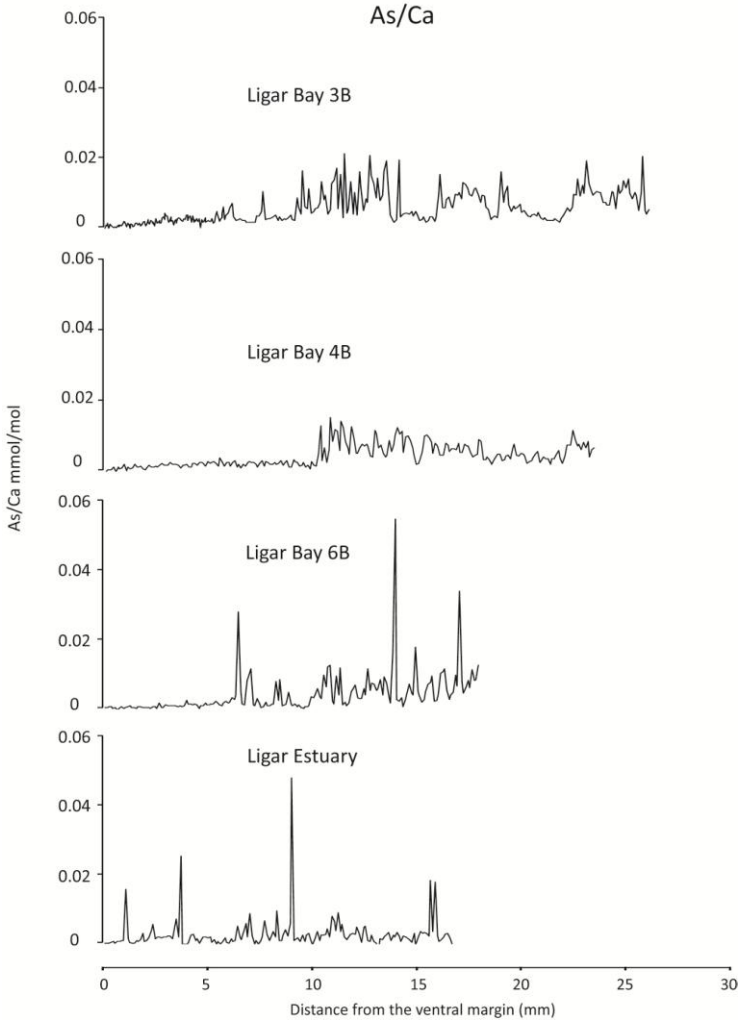

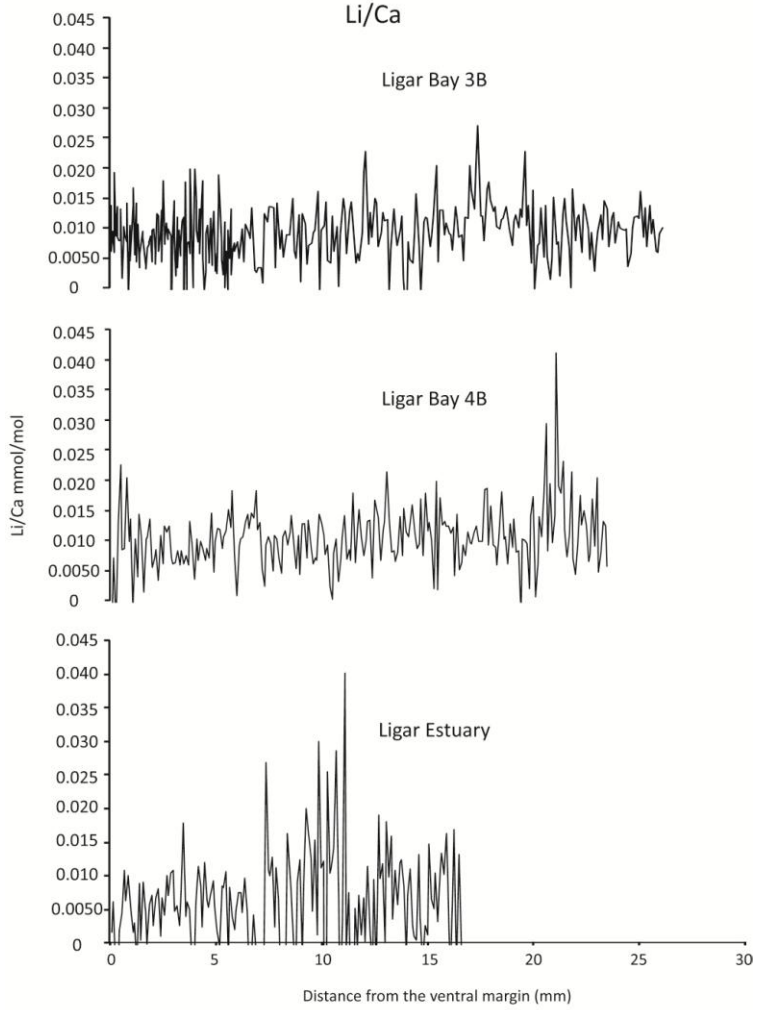

Figure 3.12 (Left) Li/Ca ratios measured in transects in *A. stutchburyi* shells from Ligar Bay and Ligar Estuary.

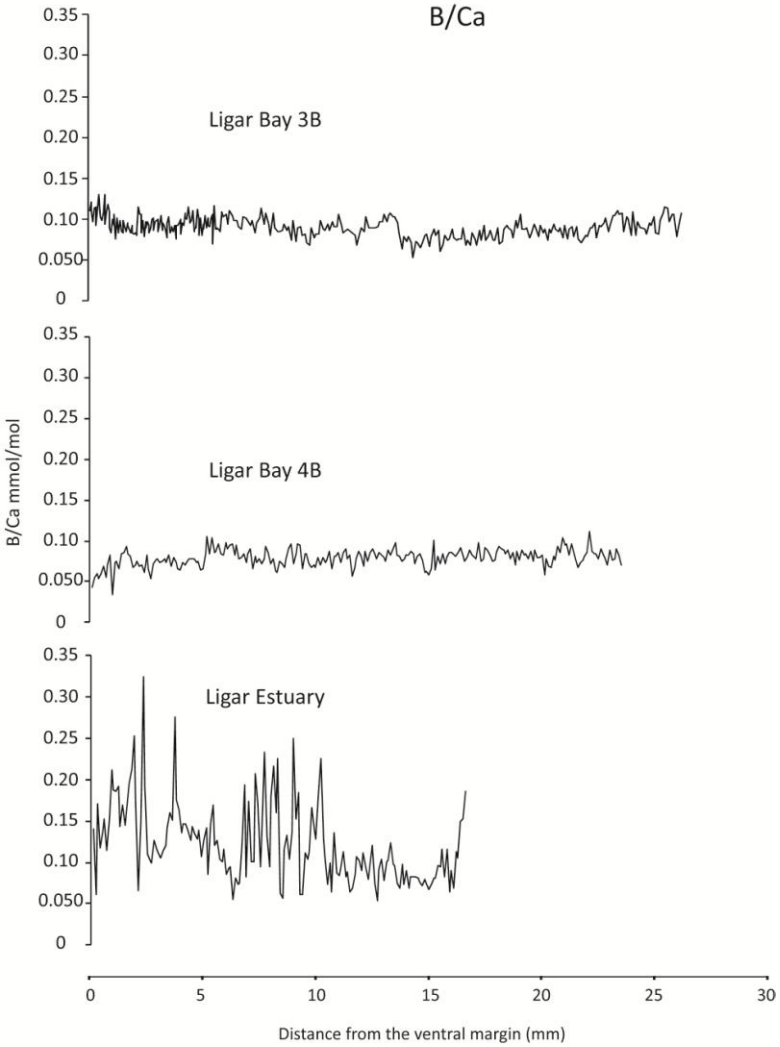

Figure 3.13 (Right) B/Ca ratios measured in transects in *A. stutchburyi* shells from Ligar Bay and Ligar Estuary.

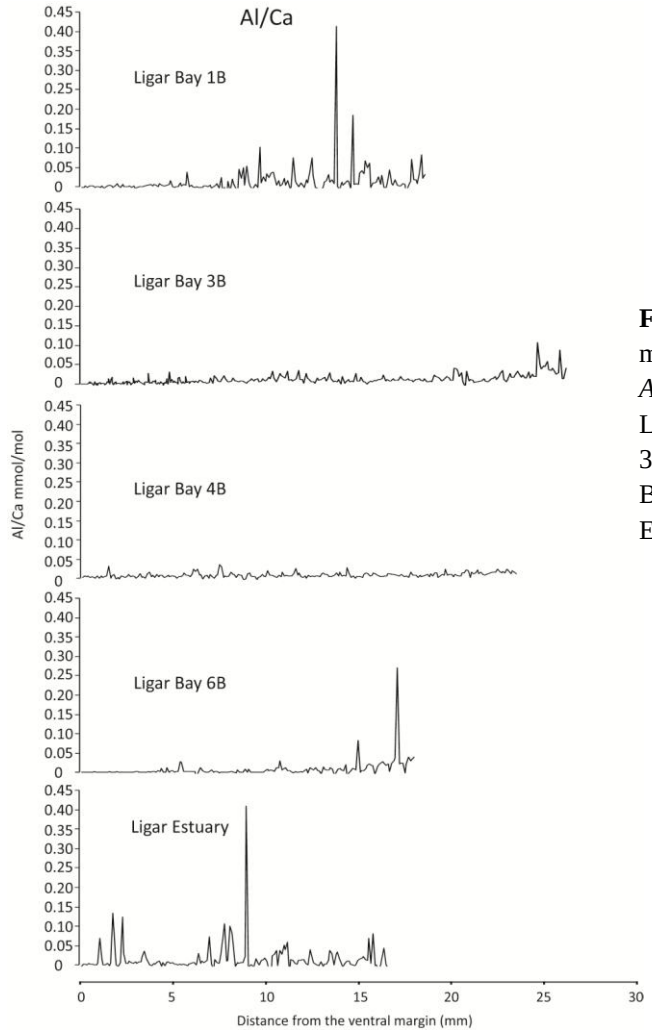

Figure 3.14 Al/Ca ratios measured in transects in *A. stutchburyi* shells from Ligar Bay 1B, Ligar Bay 3B, Ligar Bay 4B, Ligar Bay 6B and Ligar Estuary.

Table 3.1 Summary of the range in TE/Ca ratios for the Ligar Bay and Ligar Estuary shells.

		TE/Ca (mmol/mol)										
Shell		Li/Ca	B/Ca	Mg/Ca	Al/Ca	Mn/Ca	Cu/Ca	Zn/Ca	As/Ca	Sr/Ca	Ba/Ca	U/Ca
Ligar 1B	Minimum	-	-	0.40	0.00	0.00	-	0.00	-	1.0	0.00048	-
	Maximum	-	-	3.9	0.41	0.011	-	0.026	-	3.0	0.017	-
Ligar 3B	Minimum	0.00	0.053	0.58	0.00	0.00	0.0016	0.00	0.00	0.98	0.00031	0.00
	Maximum	0.027	0.13	4.1	0.11	0.01	0.059	0.011	0.021	2.6	0.039	0.00044
Ligar 4B	Minimum	0.00	0.033	0.28	0.00	0.00	0.00025	0.00	0.00	1.0	0.00037	0.00
	Maximum	0.041	0.11	2.6	0.035	0.0066	0.0041	0.011	0.015	3.2	0.046	0.00047
Ligar 6B	Minimum	-	-	0.14	0.00	0.00	0.00066	0.00	0.00	1.0	0.00035	0.00
	Maximum	-	-	2.2	0.27	0.011	0.021	0.019	0.055	3.5	0.012	0.00078
L. Estuary	Minimum	0.00	0.053	0.42	0.00	0.00	0.00023	0.00	0.00	1.3	0.00065	0.00
	Maximum	0.040	0.32	4.0	0.57	0.37	0.044	0.020	0.048	3.2	0.0084	0.00082

3.1.2.2 Individual Ligar Bay transects

Ligar Bay 1B

The Mg/Ca record consists of high-frequency peak and troughs (0-1 mm), on either side of one larger semi-sinusoidal variation centred at 10 mm distance from the ventral margin (Figure 3.15). The Mn/Ca and Ba/Ca ratio records followed a similar pattern to Mg/Ca, but the variations between peaks and troughs are more exaggerated. Sr/Ca ratios varied in a similar pattern to Mg/Ca record, except there was no pronounced semi-sinusoidal change at ca. 10 mm. The annual growth band G4 coincided with the minima on one side of this sinusoidal shape for Mg/Ca, Mn/Ca and Ba/Ca (Figure 3.15). The growth bands G2 and G4 appear to coincide with minima in the Mg/Ca and Mn/Ca records, but no other growth bands or increments appeared to correlate with the chemistry.

There is an ontogenetic decrease (i.e. a decrease in TE/Ca ratios as the clam grew older) in Mg/Ca, Sr/Ca, Mn/Ca, Ba/Ca and Zn/Ca ratios, as well a decrease in the amplitude of variations from peak to trough. For example, in the Mg/Ca record, the difference between peak and trough decreased from 1.5 mmol/mol at 14 mm, to 0.9 mmol/mol at 4 mm from the ventral margin. One variation in the older half of the Zn/Ca record was an increase from 0.0004-0.026 mmol/mol. However, in the Ba/Ca record, a sharp peak to 0.017 mmol/mol at 4.2 mm from the ventral margin interrupted the trend of lower amplitude Ba/Ca ratio variations seen in the younger part of the shell.

Ligar Bay 3B

In the Ligar Bay 3B shell, Mg/Ca and Sr/Ca records were characterised by four sharp increases and decreases (0.5-1.0 mmol/mol) at 25, 22, 14, 9 (for Sr/Ca) and 6 mm distance from the ventral margin, which were interspersed with periods with smaller

ratio variations (0-0.5 mmol/mol). Two of these decreases, at 6 mm and 14 mm, coincided with the annual growth bands G4 and G5 (Figure 3.16). In the Mg/Ca record, which was smoother than the Sr/Ca record, the ratios within 6-0 mm distance from the ventral margin, in the youngest portion of the record, form an almost sinusoidal shape. One annual growth band (G2) sat on a small decrease that interrupted this sinusoidal shape, and another (G3) was situated at the base of the shape at 4.5 mm (Figure 3.16). Mn/Ca ratios and U/Ca ratios both followed a similar pattern to Mg/Ca and Sr/Ca but with larger (relative) variations. The predominant feature in the Ba/Ca record was the 3-point peak (up to 0.039 mmol/mol) around 7-9 mm distance from the ventral margin. However, when this peak was excluded from the Ba/Ca data, the remaining Ba/Ca record was similar to the Mn/Ca record in the Ligar Bay 3B transect, and the Ba/Ca ratios were within a range comparable to those in Ligar Bay1B, not being higher than 0.016 mmol/mol. All the TE/Ca records taken in the Ligar Bay 3B shell showed an ontogenetic decrease accompanied by a decrease in the amplitude of variations, although this did not occur for the Cu/Ca, B/Ca and Li/Ca ratios (Figure 3.9, 3.12 and 3.13).

Ligar Bay 1B

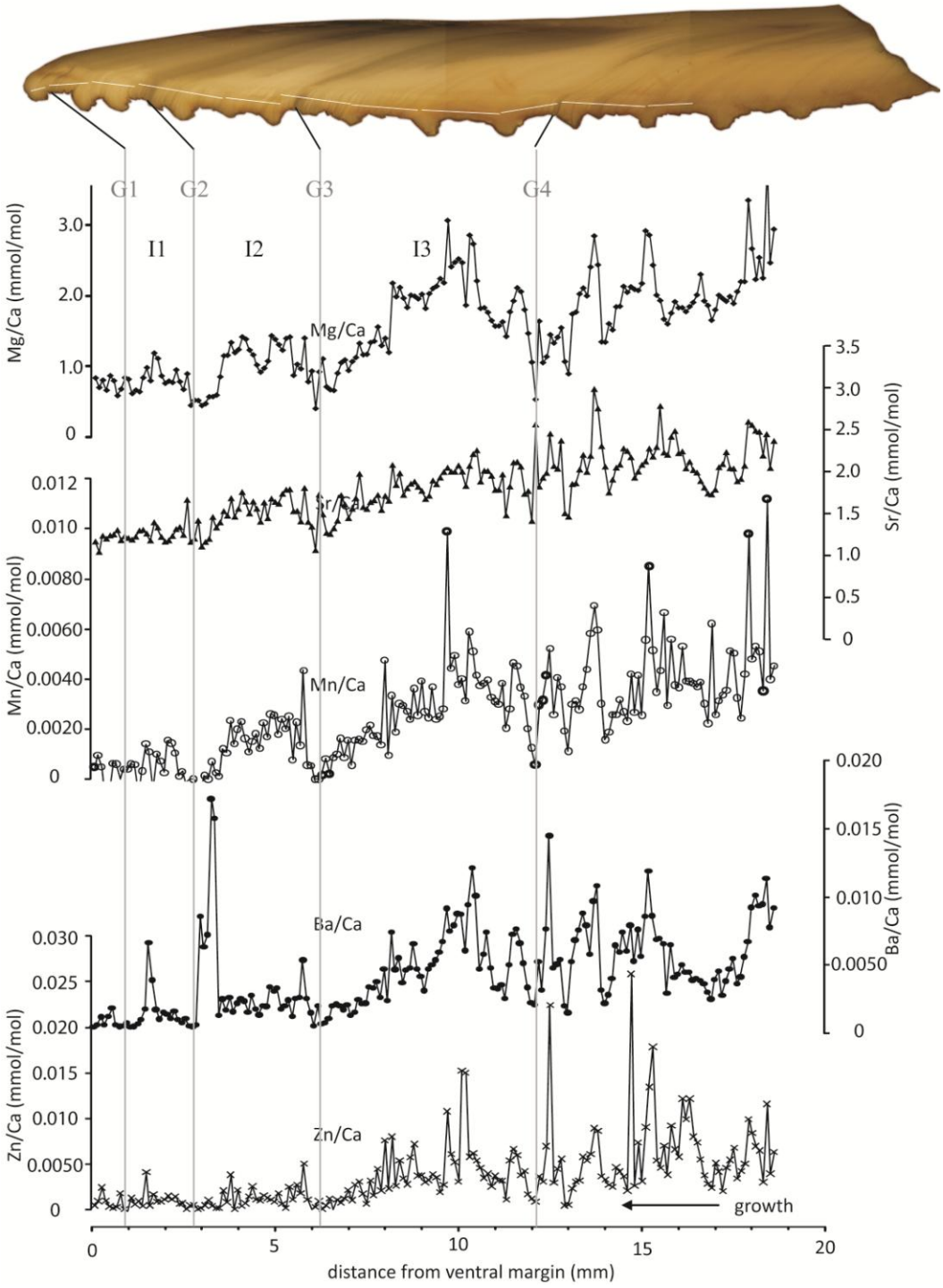

Figure 3.15 Ligar Bay 1B TE/Ca ratios transects: Mg/Ca, Sr/Ca, Mn/Ca, Ba/Ca and Zn/Ca.Grey lines are annual growth bands identified on the shell (photograph) I1-I3 refer to the annual growth increments identified. White lines on the shell show the path of LA-ICP-MS analysis.

Ligar Bay 3B

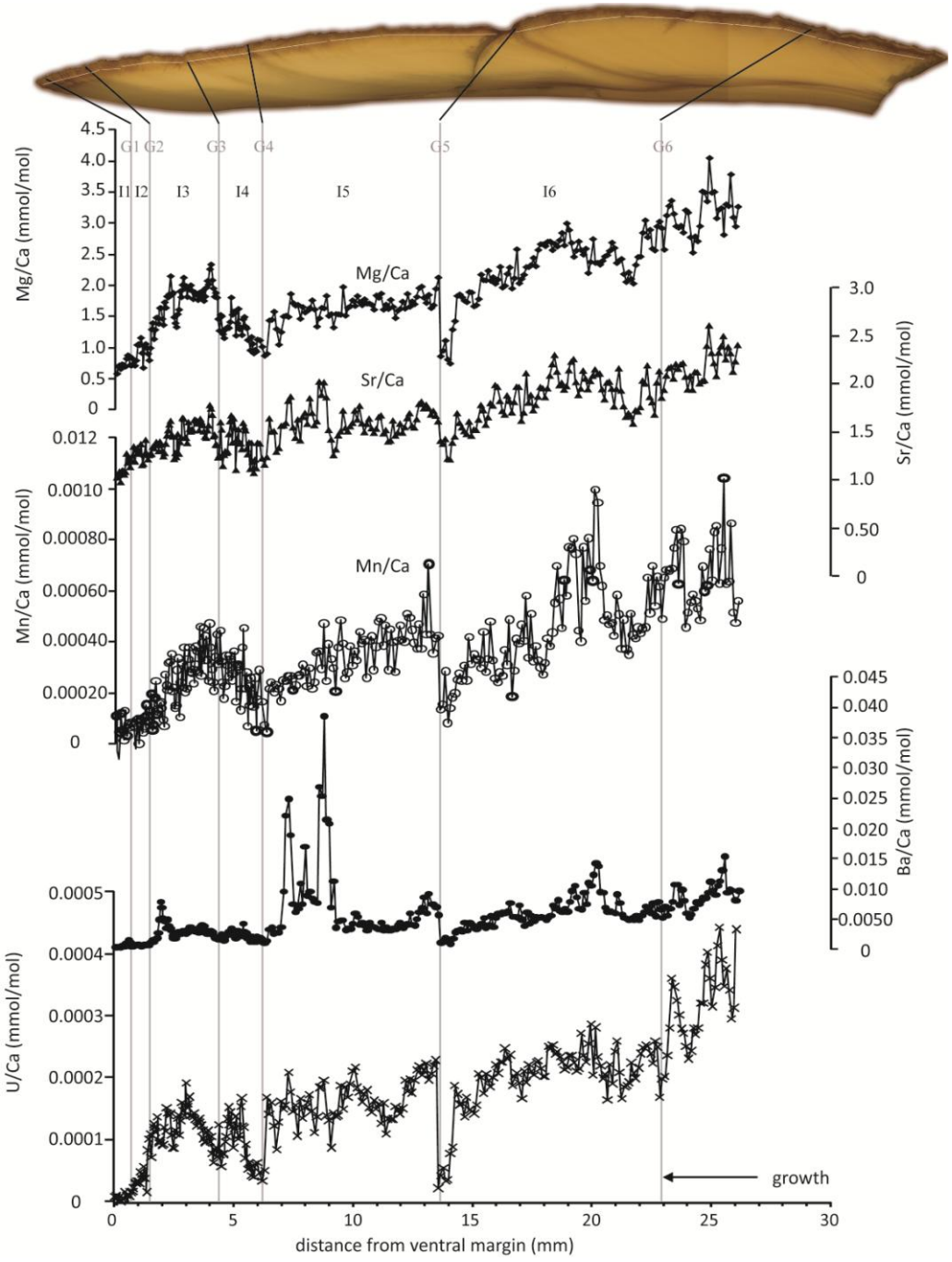

Figure 3.16 Ligar Bay 3B TE/Ca ratios transects: Mg/Ca, Sr/Ca, Mn/Ca, Ba/Ca and U/Ca. Grey lines are annual growth bands identified on the shell (photograph) I1-I6 refer to the identified annual growth increments. White lines on the shell mark the path of LA-ICP-MS analysis.

Ligar 4B

Throughout the Mg/Ca record there were few variations greater than 0.40 mmol/mol, apart from a ~0.80 mmol/mol decrease at 15 mm from the ventral margin, and a gradual decrease of ~1.2 mmol/mol in the 2 mm closest to the ventral margin (Figure 3.17). The Sr/Ca record differed from the Mg/Ca record in that it contained three peaks, at 5, 11, 14 and 17 mm from the ventral margin, amongst the periods with smaller variations. Mn/Ca ratios formed a record with reasonably uniform variations across it (between 0.0005-0.0010 mmol/mol). Ba/Ca ratios in the Ligar Bay 4B shell were quite similar to the Ligar Bay 3B record, including the 3-point peak. Excluding the 3-point peak, the Ba/Ca ratios were not above 0.010 mmol/mol in the Ligar Bay 4B shell. U/Ca ratios followed a similar pattern as the Sr/Ca record, but with greater variation. As with the previously described Ligar Bay shells, there was an ontogenetic decrease in TE/Ca ratios accompanied by a decrease in the amplitude of variations, although this was not evident for Cu/Ca, B/Ca, Al/Ca and Li/Ca ratios. The growth patterns identified in 4B did not appear to correlate with the chemistry, except for one annual growth band – G5, which coincided with the beginning of the largest decreases in the Mg/Ca, Sr/Ca, Mn/Ca, Ba/Ca and U/Ca records ~15 mm from the ventral margin.

Ligar Bay 6B

The youngest portion of the Mg/Ca record had a small peak to 1.0 mmol/mol, but then was flat, not exceeding 0.60 mmol/mol, until 9 mm from the ventral margin. After this distance, there were two sinusoidal patterns in the record, centred at 10 and 12 mm from the ventral margin, followed by a larger semi-sinusoidal shape that contained sharp variations with a peak at 16 mm from the ventral margin (Figure 3.18). The Mn/Ca, Ba/Ca and U/Ca ratios had records that were very similar to this pattern. However, the Sr/Ca record was quite unusual in the Ligar Bay 6B shell.

Ligar Bay 4B

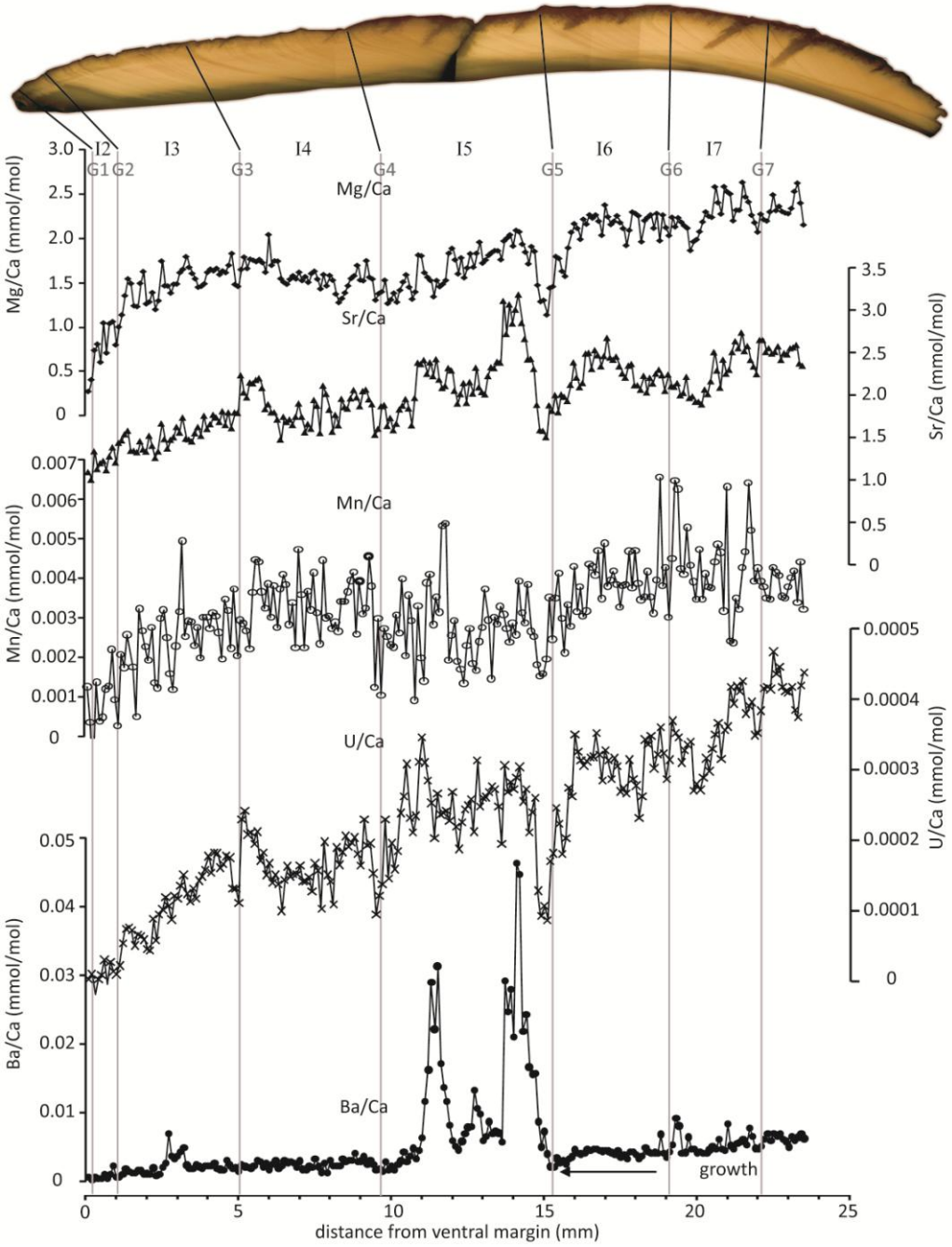

Figure 3.17 Ligar 4B TE/Ca ratios transects: Mg/Ca, Sr/Ca, Mn/Ca, Ba/Ca and U/Ca.Grey lines are annual growth bands identified on the shell (photograph) I1-I6 refer to the identified annual growth increments.

Ligar Bay 6B

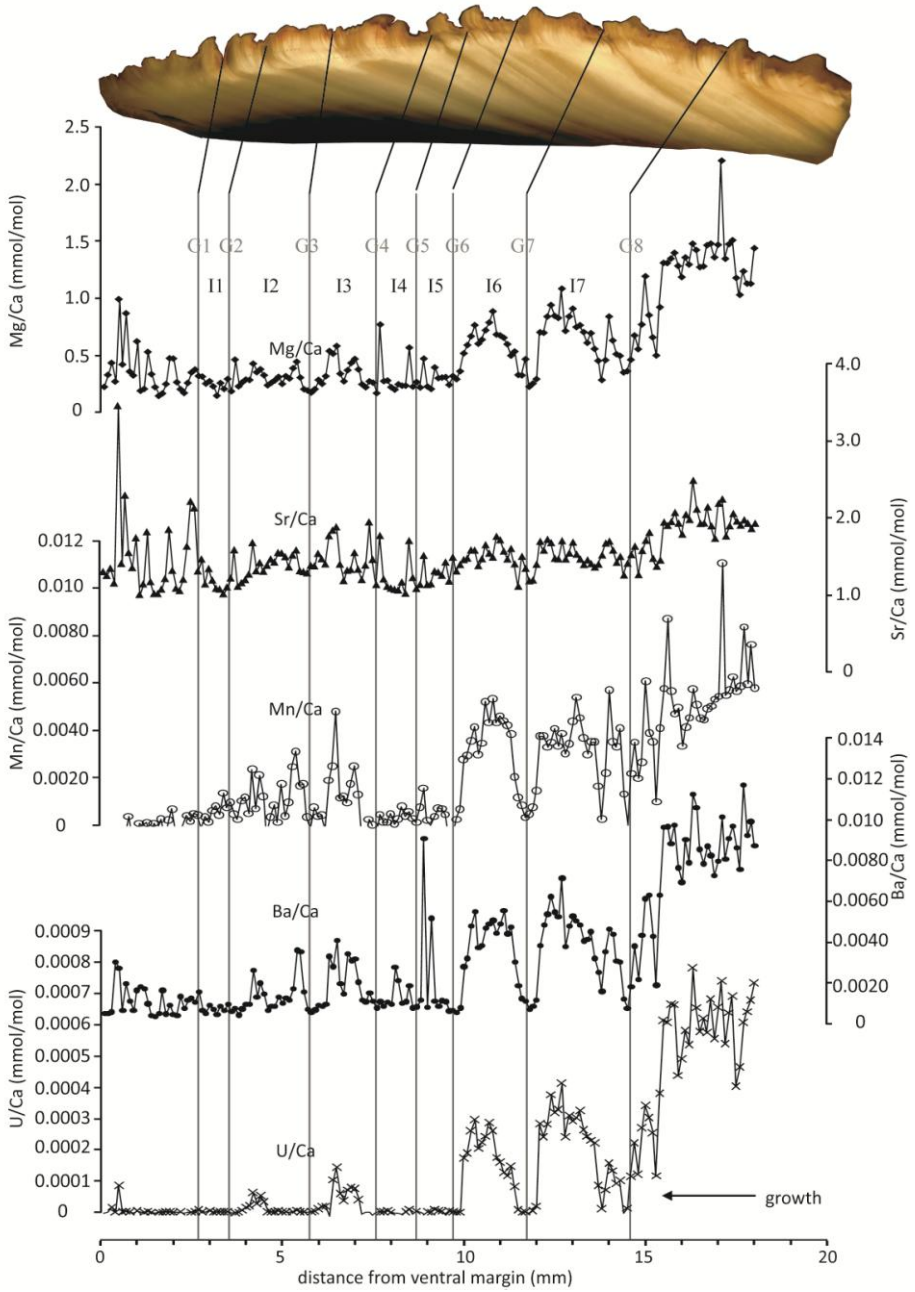

Figure 3.18 Ligar 4B TE/Ca ratios transects: Mg/Ca, Sr/Ca, Mn/Ca, Ba/Ca and U/Ca. Grey lines are annual growth bands identified on the shell (photograph) I1-I6 refer to the identified annual growth increments.

It consisted of quite sharp variations (up to 2.3 mmol/mol increases) in the youngest part of the transect, within 0-8 mm distance of the ventral margin, and the latter half of the record appeared to be a muted version of the patterns seen in the latter half of the Mg/Ca, U/Ca, Mn and Ba/Ca records. Apart from Sr/Ca and Cu/Ca ratios, there was an ontogenetic decrease in TE/Ca ratios accompanied by a decrease in the amplitude of variations. For example in the Mn/Ca record, ratios in the oldest portion are an order of magnitude larger than at the end of the clam's life (0.0011 compared to 0.00010 mmol/mol). There was some correlation between shell chemistry and annual growth bands – as growth bands G6, G7 and G8 coincided with minima of the sinusoidal chemical variations observed (Figure 3.18).

Ligar Estuary

The Ligar Estuary Mg/Ca record was most similar to the Ligar Bay 1B record and contained more and larger variations than the other Ligar Bay shell records (Figure 3.19). In the available Sr/Ca record (6.6-15 mm from the ventral margin) ratios followed the Mg/Ca record. Ba/Ca and U/Ca ratios also followed the same pattern; which was similar to the Mg/Ca record. The pattern of the Mn/Ca record was also similar except for seven large spikes superimposed on it, the largest of which was a sharp increase of 0.37 mmol/mol. The was no clear trend of ontogenetic decrease in TE/Ca ratios observed in the Ligar Estuary records, except for the Mg/Ca record; although it was less pronounced than the ontogenetic decreases observed in the Ligar Bay shells. In fact, in many of the TE/Ca records – Ba/Ca, U/Ca, Zn/Ca, B/Ca and Cu/Ca – there were larger variations in the younger sections. In others – As/Ca and Al/Ca – there were sharp increases throughout the record (Figures 3.9-3.14).

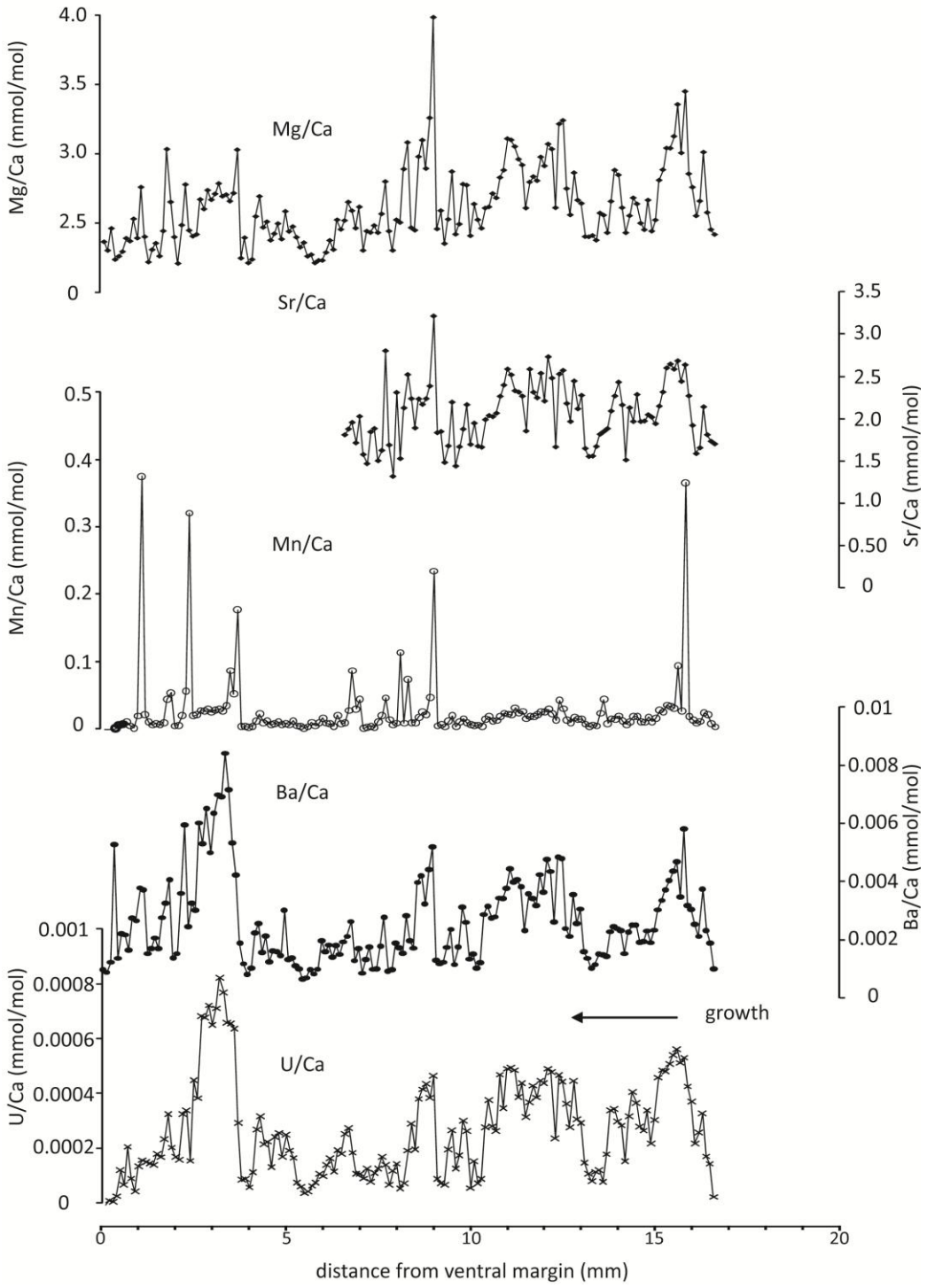

Figure 3.19 Ligar Estuary TE/Ca ratios transects: Mg/Ca, Sr/Ca, Mn/Ca, Ba/Ca and U/Ca.

3.1.2.3 Trace element/Ca ratio transects for A. stutchburyi at other New Zealand sites

Kawhia

The Kawhia Mg/Ca, Sr/Ca, Mn/Ca, Ba/Ca and U/Ca records consisted of a series of peak-trough variations (<1 mm width), and one saw-tooth pattern from 8-13 mm from the ventral margin on which these variations were superimposed (Figure 3.20). The Mn/Ca, Sr/Ca and U/Ca ratio variations appeared more amplified than the variations in the Ba/Ca and Mg/Ca records. There was a significant ontogenetic decrease and decrease in the amplitude of variations for all TE/Ca ratio records, except for in the Zn/Ca and Cu/Ca records. The relative ontogenetic decreases observed were similar to those found in the Ligar Bay shells – for example Mn/Ca ratios decrease by one order of magnitude from the oldest region of the shell to the youngest (even though Mn/Ca ratios overall were higher at Kawhia than in the Ligar shells).

Raglan

The Mg/Ca, Sr/Ca, Mn/Ca, Ba/Ca and U/Ca records in the Raglan shell mostly consist of small variations (e.g. < 0.5 mmol/mol for Mg/Ca ratios) interrupted by several sharp larger variations (up to 1.0 mmol/mol for Mg/Ca) (Figure 3.21). There was a large decrease in Mn/Ca, Mg/Ca and U/Ca ratios 6-5 mm from the ventral margin to much lower ratios in the youngest portion of the shell. This change was preceded by a decrease in ratios 11 mm from the ventral margin, of comparable amplitude, which interrupted higher TE/Ca ratios in the older section of the shell. An ontogenetic decrease was also observed in the Sr/Ca and Ba/Ca records, although it was less amplified.

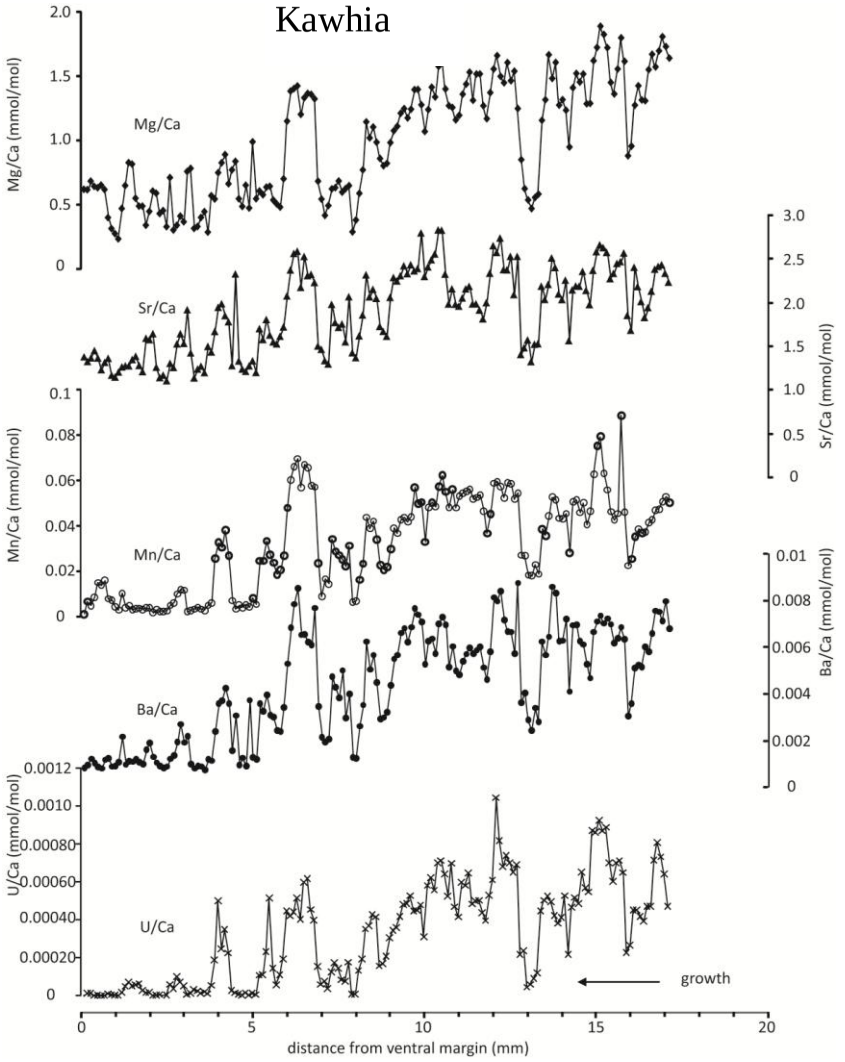

Figure 3.20 (Left): Mg/Ca, Sr/Ca, Ba/Ca, Mn/Ca and U/Ca ratios from the Kawhia shell.

Figure 3.21 (Right): Mg/Ca, Sr/Ca, Ba/Ca, Mn/Ca and U/Ca ratios from the Raglan shell.

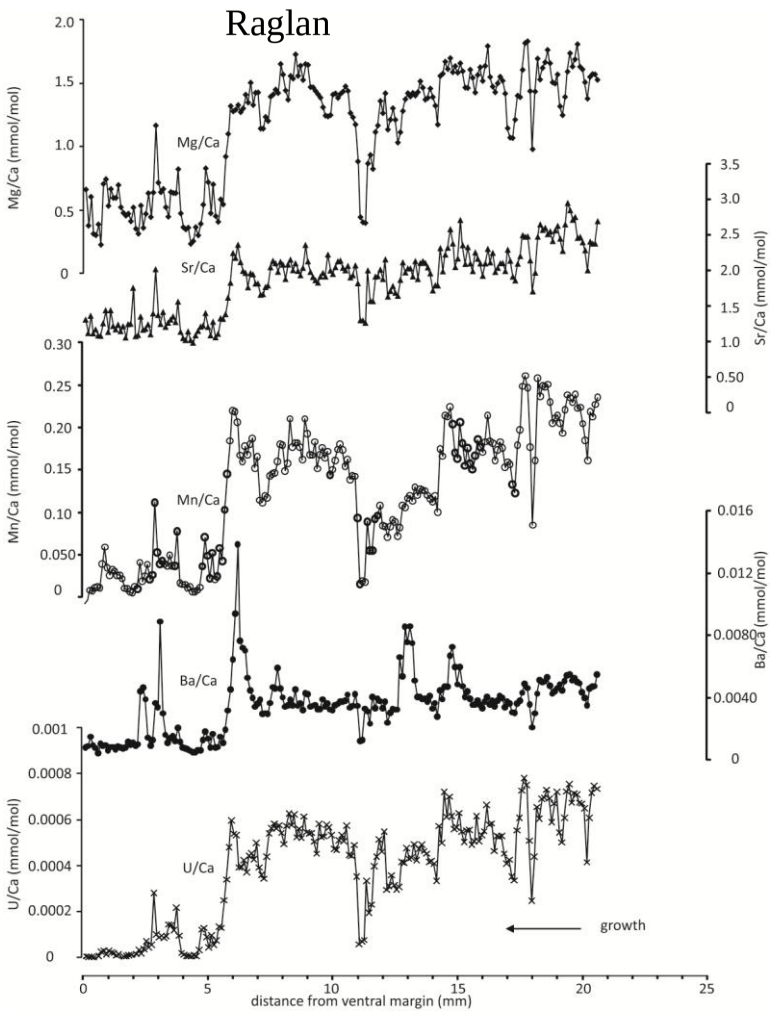

Miranda

The Mg/Ca, Sr/Ca, Ba/Ca and U/Ca records in the Miranda shell were characterised by moderate variations (~0.5, ~0.6, ~0.005 and 0.0003 mmol/mol, respectively) superimposed on a gradual ontogenetic decrease in TE/Ca ratios (Figure 3.22). Whereas a decrease in the amplitude in variations commonly accompanied the ontogenetic decrease in ratios in the other shell records, this was not the case in for Mg/Ca, Sr/Ca, Ba/Ca and U/Ca in the Miranda shell. Mn/Ca ratios exhibited a wide range, between 0.00-1.60 mmol/mol, and the Mn/Ca record included three large peaks, which apart from this was comparable to the Mg/Ca, Sr/Ca, Ba/Ca and U/Ca records.

Kaiaua

The records of Mg/Ca, Mn/Ca, Ba/Ca and U/Ca in the Kaiaua shell consisted of a series of sinusoidal variations, which was unique out of all the *A. stutchburyi* analysed (Figure 3.23). The amplitude and width of these variations generally decreased from the older sections to the youngest section. For example, in the Mg/Ca record, the penultimate variation stretches over ~4 mm (from trough-trough), whereas the three sinusoidal variations located between 5.5-2.5 mm from the ventral margin are each only approximately 0.75 mm from trough-trough. This pattern of variation was also present in the Sr/Ca record, although the variations were more subdued.

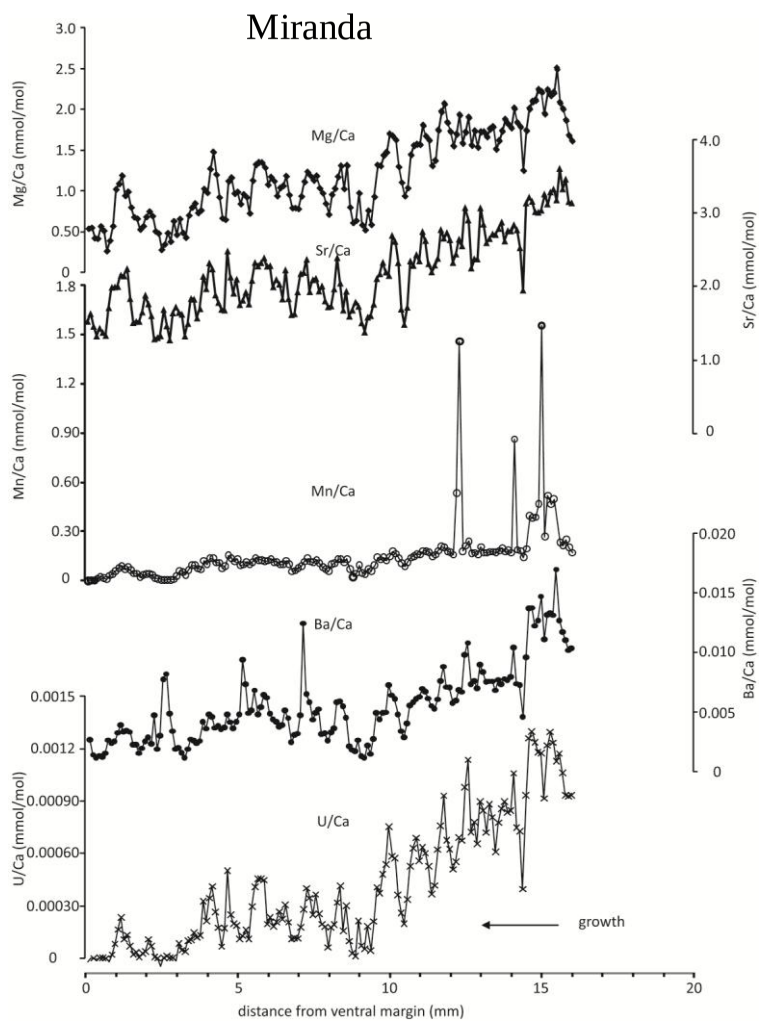

Figure 3.22 (Left): Mg/Ca, Sr/Ca, Ba/Ca, Mn/Ca and U/Ca ratios from the Miranda shell.

Figure 3.23 (Right): Mg/Ca, Sr/Ca, Ba/Ca, Mn/Ca and U/Ca ratios from the Kaiaua shell.

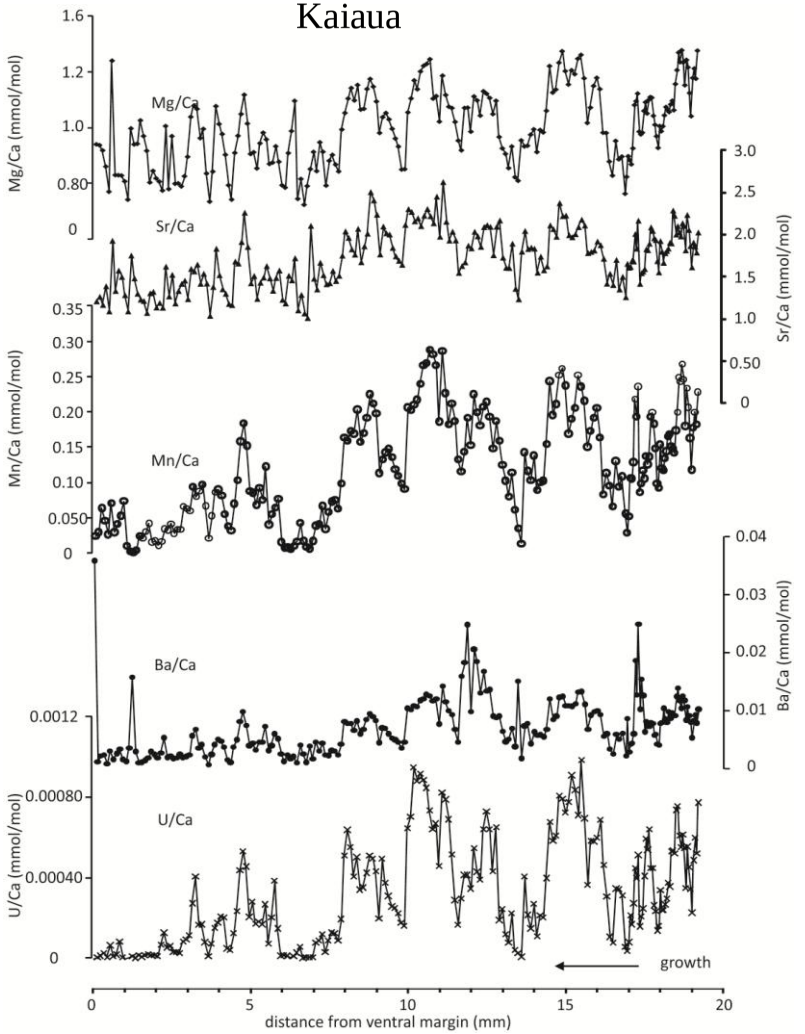

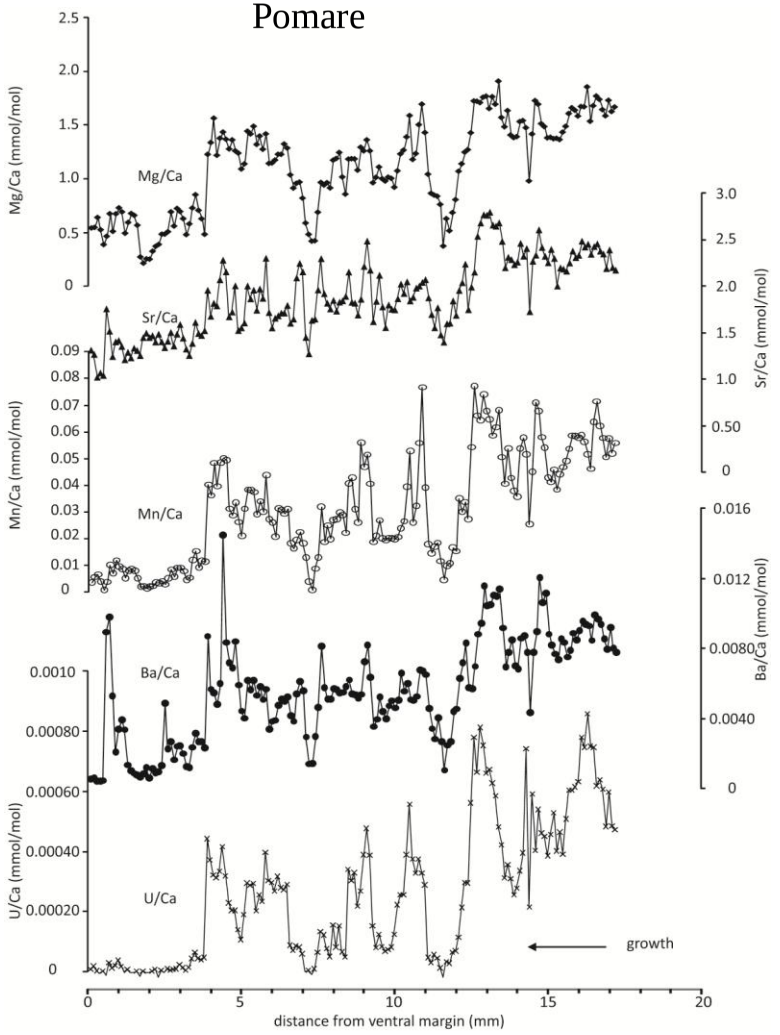

Figure 3.24 (Left): Mg/Ca, Sr/Ca, Ba/Ca, Mn/Ca and U/Ca ratios from the Pomare shell.

Figure 3.25 (Right): Mg/Ca, Sr/Ca, Ba/Ca, Mn/Ca and U/Ca ratios from the Manakau shell.

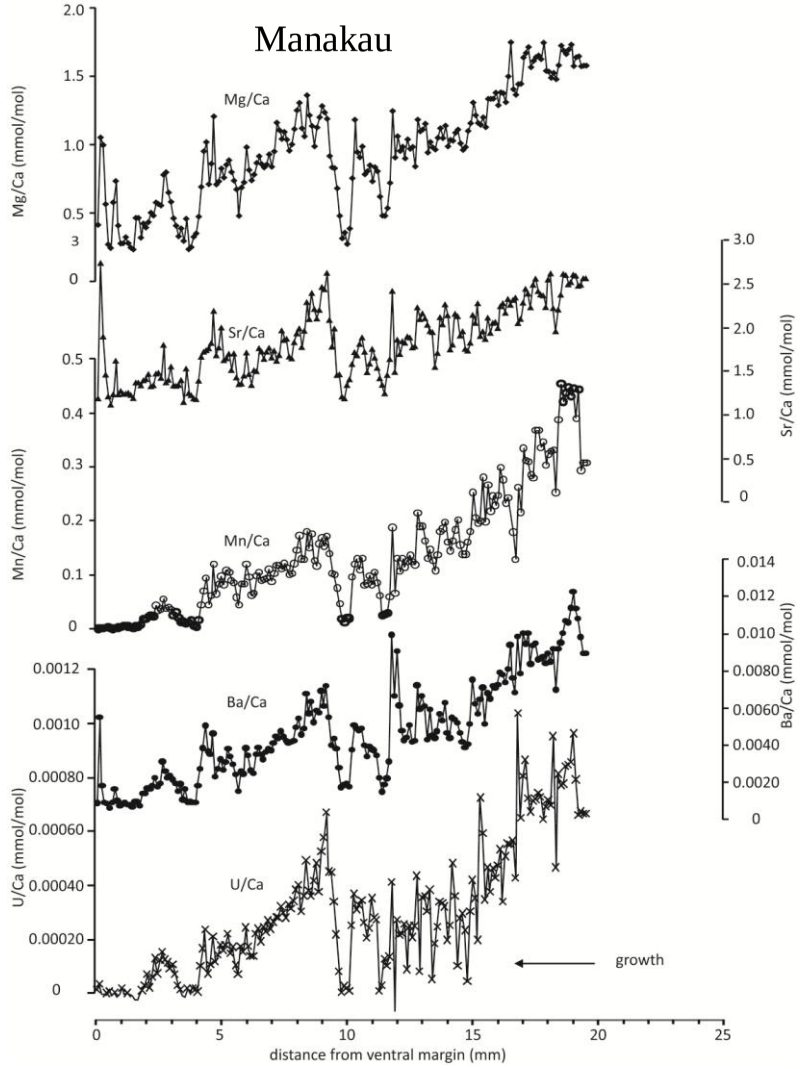

Pomare

The Pomare shell Mg/Ca, Mn/Ca, U/Ca, Ba/Ca and Sr/Ca records consisted of semi-sinusoidal variations, with significant troughs located at 4, 7 and 11.5 mm from the ventral margin (Figure 3.24). There was an ontogenetic decrease in ratios and the amplitude of the ratio variations generally decreased in the younger sections of the shell; except for the Ba/Ca record, which contained two spikes at 4.4 and 7 mm from the ventral margin.

Manakau Harbour

Each of the Mg/Ca, Mn/Ca, Sr/Ca, U/Ca, and Ba/Ca records from the Manakau Harbour shell contained two saw-tooth patterns, which were separated by a large decrease in ratios at ~10 mm from the ventral margin (Figure 3.25). As seen in several of the other shells with higher average Mn/Ca ratios, there were several spikes in Mn/Ca superimposed on this pattern in the oldest section of the record. There was a significant ontogenetic decrease over the Mg/Ca, Mn/Ca, Sr/Ca, U/Ca, and Ba/Ca records, although this was not present in the other TE/Ca records. In the B/Ca record there was an ontogenetic increase.

3.1.3 Inner versus outer shell averages

The general trend of decreasing TE/Ca ratios with the age of the clam can most clearly be observed in a comparison of the averages of the ratios measured from the half of each shell transect closest to the umbo (the "inner" half), with the averages of the ratios measured from the outside half of each shell transect closest to the ventral margin (the "outer" half) (Figures 3.26-3.27). Except for Ligar Estuary, this was the case for Mg/Ca, Al/Ca, Li/Ca, Sr/Ca, Ba/Ca, U/Ca, Mn/Ca and As/Ca shell ratios, where all inner shell ratio averages were higher than outer shell ratio averages, indicating that more of those

trace elements were substituted for Ca in the earlier stages of each clam's life. For example Mg/Ca ratios were on average between 0.5-1.0 mmol/mol greater in the oldest halves of each shell. For the Cu/Ca, B/Ca and Zn/Ca shell ratios this pattern was not evident; average B/Ca shell ratios remained very similar in both sections of the shell for all samples, while Zn/Ca and Cu/Ca average ratios were variable between inner and outer sections, across the samples.

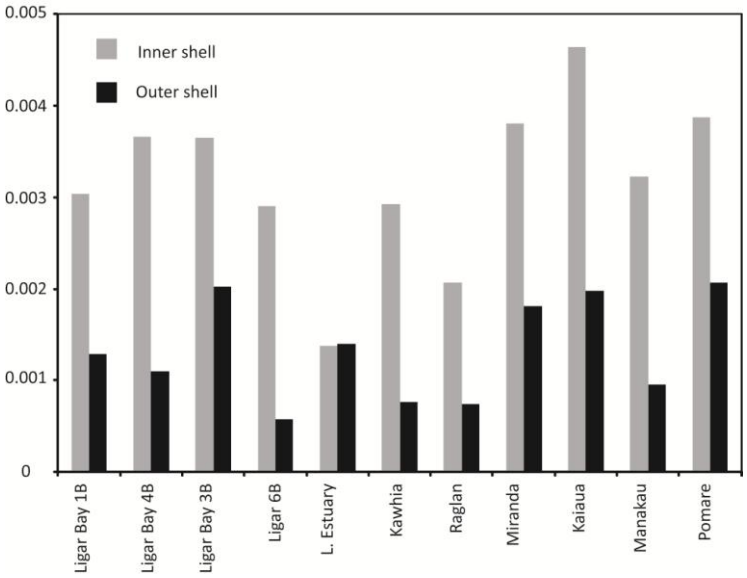

Figure 3.26
Comparison of average Mg/Ca ratios from the inner (oldest) transect of the *A. stutchburyi* shells and outer (youngest) half of the shells.

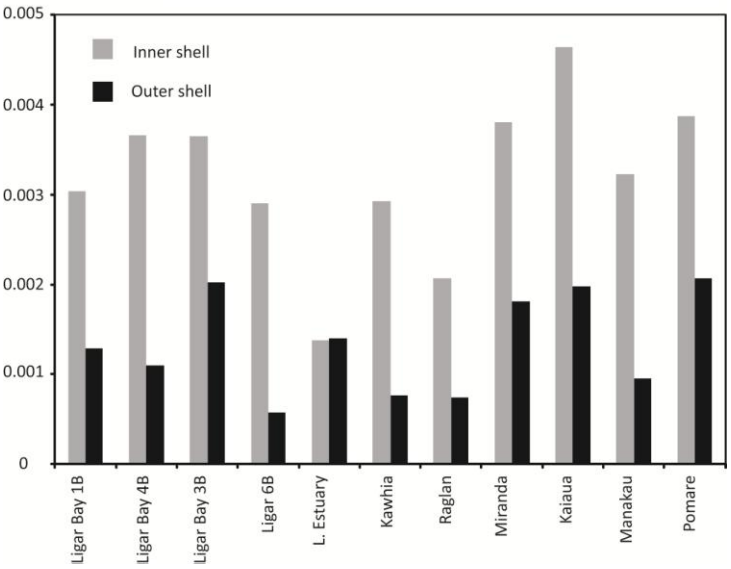

Figure 3.27
Comparison of average Ba/Ca ratios from the inner (oldest) transect of the *A. stutchburyi* shells and outer (youngest) half of the shells.

3.1.4 Correlations between trace elements

There was a significant correlation throughout the dataset for all *A. stutchburyi* shells from all sites of Mg/Ca ratios, with Mn/Ca, Sr/Ca, Ba/Ca and U/Ca ratios (Table 3.2). The strongest correlations were observed between Mg/Ca ratios and U/Ca ratios in the Raglan and Miranda shells, which displayed linear regressions with r^2 values of 0.92 and 0.91 respectively. The only weak correlation between Mg/Ca and U/Ca ($r^2 = 0.45$) was in the Ligar Estuary shell – all other Mg/Ca-U/Ca correlations had $r^2 > 0.72$. Mg/Ca always showed a significant correlation with Sr/Ca, with r^2 values ranging between 0.56–0.86. Correlations between Mg/Ca and Mn/Ca were typically significant, except for two exceptions – the Ligar Estuary ($r^2 = 0.28$) shell, and Ligar 4B ($r^2 = 0.42$). For half of the shells there was a strong correlation between Mg/Ca and Ba/Ca, but for the remaining shells, correlation was insignificant (e.g. Ligar Bay 4B $r^2 = 0.051$ and Ligar 3B $r^2=0.21$).

The slopes, for the Mg/Ca-U/Ca regressions, and thus sensitivity of co-variation, were similar between sites and also between shells within the Ligar Bay site (Table 3.2). The sensitivity of the other trace element correlations with Mg/Ca was more variable, particularly the linear regressions for Mn/Ca-Mg/Ca, where the highest slope (0.27) was two orders of magnitude higher than the lowest (0.0026). However, the Ligar Bay shells tended to have similar slopes when plotted against Ba/Ca and Mn/Ca.

Additionally, there were noticeable correlations between Mn, Ba, Sr and U. Mn/Ca ratios correlated significantly with Ba/Ca, Sr/Ca and U/Ca ($r^2 = 0.60$-0.92) in all but the Ligar Bay shells; although these had low average Mn/Ca ratios (Figure 3.30). The slope values varied within each correlation with Mn by up to an order of magnitude. Sr/Ca showed some strong correlations with Ba/Ca in most of the dataset ($r^2 = 0.46$-0.87), but not within the Ligar Bay shells or the Ligar Estuary shell. Similarly, Sr/Ca and U/Ca

were strongly correlated (r^2 = 0.66-0.90) within each of the shells except for Ligar Estuary and Ligar 6B. The sensitivity for these correlations with Sr was less variable than when Mn was included, especially Sr/Ca-U/Ca. Ba/Ca and U/Ca had the most significant correlation between each other (r^2 = 0.47-0.88), except for within the Ligar Bay 3B and Ligar Bay 4B shells.

No other trace elements showed significant correlations with the others, with the exception of Al/Ca. Within the Kawhia shell data, Al/Ca showed significant correlations with Mg/Ca, Mn/Ca, Sr/Ca, Ba/Ca and U/Ca, with r^2 values of 0.58, 0.74, 0.73, 0.80 and 0.65 respectively. The only other significant correlations seen for Al/Ca were in the Ligar 6B shell data, where Al/Ca was weakly correlated with Mn/Ca (r^2 = 0.53) and U/Ca (r^2 = 0.58).

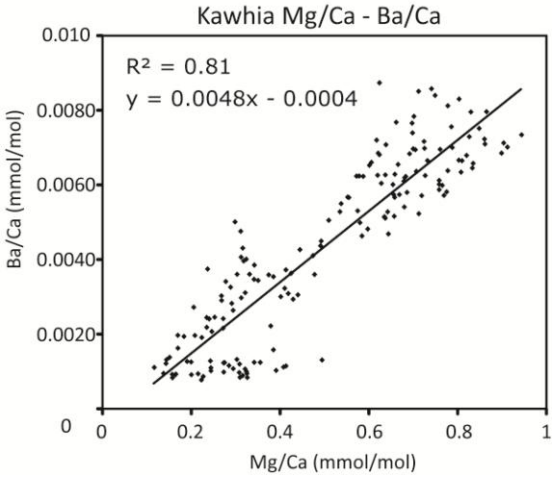

Figure 3.28 Correlation between Mg/Ca and Ba/Ca ratios from the Kawhia shell.

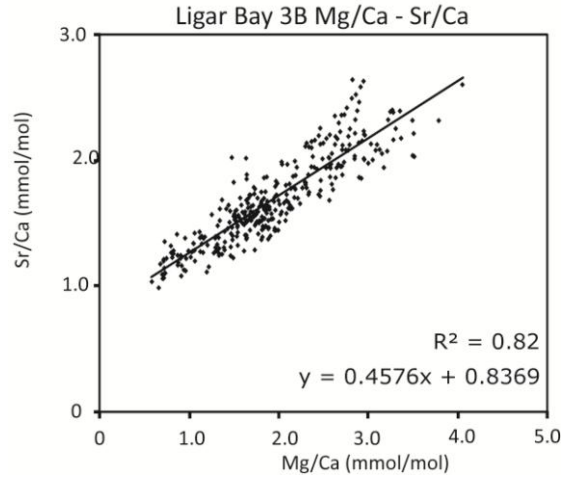

Figure 3.29 Correlation between Mg/Ca and Sr/Ca ratios from the Ligar Bay 3B shell.

Trace Element Correlations

	Mg								Ba	
variable	Mn		Sr		Ba		U		U	
Shell	m	r^2	m	r^2	m	r^2	m	r^2	m	r^2
Ligar 1B	0.0026	**0.74**	0.48	**0.65**	0.0031	**0.41**	-	-		
Ligar 3B	0.0025	**0.66**	0.46	**0.80**			0.00010	**0.82**		
Ligar 4B	0.0018	**0.42**	0.78	**0.62**	0.0034		0.00020	**0.78**		
Ligar 6B	0.0049	**0.74**	0.65	**0.56**	0.0067	**0.83**	0.00050	**0.90**	0.07	**0.88**
Ligar estuary			0.55	**0.74**	0.0017	**0.42**	0.00020	**0.45**	0.10	**0.75**
Kawhia	0.042	**0.81**	0.92	**0.77**	0.0048	**0.81**	0.00050	**0.85**	0.10	**0.81**
Raglan	0.15	**0.87**	0.95	**0.84**	0.0029	**0.47**	0.00050	**0.92**	0.083	**0.47**
Miranda	0.17	**0.73**	0.97	**0.86**	0.0053	**0.71**	0.00070	**0.91**	0.10	**0.79**
Kaiaua	0.24	**0.73**	0.66	**0.67**	0.011	**0.48**	0.00080	**0.72**	0.046	**0.54**
Manakau	0.27	**0.84**	0.91	**0.83**	0.0067	**0.89**	0.00060	**0.82**	0.085	**0.88**
Pomare	0.045	**0.90**	0.81	**0.73**	0.0058	**0.72**	0.00050	**0.80**	0.063	**0.64**

	Mn						Sr			
variable	Sr		Ba		U		Ba		U	
Shell	m	r^2	m	r^2	m	r^2	m	r^2	m	r^2
Ligar 1B	160	**0.63**					0.0050	**0.40**		
Ligar 3B					0.033	**0.66**			0.00020	**0.79**
Ligar 4B									0.00020	**0.73**
Ligar 6B			1.1	**0.79**	0.084	**0.76**	0.0053	**0.40**		
Ligar estuary										
Kawhia	20	**0.80**	0.11	**0.88**	0.012	**0.85**	0.0047	**0.87**	0.00050	**0.79**
Raglan	5.9	**0.88**	0.018	**0.47**	0.0032	**0.92**	0.0029	**0.51**	0.00050	**0.90**
Miranda	4.5	**0.66**	0.025	**0.65**	0.0031	**0.75**	0.0051	**0.74**	0.00060	**0.87**
Kaiaua	3.9	**0.74**	0.044	**0.60**	0.0032	**0.82**	0.0089	**0.46**	0.00060	**0.66**
Manakau	3.1	**0.72**	0.023	**0.89**	0.0020	**0.86**	0.0062	**0.82**	0.00050	**0.69**
Pomare	18	**0.78**	0.12	**0.73**	0.010	**0.83**	0.0065	**0.81**	0.00050	**0.71**

Table 3.2 Correlations were calculated between Mg/Ca, Sr/Ca, Mn/Ca, Ba/Ca and U/Ca across the entire dataset of all individuals of *A. stutchburyi* that were analysed. All correlations that produced a correlation coefficient ≥ 0.40 are shown in the table, and correlation coefficients and slope (m) values are displayed from the linear regressions made through correlation pairs.

3.1.5 Shell averages of trace element/Ca ratios

Shell averages of TE/Ca ratios were calculated for each shell sample by averaging all the points from one transect across that shell. These averages are shown in Figures 3.30 and 3.31. The length of LA-ICP-MS transects and shell growth rate both varied between all *A. stutchburyi* analysed. Therefore, it should be noted that these 'averages' could incorporate a degree of error where ontogenetic variations in TE/Ca have been captured to varying degrees between the shells.

With the exception of Ligar Bay 6B (0.56 mmol/mol), the highest average Mg/Ca ratios (1.23-1.88 mmol/mol) were observed in the Ligar Bay shells. Even the highest average Mg/Ca ratios are still far below the Mg/Ca ratio of seawater – 5.2 mmol/mol (Elderfield, 2006). The average Mg/Ca ratios in *A. stutchburyi* did not show an increase coinciding with decreasing latitude (and thus increasing average SST) that could imply a positive correlation between Mg/Ca and sea temperature. Rather, Ligar Bay is the southernmost location, which would suggest an inverse correlation with SST if there was a relationship at all. The Ligar Estuary shell had an average Mg/Ca ratio of 0.61 mmol/mol that was more comparable to Ligar bay 6B and to the remaining locations that had ratios varying between 0.38-0.60 mmol/mol.

The average Sr/Ca *A. stutchburyi* ratios were ~10 times lower than that of average modern seawater Sr/Ca - 8.9 mmol/mol (Elderfield, 2006). Average Sr/Ca shell ratios also appeared to show no correlation with latitude, with all average ratios observed in a close range of 1.5-2.0 mmol/mol.

A significant site variation was present in the Mn/Ca shell ratios, whereby the four Ligar Bay shells had average Mn/Ca ratios (0.0020-0.0036 mmol/mol) that were an order of magnitude lower than the Mn/Ca ratios observed in shells from the remaining locations. Four shells (Raglan, Miranda, Kaiaua and Manakau) had particularly high

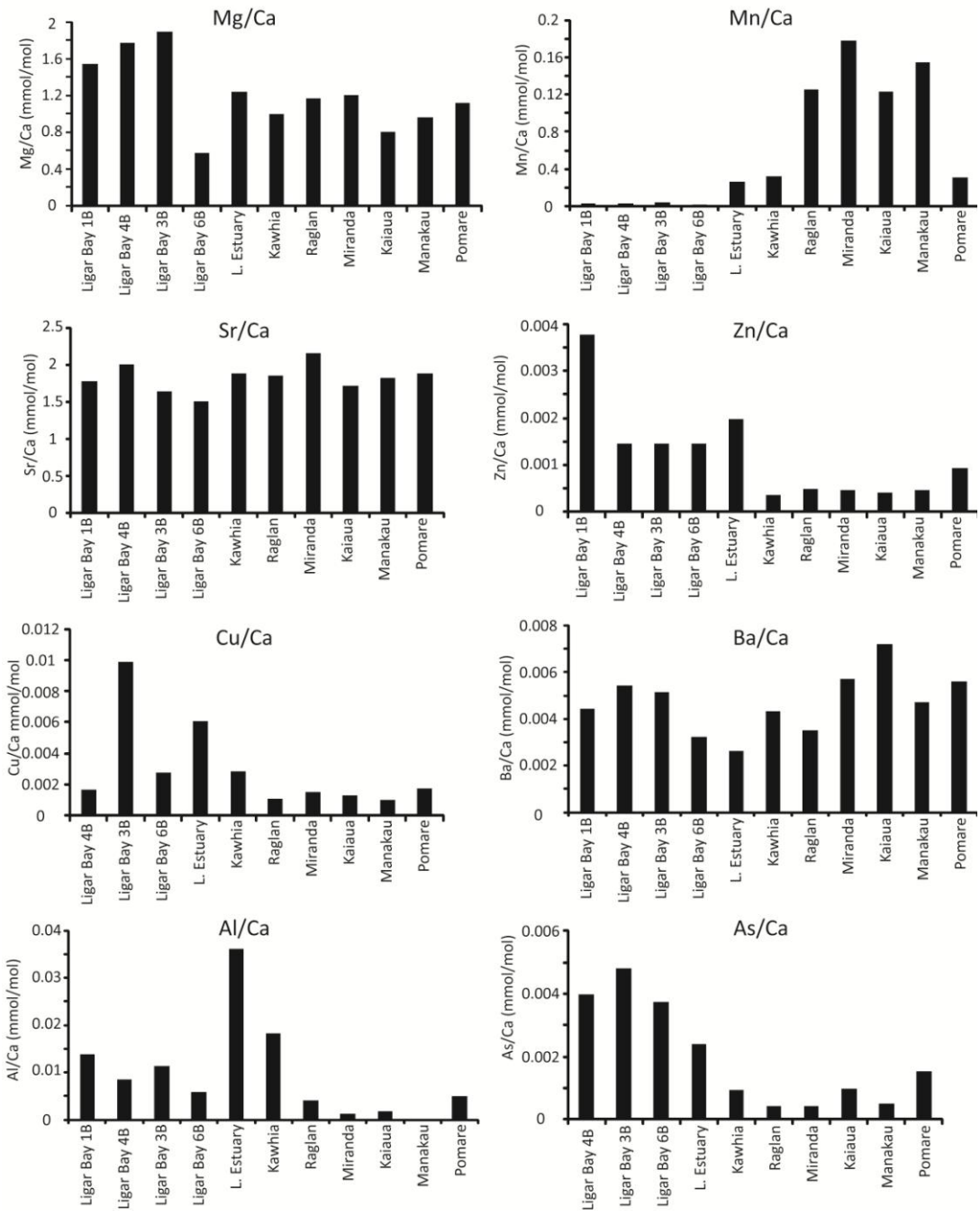

Figure 3.30 Whole-shell averages for Mg/Ca, A/Ca, Mn/Ca, Cu/Ca, Zn/Ca, As/Ca, Sr/ca and Ba/Ca. Shell samples, on the horizontal axis are in order of decreasing latitude –i.e. Ligar Bay shells were the most southern site, Pomare shell was from the most northern site.

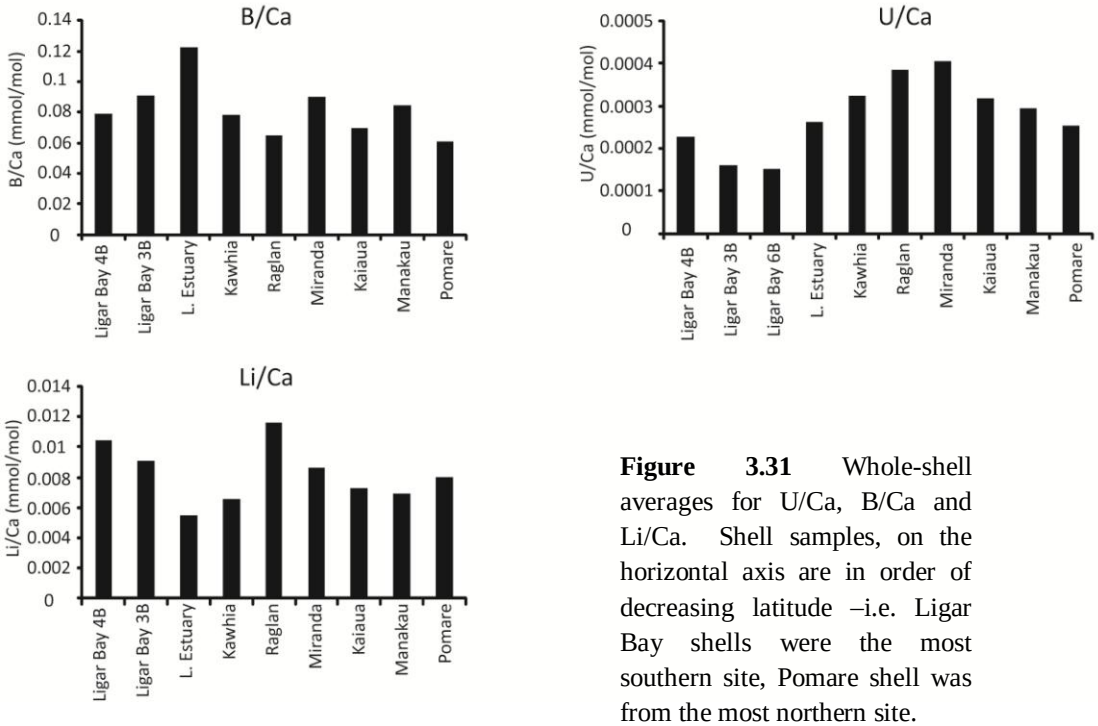

Figure 3.31 Whole-shell averages for U/Ca, B/Ca and Li/Ca. Shell samples, on the horizontal axis are in order of decreasing latitude –i.e. Ligar Bay shells were the most southern site, Pomare shell was from the most northern site.

Mn/Ca ratios ranging between 0.12-0.18 mmol/mol. The shells from Kawhia and Pomare displayed Mn/Ca ratios - 0.032 and 0.031 mmol/mol respectively - approximately three times lower than the shells with the highest Mn/Ca ratios. The average Mn/Ca ratio of the Ligar Estuary shell (0.026 mmol/mol), was intermediate between the Kawhia and Pomare shells and the low Mn/Ca Ligar Bay shells.

The TE/Ca ratios of several of the heavy metals (Zn/Ca, Cu/Ca, As/Ca) also showed a significant difference between the *A. stutchburyi* from Ligar Bay and the shells from the other sites. The clearest variation was present in the As/Ca shell ratios in which the average As/Ca ratios of the Ligar Bay shells were an order of magnitude higher than the average ratios of the shells from the other locations; with the exception of the Ligar Estuary shell, which had an average ratio just higher than the non-Ligar Bay shells. Amongst the average Zn/Ca shell ratios, all the Ligar Bay shells and the Ligar Estuary shell displayed the highest ratios, with one Ligar Bay shell (1B) having a Zn/Ca ratio an order of magnitude higher than all the other samples. Similarly, another Ligar Bay shell

(3B), and also the Ligar Estuary shell, had Cu/Ca ratios that were significantly higher than all other average Cu/Ca ratios.

The average Ba/Ca, Li/Ca and B/Ca shell ratios all fall within a reasonably restricted range (0.0026-0.0072, 0.0055-0.012 and 0.061-0.12 mmol/mol, respectively). Average U/Ca shell ratios were very low, falling in the range of 0.00015-0.00040 mmol/mol. There was a noticeable site difference in the average Al/Ca ratios, as the Ligar Bay shells and Ligar Estuary shell had higher average Al/Ca ratios than all the other locations but for the Kawhia shell.

3.2 Sediment major elements

The major element analyses for Mg, Mn, Al and Ca (Table 3.3) obtained for sediment samples were converted into Mg/Ca, Mn/Ca and Al/Ca ratios in mmol/mol (Table 3.4). Comparison of the sediment TE/Ca ratios with average shell TE/Ca ratios demonstrates there is no correlation between the two (Table 3.4). For example, Mg/Ca ratios are highest in Ligar Bay (1.4 mmol/mol), but the sediment analysed from Ligar Bay has the second lowest Mg/Ca ratios (169 mmol/mol).

Table 3.3 XRF major oxide analysis of sediment collected at each site. Reported in weight %. .

Shell	Kawhia	Kaiaua	Ligar Bay	Manakau	Miranda	Pomare	Raglan
SiO_2	61.7	61.8	80.6	74.0	72.4	68.0	45.0
Al_2O_3	13.9	7.87	10.1	10.0	9.83	10.7	11.8
Fe_2O_3	6.21	2.52	1.17	4.60	2.92	4.32	23.2
CaO	5.68	12.0	1.22	2.10	4.12	3.72	7.48
MgO	3.47	0.570	0.150	1.00	0.730	0.880	4.42
SO_3	<0.01	0.280	<0.0100	0.00	0.220	0.190	<0.0100
K_2O	1.83	1.19	3.38	1.40	1.79	1.77	1.22
Na_2O	2.80	1.78	2.44	2.00	2.37	1.56	2.24
MnO	0.120	0.0400	0.0100	0.100	0.0600	0.0300	0.310
TiO_2	0.700	0.470	0.260	0.800	0.580	0.480	2.69
P_2O_5	0.150	0.0600	0.0300	0.100	0.0600	0.150	0.230
LOI	3.23	11.0	0.540	3.40	4.57	8.02	0.980
SUM	99.9	99.5	99.9	100	99.6	99.9	99.6

Table 3.4 Mg/Ca, Al/Ca and Mn/Ca ratios in mmol/mol for sediment samples compared with average Mg/Ca, Al/Ca and Mn/Ca ratios for each shell

Sediment	Kawhia	Kaiaua	Ligar Bay	Manakau	Miranda	Pomare	Raglan
mmol/mol							
Mg/Ca	847	70	169	643	244	329	818
Al/Ca	2700	724	9130	5350	2620	3180	1740
Mn/Ca	16.2	2.94	6.43	21.4	11	5.87	32.5
Average shell							
mmol/mol							
Mg/Ca	0.99	0.81	1.4	0.96	1.2	1.1	1.2
Al/Ca	0.018	0.0018	0.0099	0	0.0012	0.0049	0.0041
Mn/Ca	0.032	0.12	0.0029	0.15	0.18	0.031	0.13

CHAPTER 4.0 DISCUSSION

4.1 *A. stutchburyi* sclerochronology

4.1.1 Extracting a high-resolution chronology; the limitations of sclerochronology

Producing a high-resolution chronology for geochemical data measured in mollusc shells is integral to the purpose of using the shell chemistry as a paleoenvironmental proxy. *A. stutchburyi* offers the potential to resolve geochemical data up to a sub-daily level, as it deposits micro-increments with a circa-tidal periodicity (McKinnon, 1996). For several species, including the sub-tidal scallop *Pecten maximus* (Lorrain, 2005), and the long-lived bivalve *Arctica islandica* (Schöne et al., 2011), counting the number of micro-increments (in cross-section) of the mollusc can provide a high-resolution chronology – down to daily information, depending on sample spacing. However, this method relies on sufficient knowledge of the growth line deposition and also on individual micro-increments being clearly visible - usually under a reflected light microscope, with an etching and dying treatment such as Mutvei's solution (Schöne et al., 2005). For most species, micro-increments/daily growth lines are not clearly visible throughout the shell and thus counting them does not provide an accurate chronology (Schöne, 2008).

A. stutchburyi shells analysed in this study do not have clearly visible daily growth lines throughout their shells; individual micro-increments were only identifiable in some regions in the shells, mostly in the sections that formed while the individuals were young. Several techniques were utilised to try to view the tidal micro-increments in *A. stutchburyi* shells after LA-ICP-MS analysis. Firstly the shells, which were in polished,

3.5 mm epoxy mounts, were viewed at 108x magnification under a reflected light, binocular microscope (Figure 4.1). In each shell some micro-increments were visible at this scale, but in many regions on each shell these were not individually identifiable and could not be counted. Secondly, the shells were viewed at 200x magnification under a reflected light, microscope (Figure 4.2). The higher magnification microscope revealed micro-increments in only two of the 11 shell samples (Ligar Bay 1B and Ligar Bay 4B); most likely as growth structures had been removed by polishing during preparation for LA-ICP-MS analysis. In the two shells where growth structures had not been polished off, the micro-increments were not clear enough across the entire shell to allow these to be counted.

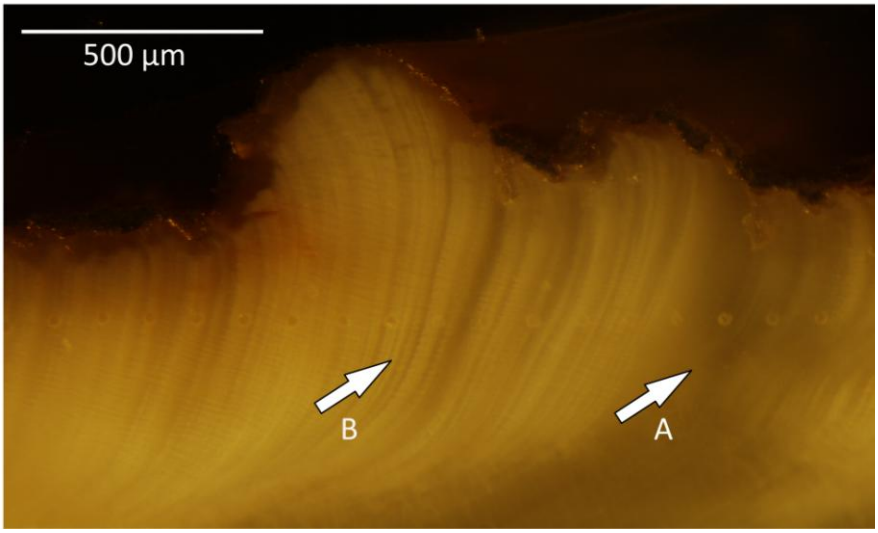

Figure 4.1

Photograph taken of growth patterns on Ligar Bay 1B shell under reflected light at 108x magnification. **A** indicates where micro-increments are not seen – coinciding with an annual macro-growth band. **B** indicates where micro-increments are distinguishable.

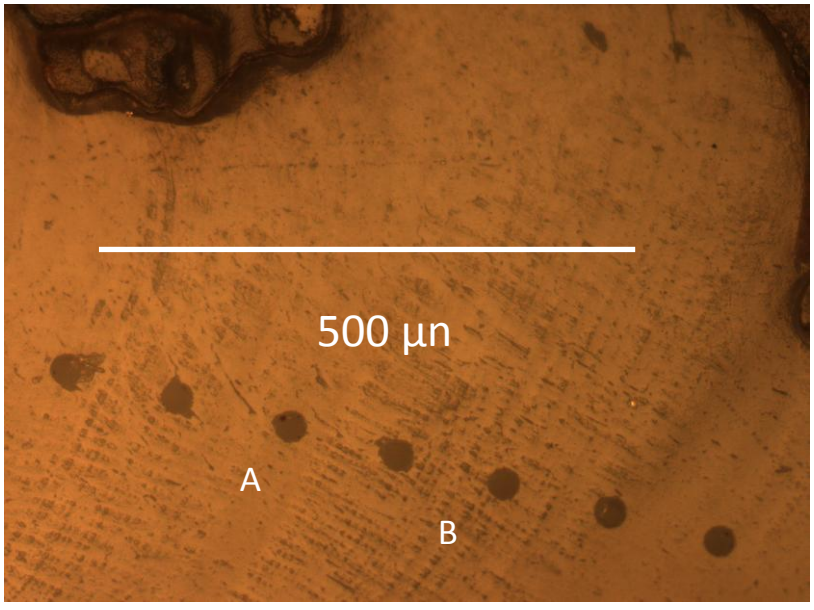

Figure 4.2

Photograph taken of growth patterns on Ligar Bay 1B shell under reflected light at a higher magnification – 200x. Areas marked with **A** indicates where micro-increments are not seen. Areas marked with **B** indicates where micro-increments are distinguishable.

Etching was subsequently attempted on a mounted sample that had not been analysed by LA-ICP-MS using Mutvei's solution (1.6 g alcian blue powder, 125 mL 1% acetic acid and 125 mL 25% glutareldahyde). This solution enhances growth structures by etching out the $CaCO_3$ within the growth increments and staining mucopolysaccharides and glucosamids in the organic growth-lines blue (Schöne et al., 2005; Schöne, 2008). The trial shell used was immersed for 25 min in the solution under constant stirring at 45 °C, air dried and then viewed under a microscope. It was then immersed under the same conditions for another 25 min (total of 50 min) before being viewed again. The Mutvei's solution etched the shell to varying depths making it difficult to see the shell in clear focus under the higher magnification microscope. Under the lower magnification microscope the etching with Mutvei's solution revealed the micro-increments on the shell that had already been visible more clearly, but there were still regions where micro-increments were present but not clearly distinguishable, and regions where there appeared to be no micro-increments at all (Figure 4.3).

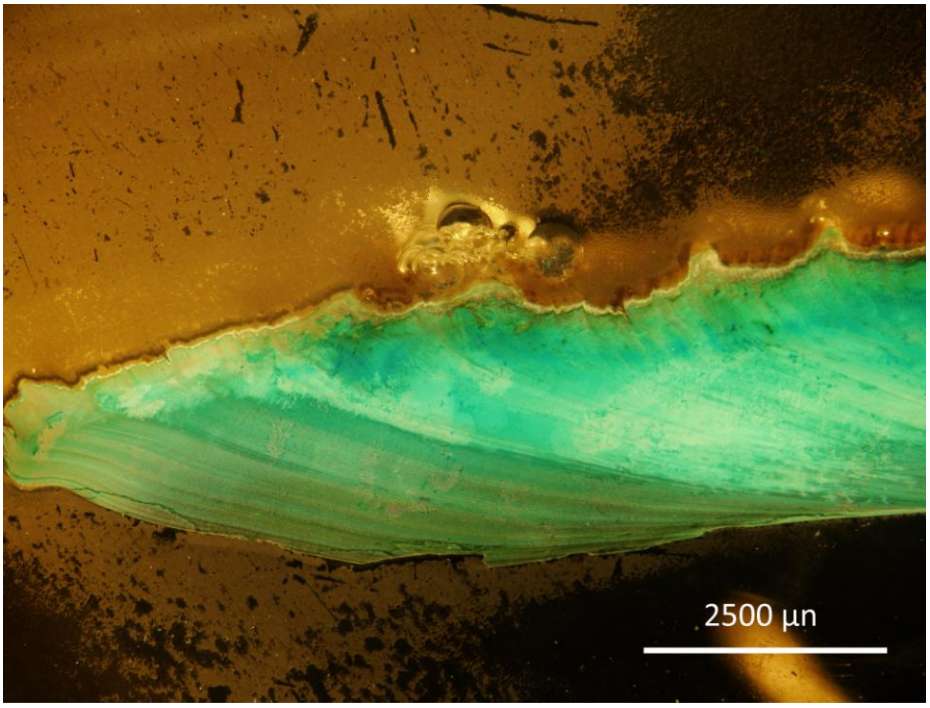

Figure 4.3 Photograph of Ligar Estuary shell after 25 min immersion in Mutvei's solution, taken at 40x magnification with a reflected light microscope.

The absence of micro-increments in particular regions is not unexpected considering what is known about *A. stutchburyi*'s growth and general observations about bivalves living in the intertidal zone. McKinnon (1996) reported that *A. stutchburyi* from Port Chalmers in Dunedin did not deposit a micro-increment for each high tide and, during winter, micro-increment addition ceased - although there was variation between the individuals as to the exact months that this spanned. In some individuals, McKinnon (1996) also observed a short break in micro-increment deposition during spawning in January-February. This could explain why regions without micro-increments in *A. stutchburyi* in the current study were often located where annual growth bands were identified (appearing as dark blue regions for the shell emerged in Mutvei's solution), but also why smaller regions without micro-increments were variably observed in the shell macro-increments between annual bands.

However, it is also likely that the timing and amount of micro-increment growth and cessation varied between individuals at different sites, and between individuals from Ligar Bay. Bivalves are sensitive to their environmental conditions (Schöne, 2008). Micro-incremental deposition ceases in response to changes in temperature (some species' temperature-induced growth cessation coincides with spawning), or when conditions outside physiological tolerance occur – such as storm surges. (Schöne, 2008; Brockington and Clarke, 2001). Therefore shells of the same species living in different temperature/environmental conditions are likely to respond to the local conditions and stop depositing micro-increments at different times of year. This has been observed in a number of species, including: *A. islandica* (Schöne et al., 2005; Schöne 2008), *Mercenaria mercenaria* (Dalton and Menzel, 1983); and *M. donacium* (Carré et al., 2005). Ligar Bay *A. stutchburyi* live in warmer water temperatures than those studied in Dunedin, so it might be expected that winter growth cessation lasts for a shorter time in the Ligar Bay individuals, and perhaps for an even shorter time in the *A. stutchburyi*

collected from sites further north (e.g. Pomare in the Bay of Islands). Furthermore, micro-increment growth is affected by the position of individuals in the intertidal zone, as the length of time shells are submerged for during the high tide controls growth time (Schöne, 2008; Evans, 1972; Goodwin et al., 2001; Miyaji et al., 2007). Thus, the individuals higher in the zone may experience cessation during neap tides that the individuals in the low tide zone do not. In conclusion, there are many complicating factors affecting micro-increment deposition that explain why regions with no micro-increments were observed in *A. stutchburyi* in this study, and which could limit the accuracy of a chronology derived from counting individual increments in the clam.

Where individual micro-increments are not identifiable, some studies have instead used fortnightly changes in micro-increments caused by neap and spring tide cycles to construct a chronology (Carré et al., 2005; Carré et al., 2006). Such micro-increment changes have been observed in *A. stutchburyi* shells (McKinnon, 1996), although these were not visible throughout the *A. stutchburyi* individuals analysed in this study. Nevertheless counting fortnightly micro-increment bands is also subject to the limitations encountered when counting individual increments, as outlined above. Carré et al. (2005) could not rely on the fortnightly growth increments to date *M. donacium* shells – their study was integrated with isotopic analyses.

In fact, most TE/Ca studies of molluscs have achieved a high-resolution chronology utilising $\delta^{18}O$ isotope analyses for which it is possible to produce at least a seasonal age model (Carré et al., 2005; Carré et al., 2006; Freitas et al., 2006; Vander Putten et al., 2000; Gillikin et al., 2005). As mollusc shell $\delta^{18}O$ represents seawater temperature and seawater $\delta^{18}O$, $\delta^{18}O$ records have seasonal temperature and salinity signals, which can be correlated to different times in the year (Vander Putten et al., 2000 and Carré et al., 2005). Further, if seawater $\delta^{18}O$ and temperature are measured while the analysed

molluscs are growing, and the $\delta^{18}O$ relationship has been defined for the species, predicted shell $\delta^{18}O$ values can be calculated. These can then be compared to measured shell $\delta^{18}O$ values, and using software such as AnalySeries, specific dates can be assigned to the measured $\delta^{18}O$ values, and thus trace element records (Freitas et al., 2006). Alternatively, seawater temperatures can be calculated from measured shell $\delta^{18}O$ and modelled with measured seawater temperatures to derive a timescale (Gillikin et al., 2005). Although these latter two methods clearly cannot be used for fossil mollusc shells, they are an effective way to study the incorporation of trace elements in modern specimens because seasonal variation in the trace element records can be defined, and TE/Ca ratios can be directly compared to seawater data (such as temperature, salinity and chlorophyll) on a calendar timescale (Freitas et al., 2006).

4.1.2 Identifying annual growth bands

As discussed in Chapter 1.0, previous studies have found *A. stutchburyi* forms annual growth bands during winter, most likely in July (McKinnon, 1996; Coutts, 1974). In this study annual bands were identified in *A. stutchburyi* after LA-ICP-MS analysis, using photographs taken of the cross-sectioned shells with a camera mounted on a reflected light microscope at 108x magnification. The observations outlined by McKinnon (1996) were followed; annual bands are often accompanied by a notch at the shell surface, and usually form a complete dark band from the base of the shell to the surface. However, these characteristics were not always present or clear in all *A. stutchburyi* samples (Figures 4.4-4.5). The region of shell within ~5 mm of the ventral margin was often complex because there were multiple dark bands (Ligar Bay 3B), or there were no clear micro- or macro-growth patterns and the region was homogeneously dark (Ligar Bay 6B and Kaiaua). Slow-down of growth, permanently, or intermittently, probably caused these patterns near the ventral margin as dark extra-crystalline organic

material forms when growth ceases and valves are shut (Panella, 1975; Palmer, 1995; Takesue and van Geen, 2004), and *A. stutchburyi* growth slows significantly with ontogeny (McKinnon, 1996). This trend was observed by Carré et al. (2005) when assigning a chronology to the bivalve *M. donacium.*

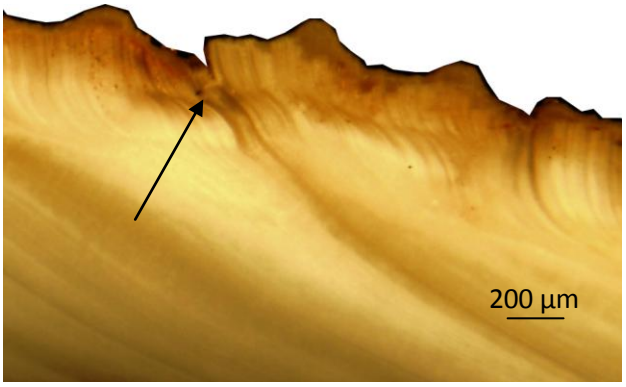

Figure 4.4 Photograph of Ligar 6B showing where an annual growth band is associated with a V shaped notch in the surface of the shell (black arrow).

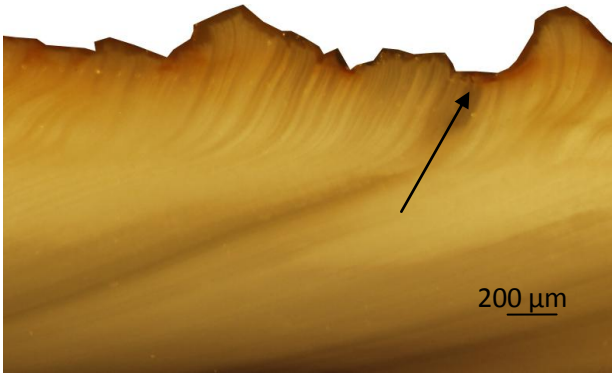

Figure 4.5 Photograph of Ligar 1B showing where an annual growth band is not accompanied by a V shaped notch (black arrow shows growth band).

Annual bands were identified on the Ligar Bay 1B, Ligar Bay 3B, Ligar Bay 4B, Ligar Bay 6B and the Kaiaua *A. stutchburyi* samples (see the annual growth bands represented by grey lines on the TE/Ca transects for these shells in Chapter 3). Due to the uncertainties involved in identifying the annual bands only the Ligar Bay 3B and Ligar Bay 4B *A. stutchburyi* were selected to create a chronology of annual resolution; as their growth bands were clearly identifiable in these individuals, and furthermore, they could be correlated by a common feature in their chemistry.

4.1.3 Constructing an annual chronology for Ligar Bay 3B and 4B shells

The starting point for assigning a common timescale to the Ligar Bay 3B and 4B shells was the 3-point Ba/Ca peaks present in both shells' Ba/Ca records (Figures 3.7, 3.16 and 3.17; Chapter 3). It was inferred that these peaks were formed at the same time, because of their strong similarity in shape and because the large increase in Ba/Ca ratios across the peaks was comparable (0.039 and 0.046 mmol/mol). Therefore, the physical location on the shells where the Ba/Ca peaks were measured could be fixed in the chronology (Figure 4.6). The method of correlating identical Ba/Ca peaks was also used by Takesue et al. (2008) to construct a chronology. In Ligar Bay 3B and Ligar Bay 4B, the annual growth bands identified in both shells on either side of the Ba/Ca peaks were interpreted to have formed during July of the same year. As the *A. stutchburyi* clams were alive when they were collected in April 2008, this date was assigned to the end of the 3B and 4B records. Both shells had to contain the same number of annual bands between the Ba/Ca peak in each shell and the end of each shell, which could not yet contain the winter annual band for 2008. In 4B there were four annual bands that could be confidently identified in this section of the shell. In 3B there were only three clearly identifiable bands because at the end of the shell there were a number of dark thin dark bands interspersed with lighter banding. A fourth annual band was inferred to be near the end of Ligar Bay 3B based on the fourth Ligar Bay 4B band, although for the reasons previously stated it could not be pinpointed. Counting backwards from winter 2007, the last possible winter band to form; the Ba/Ca peaks were formed between winter 2003 and winter 2004. Before the Ba/Ca peaks, annual bands were clear in both shells and could be assigned dates working backwards from winter 2003.

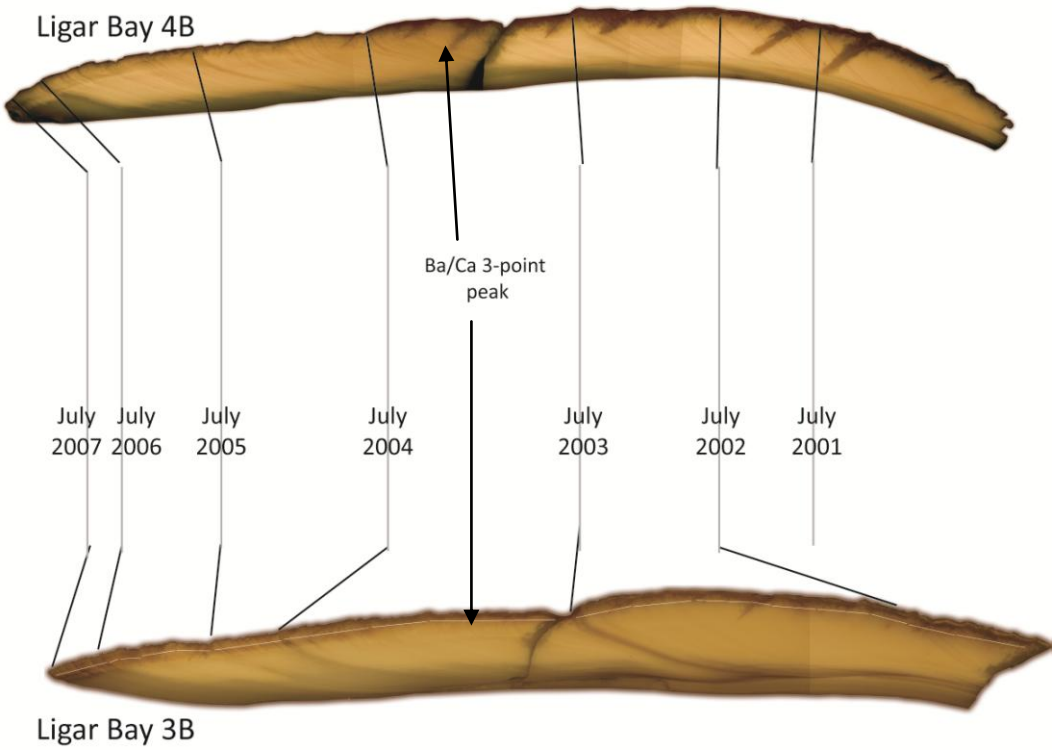

Figure 4.6 Schematic diagram showing the relationship interpreted between annual growth bands on Ligar Bay 3B and Ligar Bay 4B shells. Years from 2007 have been assigned. The annual increment in which the 3-point Ba/Ca peaks were found is identified. (Not to scale)

4.2 Factors affecting trace element incorporation in *A. stutchburyi*

4.2.1 A. stutchburyi growth rate

Growth rate was calculated in mm per year for 23 annual growth increments in *A. stutchburyi* from Ligar Bay. The amount of annual growth was approximated by the number of laser ablation spots (of known spacing) between annual growth bands. The annual growth measured by this method most likely represents the amount of shell extension in the maximum growth direction, down which the LA-ICP-MS analysis was conducted. This is because laser ablation transects followed the geometry of the shell. Carré et al. (2006) suggested growth rate is better quantified by measuring the width of micro-increments in the crystal growth direction (Figure 4.7) rather than measuring shell extension, because shell extension varies down different growth directions, and also within a growth direction because of shell curvature.

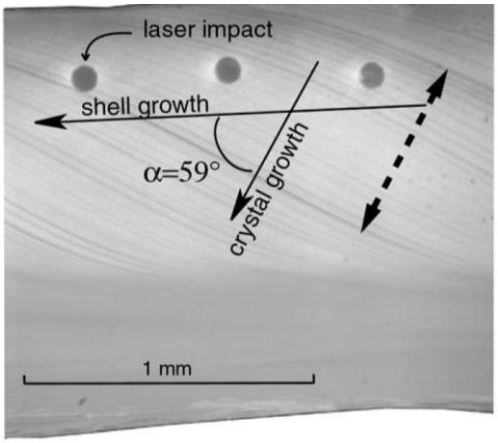

Figure 4.7 Photograph showing the difference between shell growth direction (shell extension) and the crystal growth direction (perpendicular to micro growth lines). Shell extension (growth) was measured in *A. stutchburyi* by adding the distance between consecutive laser ablation points (labelled 'laser impact' in the photograph). Figure taken from Carré et al. (2006).

However, this requires accurate identification of micro-increments and their deposition periodicity, which was not possible for *A. stutchburyi*. Other studies have utilised shell extension rate to estimate growth rate (Gillikin et al., 2005; Klein et al., 1996), and it is argued for this study that this method provides a valid estimation of growth rate for correlation with trace element data that is annually resolved. Nevertheless, the

measurements of annual shell extension potentially include error because of the variations between transects in following the geometry of the shell and because of the human error involved in identifying annual growth bands.

4.2.2 Growth rate and age correlation with trace element/Ca ratios

To compare growth rate with trace element/Ca ratios, ratios within annual increments were averaged (Table 4.1). Correlations between average element/Ca ratios and corresponding annual increment growth rate were then made.

Table 4.1 Average shell growth rate (mm/yr) compared with average trace element/Ca ratios within 23 annual growth increments in *A. stutchburyi* from Ligar Bay.

Shell, and shell increment	Years Before Death	mm/year	Li/Ca	B/Ca	Mg/Ca	Al/Ca	Mn/Ca	Cu/Ca	Zn/Ca	As/Ca	Sr/Ca	Ba/Ca	U/Ca
1B 1	0	0.60	0.017	0.10	0.75	0.00055	0.00028	0.00096	0.00083	0.00034	1.2	0.00096	0.000013
2	1	1.6	0.0078	0.095	0.82	0.0012	0.00053	0.0012	0.0010	0.00084	1.3	0.0015	0.000025
3	2	3.3	0.0092	0.10	1.0	0.0042	0.0014	0.0016	0.0012	0.0026	1.5	0.0035	0.000079
4	3	5.9	-	-	1.7	0.012	0.0027	-	0.0038	-	1.8	0.0046	-
5	4	6.4	-	-	2.0	0.025	0.0040	-	0.0061	-	2.1	0.0059	-
3B 1	0	0.60	0.0096	0.11	0.73	0.0017	0.00052	0.0041	0.00	0.00015	1.1	0.00065	4.80E-06
2	1	0.70	0.0088	0.098	0.91	0.00077	0.00076	0.0070	0.00	0.00059	1.3	0.00066	0.000030
3	2	2.75	0.0079	0.091	1.8	0.0050	0.0026	0.011	0.00032	0.0017	1.5	0.0030	0.00012
4	3	1.8	0.0074	0.097	1.3	0.0064	0.0027	0.010	0.00093	0.0025	1.4	0.0023	0.000096
5	4	7.4	0.0090	0.091	1.6	0.012	0.0034	0.015	0.0018	0.0067	1.6	0.0073	0.00016
6	5	8.9	0.010	0.081	2.2	0.012	0.0044	0.0083	0.0025	0.0055	1.8	0.0059	0.00020
4B 2	1	3.9	0.0082	0.073	1.5	0.0057	0.0024	0.0015	0.00090	0.0012	1.5	0.0022	0.00011
3	2	4.6	0.010	0.083	1.6	0.0081	0.0033	0.0017	0.0015	0.0018	1.9	0.0025	0.00017
4	3	5.5	0.011	0.079	1.7	0.0079	0.0027	0.0019	0.0018	0.0067	2.2	0.012	0.00024
5	4	3.7	0.011	0.082	2.1	0.0081	0.0038	0.0014	0.0011	0.0056	2.2	0.0040	0.00029
6	5	2.9	0.013	0.082	2.3	0.012	0.0043	0.0014	0.0019	0.0037	2.2	0.0054	0.00035
6B 2	2	0.60	-	-	0.25	0.00061	0.00053	0.0017	0.00045	0.00049	1.2	0.00072	2.23E-06
3	3	1.9	-	-	0.31	0.0053	0.0011	0.0018	0.0015	0.00093	1.4	0.0014	0.000013
4	4	1.9	-	-	0.33	0.0015	0.0010	0.0026	0.00089	0.0042	1.5	0.0018	0.000033
5	5	0.7	-	-	0.30	0.00099	0.00021	0.0019	0	0.0016	1.2	0.0013	3.90E-07
6	6	1.2	-	-	0.31	0.0016	0.00041	0.0022	0	0.0016	1.3	0.0020	1.88E-06
7	7	1.9	-	-	0.57	0.0063	0.0030	0.0024	0.0011	0.0046	1.5	0.0035	0.00015
8	8	2.8	-	-	0.62	0.0050	0.0029	0.0026	0.0020	0.012	1.5	0.0037	0.00019

If two annual increments from Ligar Bay 4B are excluded, there is significant positive correlation between growth rate and TE/Ca ratios for Sr/Ca (r^2 = 0.68), Mg/Ca (r^2 = 0.71), Mn/Ca (r^2 = 0.72), Ba/Ca (r^2 = 0.60), U/Ca (r^2 = 0.63) and Al/Ca (r^2 = 0.65), for the Ligar Bay individuals combined (Figure 4.8). No other trace elements showed significant correlations, except for B/Ca, which had a weak, negative correlation with growth rate (r^2 = 0.45).

When correlations were made separately for each shell, the strength of the correlation improved in some cases (Figure 4.9). In particular, for Sr/Ca the correlation with growth rate for each individual Ligar Bay shell was high - with correlation coefficient values of 0.92, 0.88 and 0.85 for Ligar Bay 1B, Ligar Bay 3B and Ligar Bay 6B, respectively. The slopes of the linear regressions for the Sr/Ca-growth rate correlations were variable between the shells (for example 0.16 compared to 0.065). Other than Sr/Ca, the strength of TE/Ca ratio correlation with growth rate was variable between shells. Ligar Bay 1B and Ligar Bay 3B both individually had stronger correlations between growth rate and Mg/Ca, Mn/Ca, Ba/Ca and U/Ca, whereas Ligar Bay 6B had a lower individual correlation for Mn/Ca, Mg/Ca and U/Ca, and had only a marginally higher individual correlation for Ba/Ca.

The growth rate results indicate that shell growth rate (here quantified by extension rate), significantly affects trace element incorporation. For Mg/Ca, Sr/Ca, Mn/Ca, U/Ca, Ba/Ca and Al/Ca the correlation with growth rate is positive; faster growing increments have higher average TE/Ca ratios. Sr/Ca ratios were the most dominated by growth rate, as individually the Ligar Bay shells all showed a very strong ($r^2 \geq 0.85$) correlation between Sr/Ca and growth rate. However, the exact relationship and sensitivity to growth rate is specific to individuals based on the variability in correlation strength and

linear regression slope value between the Ligar Bay shells. Schöne et al. (2011) found that in fast growing annual increments of *Arctica islandica* TE/Ca ratios

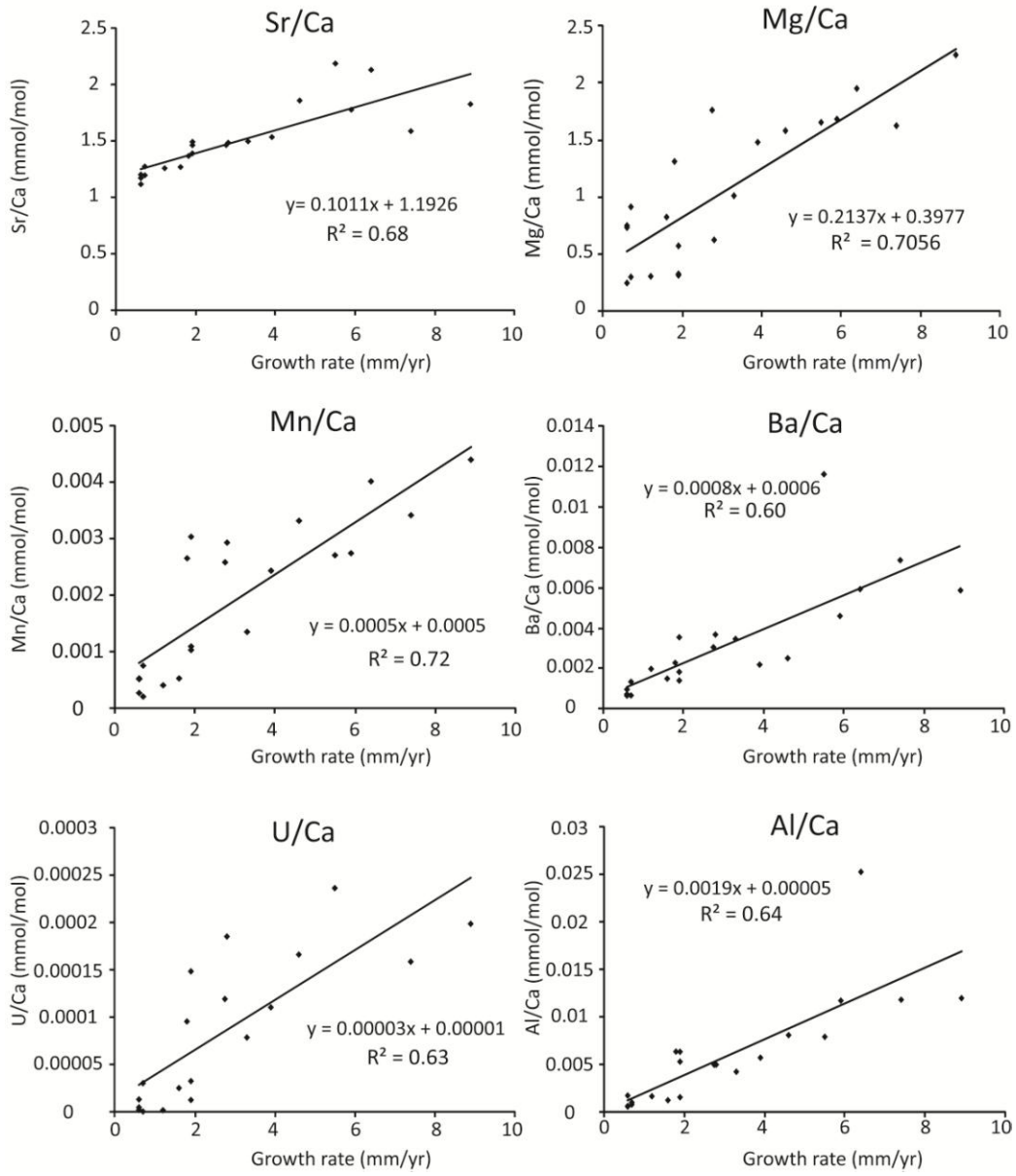

Figure 4.8 Correlations between growth rate (mm/year) for growth increments in Ligar Bay shells and average TE/Ca ratios in those same increments.

were weakly positively correlated to growth rate, but in slow growing increments (below 30-200 µm per year) there was a strong inverse correlation. For *A. stutchburyi*, shells with the highest growth rates (Ligar Bay 1B and Ligar Bay 3B) had the best correlations with growth rate, whereas Ligar Bay 6B, which had lower growth rates, had

a lower correlation coefficient for Mg/Ca (0.62), Mn/Ca (0.64), Ba/Ca (0.61) and U/Ca (0.62).

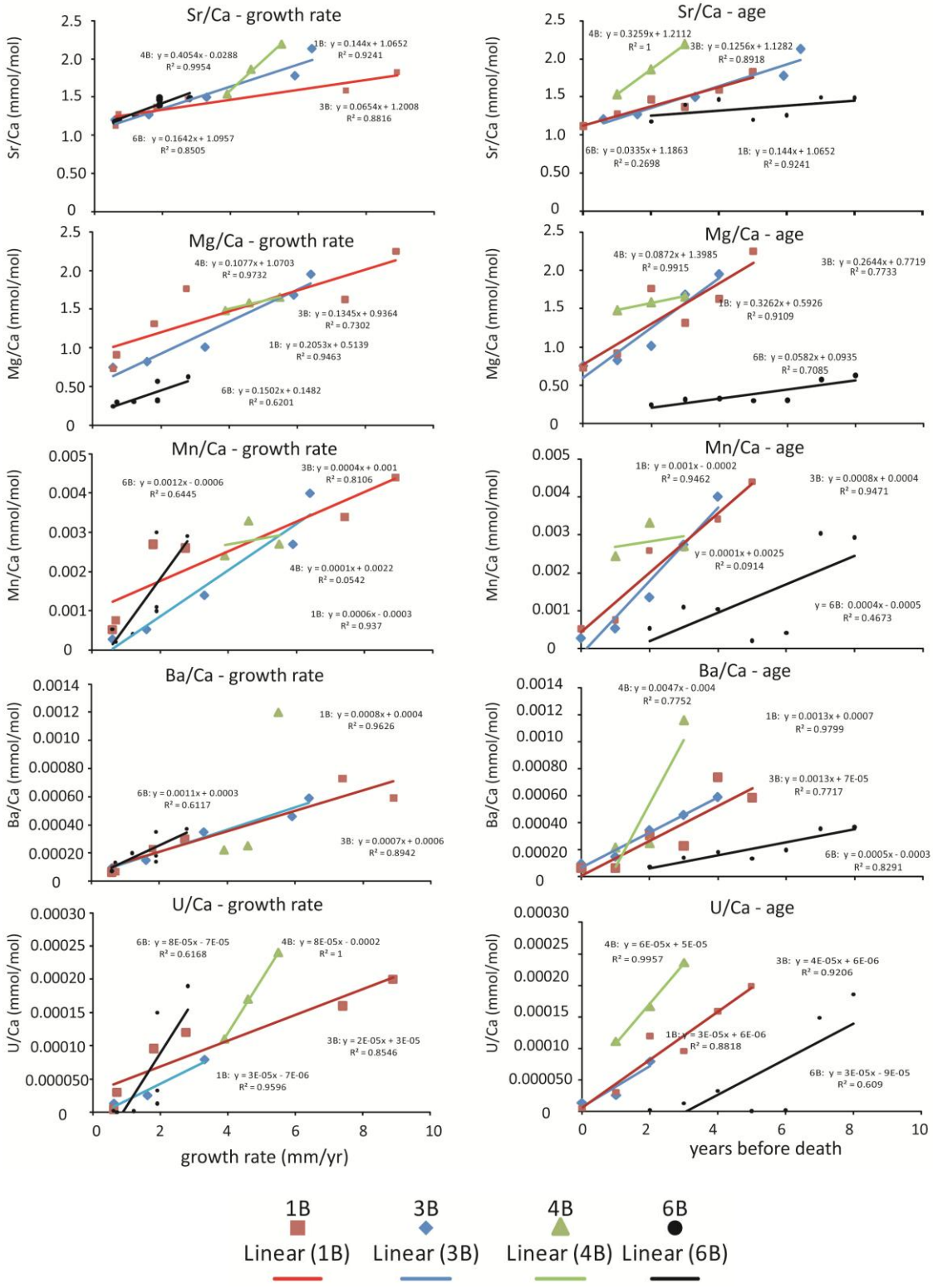

Figure 4.9 Graphs on the left-hand side show growth rate correlations with Mg/Ca, Sr/Ca, M/Ca, Ba/Ca and U/Ca for individual Ligar Bay shells. Graphs on the right-hand side show age (in years before death) correlations with Mg/Ca, Sr/Ca, M/Ca, Ba/Ca and U/Ca for individual Ligar Bay shells. Linear regression equations and r^2 values of correlations are displayed on graphs.

An ontogenetic decrease in TE/Ca ratios was observed in the records from Ligar Bay *A. stutchburyi*. Average TE/Ca ratios for annual increments were compared to the age (measured in years before death) of the increments in order to quantify this effect (Figure 4.9). There was a significant positive correlation between years before death and average TE/Ca ratios for Mg/Ca, Sr/Ca, Mn/Ca, Ba/Ca and U/Ca. As with growth rate correlation, Ligar Bay 6B had lower correlation coefficients ($r^2 < 0.7$) between age and U/Ca, Mn/Ca and Sr/Ca. This may indicate that in slower-growing *A. stutchburyi* individuals biological influences on element partitioning are weaker, and secondary effects such as temperature and ocean chemistry have more influence. Alternatively, the effect could be due to errors in identifying ages for annual bands in Ligar Bay 6B, which was particularly difficult in the youngest regions of the shell because of its slow growth rate. The overall strong correlations found between TE/Ca ratios and age is consistent with the growth rate results, as *A. stutchburyi* growth rate decreases with age.

4.2.3 Sr/Ca and Mg/Ca ratios

Mg/Ca ratios in all *A. stutchburyi* shells analysed ranged between 0.14 and 4.05 mmol/mol, and Sr/Ca ratios between 0.98 and 3.46 mmol/mol. These ratios were significantly lower than the seawater ratios of Mg/Ca - 5.2 mmol/mol, and Sr/Ca - 8.9 mmol/mol (Elderfield, 2006), which confirms that physiological, metabolic or environmental factors control the incorporation of these elements into the crystal lattice. For the Ligar Bay shells, which were collected from an open beach environment, it is unlikely that the Mg/Ca and Sr/Ca ratio variations were caused by variations in conservative seawater ratios. Further, for the remaining shells, which were collected from estuarine and mud-flat environments, Dodd and Crisp (1982) have shown that Mg/Ca and Sr/Ca ratios in estuarine waters only vary from ocean ratios at salinities below 10‰. *A. stutchburyi* are very sensitive to salinity; Marsden (2004) found that the

clams only survived 6 weeks in salinities down to 7‰ with high phytoplankton availability. At 14 ‰ salinity with low food availability, clams survived only 4 weeks. Therefore, it seems unlikely that *A. stutchburyi* were collected from estuaries and mud flats below the 10‰ salinity threshold because populations would not be sustained in that salinity environment.

The strong positive correlation with growth rate and strong negative correlation with ontogenetic age for both trace elements indicate that metabolic and physiological processes connected to the rate of mineralization and its decrease with age are the most dominant control on Mg/Ca and Sr/Ca ratios in *A. stutchburyi*. However, as growth rate and age correlations were not perfect it is likely that other influences affect the incorporation of Mg^{2+} and Sr^{2+}, and have some signal in the Mg/Ca and Sr/Ca records.

For the Ligar Bay 3B and Ligar Bay 4B shells that an annual chronology was constructed for, Mg/Ca and Sr/Ca ratios were compared to a satellite sea surface temperature (SST) record for Golden Bay, the larger, open bay in which Ligar Bay is located. Mg/Ca and Sr/Ca ratios were evenly spread between annual growth points (set to July of each year when growth bands were formed), which assumes a constant growth rate within increments. Calendar months are included on the time series graphs; although as discussed in section 4.1 above, data points were not resolved to this level and the months are extrapolated from the annual chronology.

The comparison of the Ligar Bay 4B and Ligar Bay 3B Mg/Ca and Sr/Ca records with SST (Figures 4.10 and 4.11, respectively) did not reveal an obvious relationship between the TE/Ca ratios and temperature. There was occasionally a visible positive correlation between SST and Mg/Ca and Sr/Ca ratios in the records between July-August when the ratios and SST each decreased; twice in Ligar Bay 4B, and four times in Ligar Bay 3B years (shown on Figures 4.9 and 4.10 by vertical dashed lines). Also,

between July 2005 and July 2006 Mg/Ca in the Ligar Bay 3B record appeared to show a seasonal pattern mimicking the SST record. Apart from these observations the Ligar Bay 3B and Ligar Bay 4B Mg/Ca and Sr/Ca records did not show seasonal variations with SST, and were dominated by the ontogenetic decrease in TE/Ca ratios.

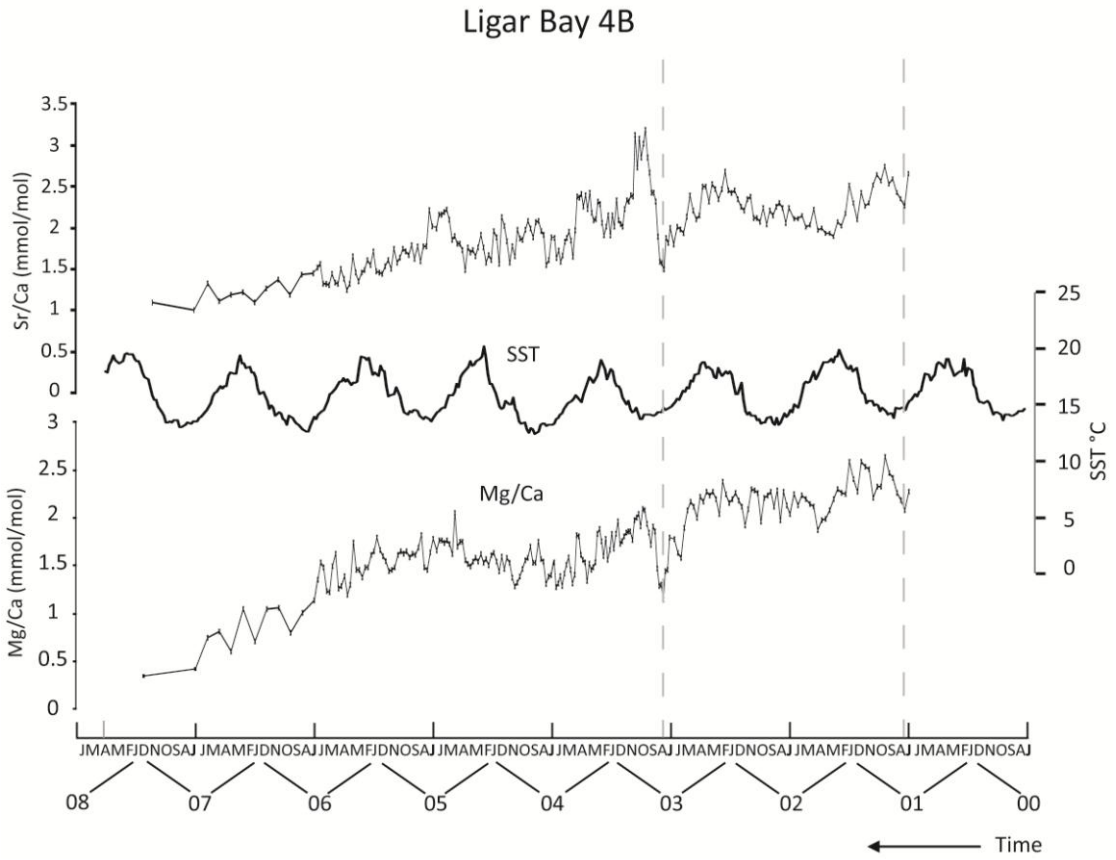

Figure 4.10 Mg/Ca (mmol/mol) and Sr/Ca (mmol/mol) records from Ligar Bay 4B plotted against time (running right to left). The plot assumes a constant growth rate between annual increments (from July to July – marked as black lines on the timescale). Years (2000-2008) are indicated by 00-08. Grey lines indicate where potential positive correlations exist between SST, Mg/Ca and Sr/Ca.

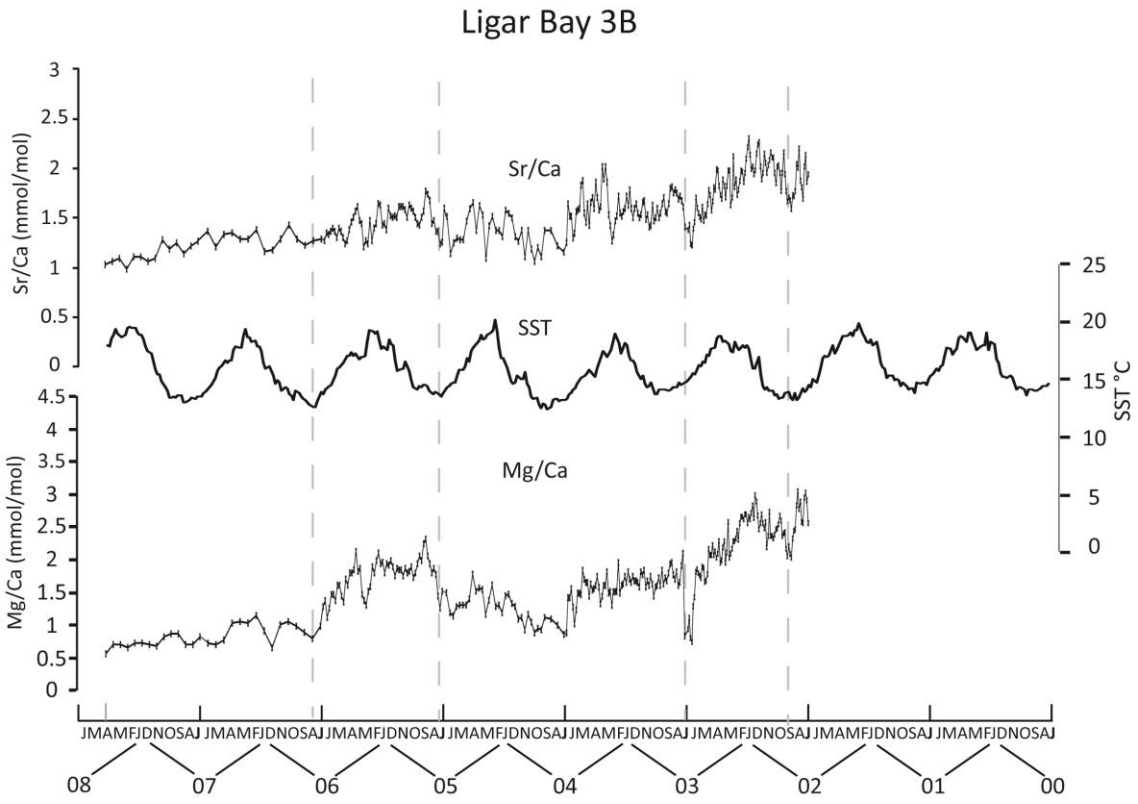

Figure 4.11 Mg/Ca (mmol/mol) and Sr/Ca (mmol/mol) records from Ligar Bay 3B plotted against time (running right to left). The plot assumes a constant growth rate between annual increments (from July to July – marked as black lines on the timescale). Years (2000-2008) are indicated by 00-08. Grey lines indicate where potential positive correlations exist between SST, Mg/Ca and Sr/Ca.

Schöne et al. (2011) attempted to mathematically eliminate the growth rate and ontogenetic effect on Mg/Ca and Sr/Ca records to test whether the remaining signal was correlated to SST. This consisted of detrending the data by dividing actual TE/Ca ratios by 'predicted' TE/Ca ratios; calculated from the linear regressions made between TE/Ca ratios and growth rate and ontogenetic age. The resulting values were then standardised: the mean of the values was subtracted from each value and they were then divided by the standard deviation of the actual/'predicted' values. This produced dimensionless measures of TE/Ca ratios. When compared to SST the detrended Mg/Ca and Sr/Ca data showed an inverse correlation to temperature (Sr/Ca r^2 = -0.64 and Mg/Ca r^2 = -0.52), whereas the original TE/Ca records had shown no correlation. This method was applied

to Mg/Ca and Sr/Ca ratios in the Ligar Bay 3B record. Ages (measured in days before death) were calculated for each ratio by extrapolating between the annual data points. The results for Sr/Ca are shown below in Figure 4.12, and demonstrate that age detrending removes the ontogenetic decrease from the records, but does not reveal any new patterns of variation, which remains the same as in the original Sr/Ca record. This was also the case for Mg/Ca ratios, not shown.

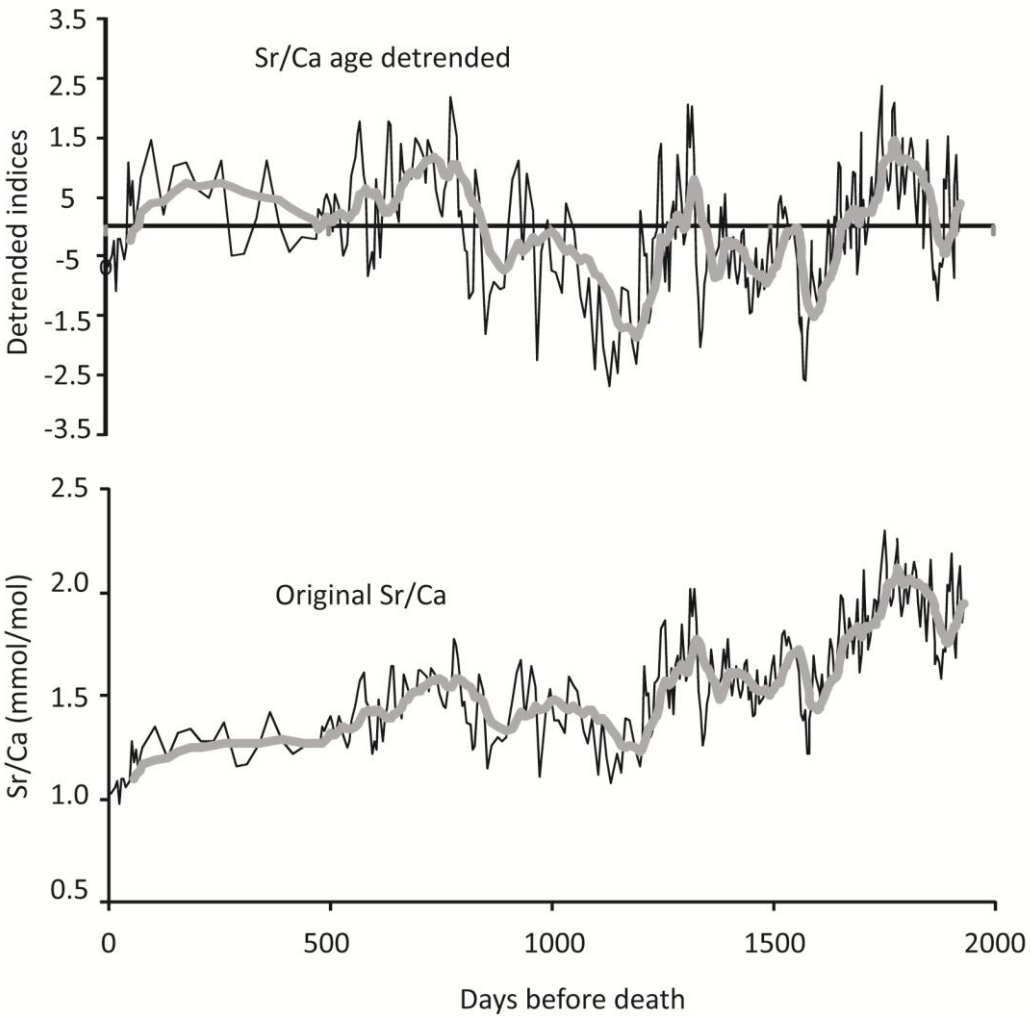

Figure 4.12 Black lines: Comparison of age-detrended Sr/Ca indices to original Sr/Ca ratios (mmol/mol) from Ligar Bay 3B. All data are plotted against the age of the shell (days before death). Grey Lines: 10 point moving average of age detrended and original Sr/Ca data.

The effect of growth rate could not be eliminated from the Ligar Bay 3B and Ligar Bay 4B Sr/Ca and Mg/Ca records following the method by Schöne et al. (2011) because there was no precise growth rate data available for all the ratios. Therefore, to remove growth rate, Mg/Ca records from Ligar Bay shells were normalised to Sr/Ca, on the basis that Sr/Ca was most highly correlated to growth rate (see section 4.2.1 above). This was done by subtracting the actual Mg/Ca ratios from predicted Mg/Ca ratios – which were calculated from linear regression of the Mg/Ca and Sr/Ca data. Plotted in time series, the Ligar Bay 4B normalised Mg/Ca record appeared visually to positively correlate with SST in at least two annual increments (Figures 4.14-4.15). Ligar Bay 3B, did not show any visual correlation (Figure 4.13).

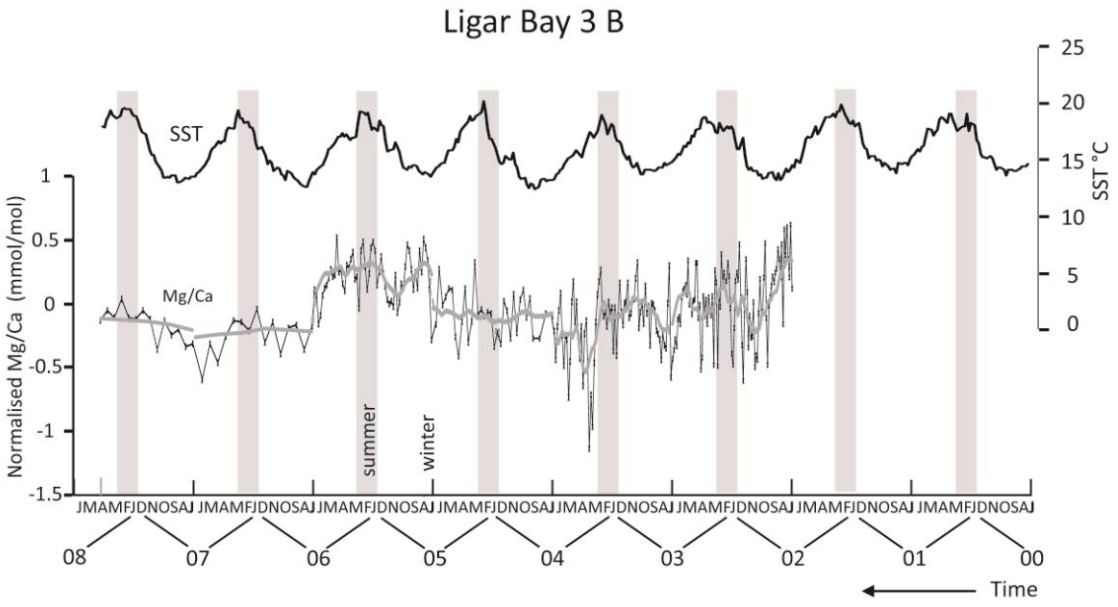

Figure 4.13 Mg/Ca ratios normalised to Sr/Ca from Ligar Bay 3B plotted against time (running right to left). The plot assumes a constant growth rate between annual increments (from July to July – marked as black lines on the timescale). Years (2000-2008) are indicated by 00-08.

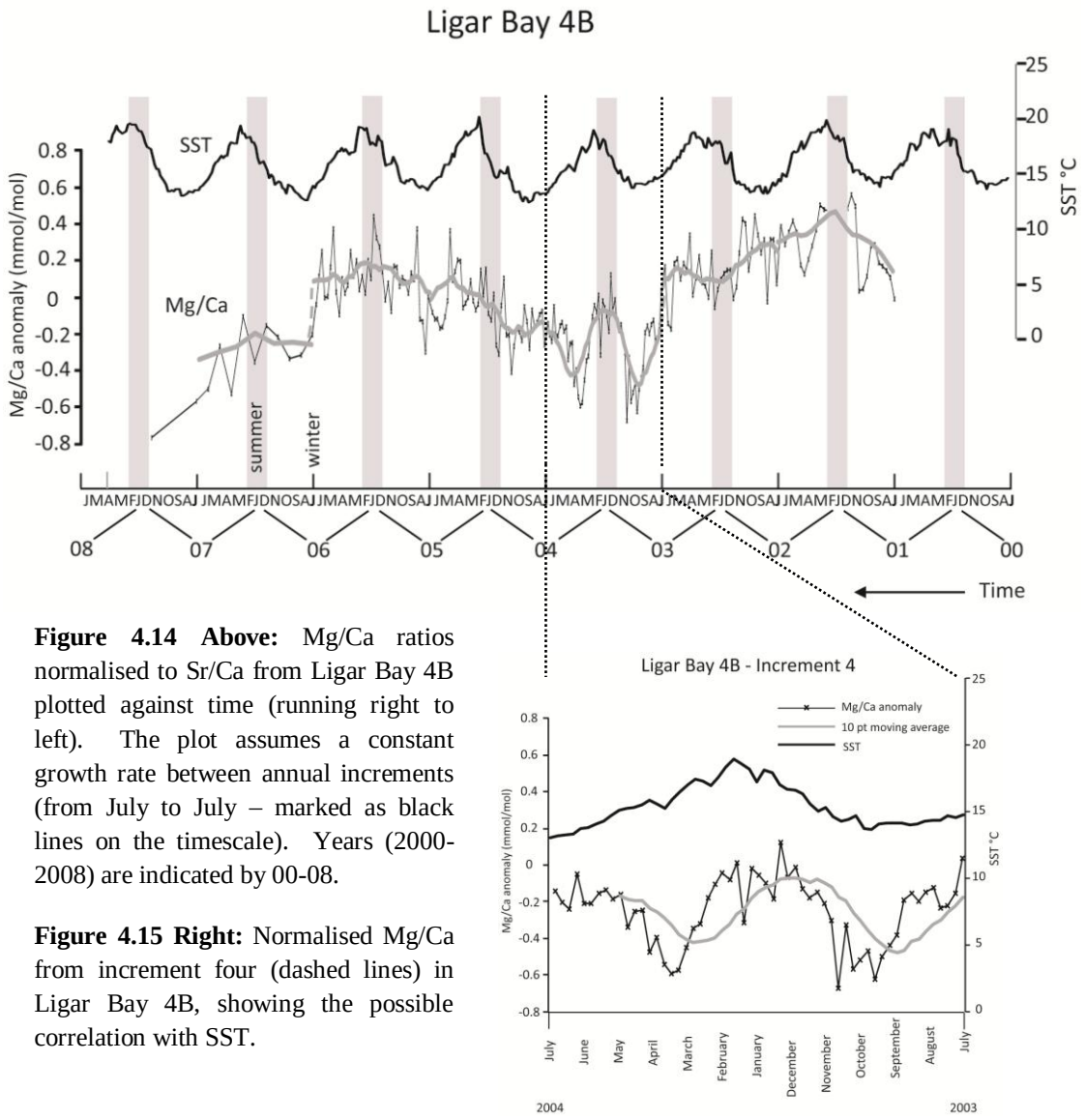

Figure 4.14 Above: Mg/Ca ratios normalised to Sr/Ca from Ligar Bay 4B plotted against time (running right to left). The plot assumes a constant growth rate between annual increments (from July to July – marked as black lines on the timescale). Years (2000-2008) are indicated by 00-08.

Figure 4.15 Right: Normalised Mg/Ca from increment four (dashed lines) in Ligar Bay 4B, showing the possible correlation with SST.

In particular, Mg/Ca ratios in increment four (Figure 4.15) seemed to follow SST. However, matching temperatures with normalised ratios only yielded a correlation coefficient of 0.012; thus no relationship was verified.

Overall, the results of this study appear to demonstrate that there is little thermodynamic dependence on the incorporation of Mg^{2+} or Sr^{2+} into *A. stutchburyi* aragonite, as the incorporation in aragonite of both ions should be inversely dependent on temperature based on inorganic studies (Kinsman and Holland, 1969; Dietzel et al., 2004; Gaetani

and Cohen, 2004). The only potential correlations with SST observed were positive. This may indicate that temperature has an indirect influence on the incorporation of Mg^{2+} or Sr^{2+}. It is possible that an indirect temperature effect would occur via the positive influence of temperature on *A. stutchburyi* growth rate, which itself had a significant positive correlation with Sr/Ca and Mg/Ca ratios (Stecher et al., 1996; Gillikin et al., 2005). McKinnon (1996) observed a strong positive relationship between *A. stutchburyi* growth rate and temperature in individuals from Dunedin (Figure 4.16). The temperature-growth rate relationship could explain the corresponding decreases in SST and Mg/Ca and Sr/Ca ratios observed during July-August as there is a slowdown in growth rate as temperatures cool.

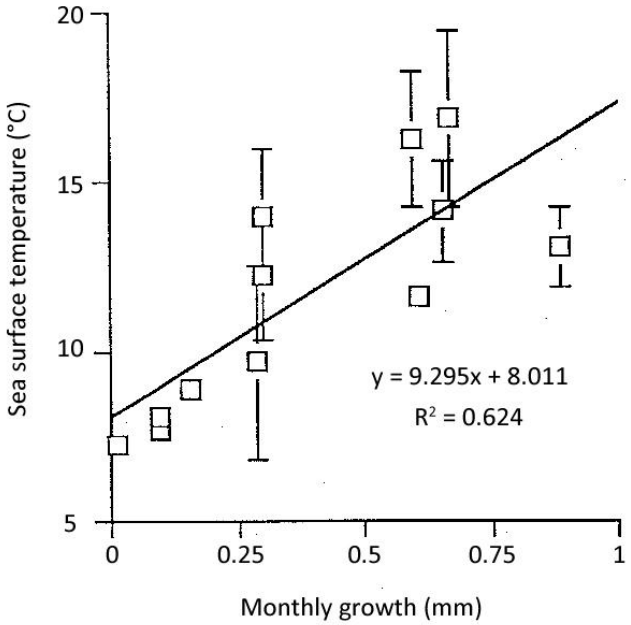

Figure 4.16 Correlation between growth rate (mm/month) and sea-surface-temperature for *A. stutchburyi* from Post Chalmers, Dunedin. Figure taken from McKinnon (1996).

Another possibility is that variations in *A. stutchburyi* shell architecture are responsible for some of the observed variations in Mg/Ca and Sr/Ca ratios in the horizontal transects. As the percentage of organic material (intra- and extra-crystalline) in the shell increases over annual growth bands, the amount of Mg^{2+} and Sr^{2+} incorporated in the shell could vary because of the different hosting properties of the organic

component compared to the mineral ($CaCO_3$) component (Vander Putten et al., 2000; Schöne et al., 2011; Foster et al., 2008). A preliminary study by Foster et al. (2008) using X-ray Absorption Near Edge Spectroscopy (XANES) on *Arctica islandica* aragonite found that Mg^{2+} was not hosted by the aragonite at all, but rather was bound to organic intra- or extra-crystalline component of the shell, which caused an increase in Mg/Ca near growth checks. Schöne et al. (2011), utilising LA-ICP-MS, observed higher Mg/Ca ratios over organic growth checks in *A. islandica*, but also found that Sr/Ca (which is hosted in aragonite) peaked in the aragonite component adjacent to the growth checks. Vertical variations in shell architecture in *A. stutchburyi* certainly affect TE/Ca ratios - as observed from LA-ICP-MS transects taken down single growth lines (Chapter 3, section 3.1). These variations occur because with distance through the *A. stutchburyi* shell, microstructure of the $CaCO_3$ crystals changes from crossed lamellar to homogeneous. Further high-resolution analysis (microprobe or XANES) is required to investigate how, if any, horizontal variations in *A. stutchburyi* shell architecture affect Sr/Ca and Mg/Ca ratios.

Finally, Mucci and Morse (1983) proposed that Mg^{2+} might directly affect the substitution of Sr^{2+} in aragonite or calcite (Chapter 1). Across the entire dataset, Mg/Ca and Sr/Ca ratios were well correlated, with a sensitivity of almost 1 for many linear regressions. However, both TE/Ca ratios are also significantly correlated to growth rate, with Sr/Ca ratios having a slightly higher correlation. On this basis, Sr^{2+} is probably not driven by Mg^{2+} incorporation, although more accurate growth rate determinations would be needed to confirm this conclusion.

4.2.4 Ba/Ca ratios

Ba/Ca ratios ranged between 0.00-0.046 mmol/mol across the analysed *A. stutchburyi* shells. Studies on both calcitic and aragonitic bivalves have reported background Ba/Ca ratios between 0.0005-0.0015 mmol/mol, interspersed with peaks between 0.004-0.045 mmol/mol (Elliot, 2009; Stecher et al., 1996; Gillikn et al., 2006). The overall range in *A. stutchburyi* Ba/Ca ratios is comparable to these reported ranges; however, very low (<0.0015 mmol/mol) 'background' Ba/Ca ratios were not prevalent in *A. stutchburyi* Ba/Ca records. Rather, for each shell, the majority of Ba/Ca ratios were >0.002 mmol/mol, and followed the same pattern as Mg/Ca, Sr/Ca, Mn/Ca and U/Ca ratios (Chapter 3). Transient peaks in Ba/Ca, which were not matched by similar peaks in the other TE/Ca records, were superimposed on these patterns. Peak amplitudes varied between individuals at different sites, and between the individuals at Ligar Bay; peaks reached 0.017, 0.025 and 0.46 mmol/mol in the Ligar Bay 1B, Kaiaua, and Ligar Bay 4B shells, respectively.

The shells with the highest Ba/Ca peaks had the poorest Ba/Ca correlations with other TE/Ca ratios - Mg/Ca, Sr/Ca, Mn/Ca and U/Ca. For example, while correlation coefficients for Ba/Ca-Mg/Ca were >0.41 for all other shells, for Ligar Bay 3B and Ligar Bay 4B, which both contained similar 3-point peaks up to 0.46 and 0.39 mmol/mol, correlation coefficients were only 0.19 and 0.05, respectively. Excluding the large 3-point Ba/Ca peak from the Ligar Bay 3B data yielded a correlation coefficient of 0.78 between Sr/Ca and Ba/Ca, and from Ligar Bay 4B data gave a correlation coefficient of 0.59 between Sr/Ca and Ba/Ca. Growth rate correlations with Ba/Ca ratios in the Ligar Bay shells were significant ($r^2 = 0.60$ for the Ligar Bay shells combined). Despite having large Ba/Ca peaks, even the individual Ligar Bay 3B Ba/Ca correlation with growth rate was strong ($r^2 = 0.89$), although the increment that included

the large Ba/Ca peak was the most offset from the linear regression. Ba/Ca ratios in the Ligar Bay shells were also significantly correlated with ontogenetic age (correlation coefficients between 0.61 – 0.96).

There has been speculation over the influences on 'background' Ba/Ca ratios and what factors cause the Ba/Ca peaks observed in mollusc shells (Lazareth, 2003; Gillikin et al., 2006; Takesue et al., 2008; Gillikin et al., 2008). It has been suggested that background Ba/Ca ratios are controlled by dissolved Ba, and thus are a proxy for salinity in estuaries (Gillikin et al., 2006; Gillikin et al., 2008). However, based on the significant correlation with growth rate and ontogenetic age it is argued here that 'background' Ba/Ca ratios (i.e. all ratios excluding the peaks where Ba/Ca record varies from other TE/Ca ratios) in *A. stutchburyi* are predominantly controlled by these biological effects. This is supported by the significant correlations between Ba/Ca and Sr/Ca ratios, which are stronger when Ba/Ca peaks are excluded, and as discussed above, Sr/Ca ratios are strongly growth rate dependent. Carré et al. (2006) found in *M. donacium* that Ba/Ca ratios (including peaks) correlated with calcification rate; with a higher correlation coefficient ($r^2 = 0.72$) when Ba/Ca ratios were on a log scale, suggesting perhaps a non-linear relationship. Takesue et al. (2008) also noticed a relationship between growth rate and Ba/Ca ratios by comparing the faster growing to the slower growing valve of *C. amurensis* shells. Further, Elliot et al. (2009) observed it was unlikely that background Ba/Ca ratios in *T. gigas* were directly controlled by the amount of dissolved Ba/Ca in seawater, because the Ba/Ca ratios required at the particular locations in San Francisco Harbour were not realistic for the background Ba/Ca ratios incorporated in the shells. Nevertheless, variations in dissolved seawater Ba/Ca cannot be ruled out as an influence for the Ba/Ca records observed in *A. stutchburyi*, at least to some extent. Ba/Ca ratios for Ligar Bay 3B were normalised against Sr/Ca ratios, using the method described for Mg/Ca ratios in the previous section, with the linear regression for Sr/Ca and Ba/Ca

excluding the Ba/Ca 3-point peak (r^2 = 0.78). The normalised Ba/Ca ratios show variations that were not present in the Ba/Ca record before eliminating the growth rate effect (Figure 4.17). Measurements of seawater Ba/Ca would be required however to produce a partition coefficient and test the relationship.

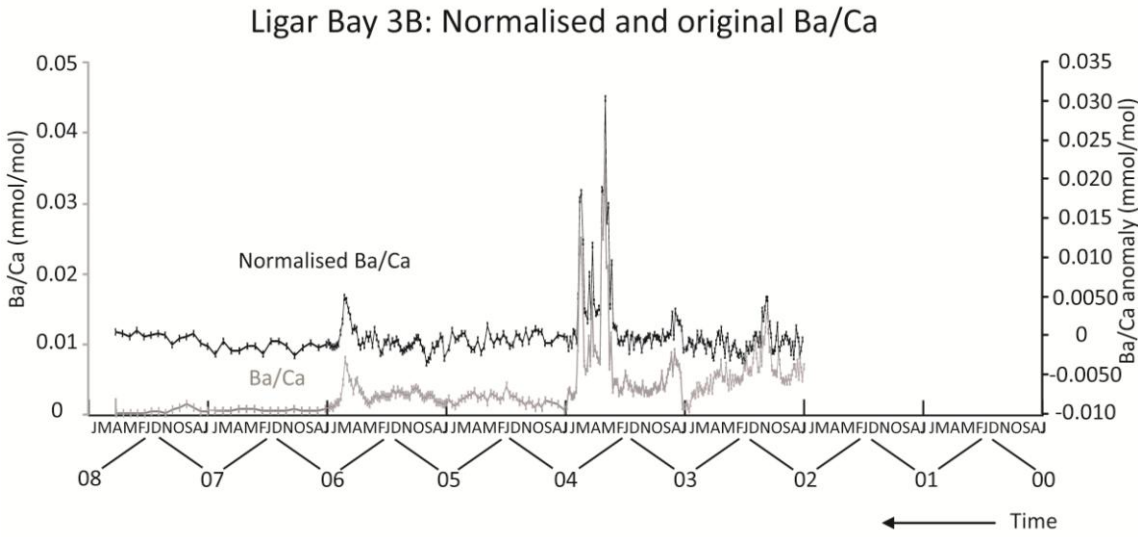

Figure 4.17 Ba/Ca ratios from Ligar Bay 3B (grey line), compared to Ba/Ca ratios from Ligar Bay 3B after being normalised to Sr/Ca (black line). Constant growth rate is assumed within each annual increment (July-June)

Ba/Ca peaks are most often associated with seasonal chlorophyll increases (Vander Putten et al., 2000; Lazareth, 2003; Gillikin et al., 2008). Elliot et al. (2009) found that peak Ba/Ca ratios observed in the giant-bivalve *Tridacna gigas* from the Indo Pacific Ocean correlated strongly with local chlorophyll maxima, (background Ba/Ca ratios and chlorophyll data plotted along a separate linear regression). The timing of Ba/Ca peaks with chlorophyll maxima indicated that increased primary productivity was the main cause of the peaks; although the factors controlling the chlorophyll maxima at each site studied varied significantly (at Cocos Island chlorophyll maxima occurred in winter compared to Palm Island when the maxima occurred in summer in response to increased rainfall providing nutrients to phytoplankton). Chlorophyll levels vary seasonally in Golden Bay in response to seasonal stratification of the water column, which is

primarily influenced by surface warming and nutrient input from rivers (Gall and Zeldis, 2003). At Ligar Bay in the southeastern region of Golden Bay chlorophyll peaks in springtime, according to 2001-2002 data (Figures 4.18-4.19). It is likely that these significant seasonal variations and peaks would be recorded in the Ligar Bay shells if Ba/Ca in *A. stutchburyi* is sensitive to chlorophyll levels. Alternatively, Ba/Ca peaks could be caused by an increase in dissolved Ba in seawater, potentially brought by river discharge in a flood (Torres et al., 2001); although Elliot et al. (2009) have pointed out that the levels of dissolved Ba required are unrealistically high given the range of the peak Ba/Ca ratios in bivalves. More information on dissolved Ba in Golden Bay, and its sources, is necessary.

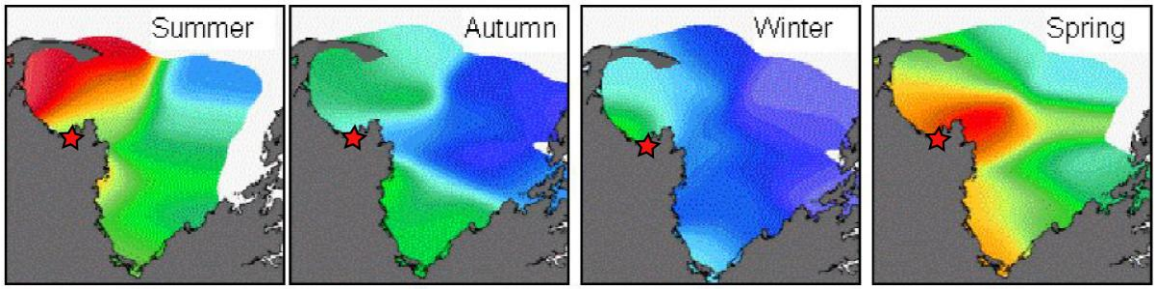

Figure 4.18 Maps of chlorophyll (phytoplankton abundance) across Golden Bay for summer, autumn, winter and spring 2001-2002. Red star shows the location of Ligar Bay. Colours represent average chlorophyll abundance from near surface to the sea bed. Low chlorophyll is shown in blue, increasing through green, to yellow, with the highest values in red. Figure taken from Gall and Zeldis (NIWA, 2003).

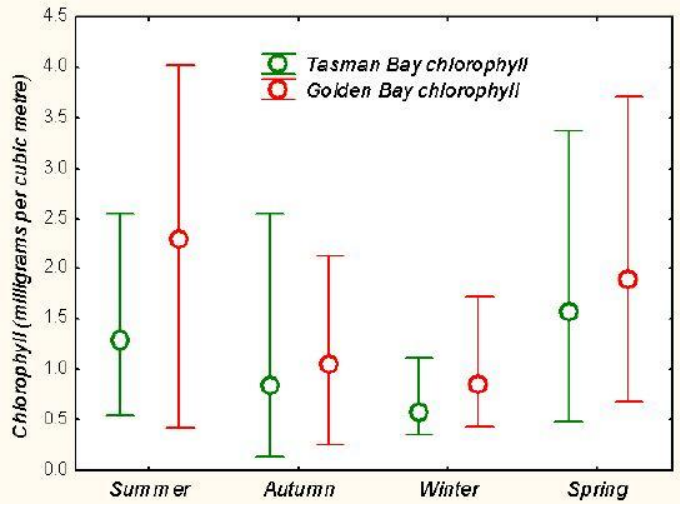

Figure 4.19 Average chlorophyll concentrations in each season of 2001-2002. Golden Bay has red circles. Bars show the maximum and minimum values. Figure taken from Gall and Zeldis (NIWA, 2003).

No quantitative chlorophyll record was available for the life span of the *A. stutchburyi* in Ligar Bay, but Ba/Ca ratios from Ligar Bay 3B and Ligar Bay 4B were put on a timescale and compared to monthly total rainfall from the nearest NIWA weather station in Takaka (Figure 4.20). The figure shows the shortcomings of the chronology developed for Ligar Bay 3B and Ligar Bay 4B, and the limitation in assuming constant growth rate between annual increments. For example, the large red circle shows where smaller peaks (0.01 mmol/mol) in each record are mismatched at the end of the record. Even so, on an annual level the 3-point peaks do not appear to correlate with a major increase in rainfall in 2003-2004, although the monthly total of rainfall might have averaged out extreme, short timescale (e.g. daily) events.

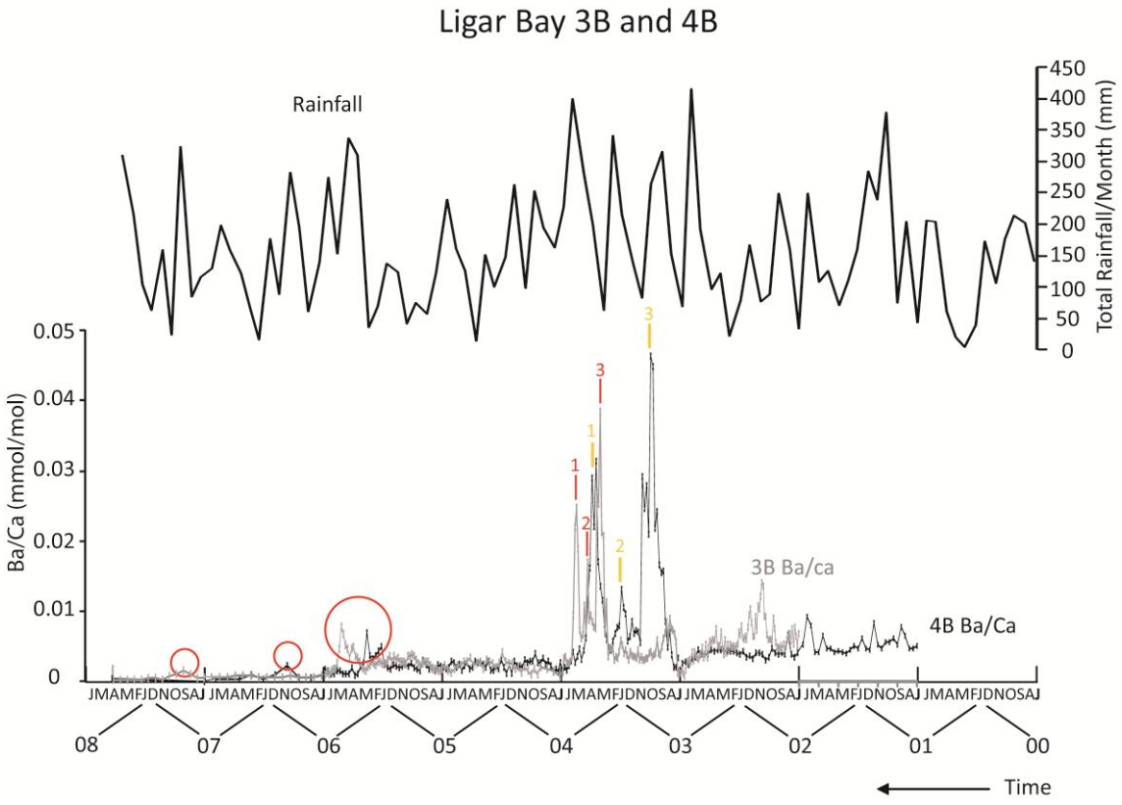

Figure 4.20 Ba/Ca ratios from Ligar Bay 3B (grey) and Ligar Bay 4B (black). Thick black line shows total monthly rainfall for July 2000-April 2008, when *A. stutchburyi* shells were collected. Yellow numbers denote the peak number on the 3-point peak in Ligar Bay 4B. Red numbers denote the peak number of the 3-point peak in Ligar Bay 3B. Large red circle shows the peak (0.01 mmol/mol, in 2006) that should correlate if the time scale was aligned correctly. Small red circles show a smaller peak in each record that is potentially the same feature, and should also be aligned.

If the cause of the peaks was seasonal chlorophyll increases, the peaks should be periodic, as has been seen in Ba/Ca peaks linked to phytoplankton blooms (Vander Putten et al., 2000; Gillikin et al., 2008). In Ligar Bay 3B and Ligar Bay 4B the large 3-point peak is unique, and there is no periodicity of peaks. There did not appear to be periodic peaks, which could be formed annually, in the Ba/Ca records for the other *A. stutchburyi* analysed in this study (Chapter 3). It is also unclear why only these two shells from Ligar Bay contain such large peaks; the peaks in Ligar Bay 1B and Ligar Bay 6B are an order of magnitude lower. It is not possible to make comprehensive interpretations without a more highly resolved chronology and chlorophyll and rainfall data to compare the Ba/Ca ratios directly with (e.g. Figure 4.21). However, the similarity between the Ligar Bay 3B and Ligar Bay 4B 3-point peaks do appear to demonstrate that an environmental process is responsible for Ba/Ca peaks rather than an endogenous one in response to spawning (postulated by Gillikin et al., 2008): the synchronicity required to produce the particular 3-point shapes, spread as they were over different widths in each shell, seems very unlikely.

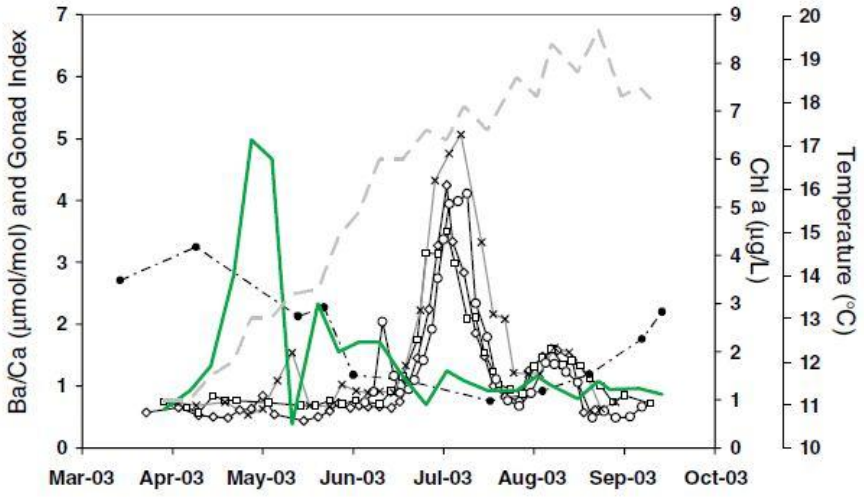

Figure 4.21 Synchronous Ba/Ca ratio peaks in three *Pecten maximus* shells. The solid green line is chlorophyll a, and the dashed grey line water temperature. The dashed black line and solid black symbols are the gonad index (representative of spawning). The high-resolution timescale of the Ba/Ca data allows from a direct comparison with chlorophyll, which reveals a delay between chlorophyll maxima and Ba/Ca peaks. Figure taken from Gillikin et al. (2008).

4.2.5 Mn/Ca and U/Ca ratios

The range in Mn/Ca ratios across *A. stutchburyi* shells was 0-1.56 mmol/mol. Mn/Ca ratios were mostly strongly correlated to Mg/Ca, Sr/Ca, Ba/Ca and U/Ca with the notable exception of the Ligar Bay shells, which contained average Mn/Ca ratios an order of magnitude lower than shells from all other sites (Chapter 3). However, even though Mn/Ca was poorly correlated with Sr/Ca in Ligar Bay 3B and Ligar Bay 4B, there was strong correlation between Mn/Ca ratios and growth rate (r^2 = 0.72) and ontogenetic age (r^2 between 0.47-0.95) in both of these shells. This suggests that growth rate and ontogenetic age are the dominant control on Mn/Ca ratios in *A. stutchburyi*, regardless of Mn^{2+} source. Growth rate control is consistent with results obtained by Carré et al. (2006) on *M. donacium* and *C. subrogosa*, which had correlation coefficients between growth rate and Mn/Ca ratios varying between 0.53-0.74.

Fluctuations in Mn^{2+} may yet be responsible for the remaining variations in Mn/Ca ratios in *A. stutchburyi* shell. The amount of Mn^{2+} in seawater is linked to oxidation-reduction conditions, as well as phytoplankton blooms, as Mn is a redox sensitive element (Miao et al., 2006; Chapter 1). Variations observed in Mn/Ca ratios in *A. stutchburyi* indicate redox conditions might influence the chemistry of its shell. Firstly, the significant variation in average Mn/Ca ratios between the Ligar Bay shells and the remaining shells (Figure 4.22) could be explained by the redox conditions expected at the respective sites. Ligar Bay was the only site where *A. stutchburyi* were collected from an open beach, with medium-coarse grained sand (sourced from the Separation Point granite batholith - Muir et al., 1995). The clams were found below low tide on a sand bar; the exposure to wave action and permeable sediment would make this a relatively oxidising environment with low Mn^{2+} production. Conversely, the other sites

were estuaries (Kawhia) and tidal mud-flats (Miranda, Manakau, Bay of Islands), which provide an anoxic environment because of organic material, fine-grained impermeable sediment, and less water disturbance. The shell from Miranda, where it was necessary to walk over extensive mud-flats for several hundred metres to find *A. stutchburyi* at low tide, had the highest average Mn/Ca ratios. The Miranda transect also contained 3 large spikes in Mn/Ca, up to 1.55, 0.86 and 1.46 mmol/mol, the magnitude of which was not seen in any of the other shell Mn/Ca records (Figure 3.22). Secondly, there was significant variation between the Mn/Ca ratios in the Ligar Bay shell records and the Ligar Estuary Mn/Ca shell record (Table 4.2 shows results from a student-t test). This variation could well be caused by variation in Mn^{2+} production via redox, as aside from redox conditions, these sites should have similar environmental parameters (SST, source of riverine, particulate Mn) because of their close proximity.

	Ligar Estuary			
	Ligar Bay 1B	Ligar Bay 3B	Ligar Bay 4B	Ligar Bay 6B
t	-6.1	-7.69	-6.69	-6.14
SD	0.00159	0.0305	0.0337	0.0362
p	<0.0001	<0.0001	<0.0001	<0.0001

Table 4.2 Results from student-t test between Ligar Estuary and each Ligar Bay shell. P (probability) is less than 0.0001 for all tests.

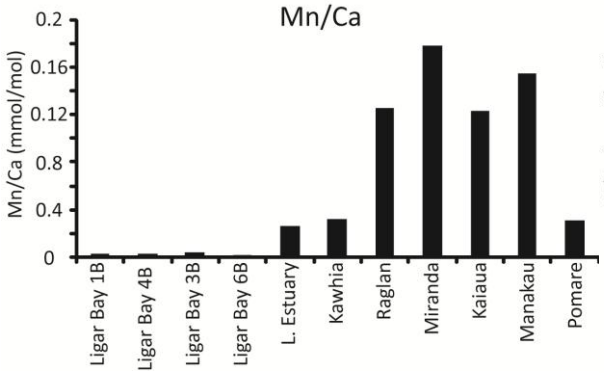

Figure 4.22 Average Mn/Ca ratios in each *A. stutchburyi* shell

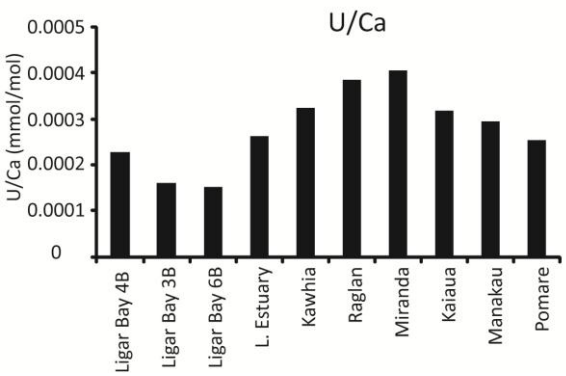

Figure 4.23 Average U/Ca ratios in each *A. stutchburyi* shell

It is difficult to eliminate the effect of growth rate from Mn/Ca ratios in the Ligar Bay 3B and Ligar Bay 4B shells so that the remaining variations can be plotted on a time series, because Sr/Ca does not correlate with Mn/Ca in these shells. If an improved chronology was constructed for the *A. stutchburyi* shells, it would enable high-resolution growth rate calculation, which could then be used to eliminate the physiological effects from the Mn/Ca data and further assess the Mn redox proxy potential.

Another possible influence on Mn/Ca ratios in *A. stutchburyi* are phytoplankton levels, which have been linked to peaks in Mn/Ca in other bivalve species (Vander Putten et al., 2000; Lazareth, 2003). As discussed above for Ba/Ca, chlorophyll variations are expected in the Ligar Bay region, and thus may transmit to Mn/Ca variations in *A. stutchburyi* shells. Where Mn/Ca ratios have been linked to chlorophyll maxima (caused by phytoplankton blooms) the Mn/Ca records have shown similar periodic peaks to Ba/Ca peaks described above (e.g. Figure 4.25). There were only several *A. stutchburyi* shells that showed peaks comparable to these on top of the pattern followed by Mg/Ca and Sr/Ca – Ligar Bay 1B, Ligar Bay 3B, Pomare and Miranda, although peaks were an order of magnitude higher at Miranda (Chapter 3). The periodicity of the peaks in Ligar Bay 1B, Ligar Bay 3B and Pomare shells could potentially be seasonal (Figure 4.24). However, a high resolution chronology, and real-time chlorophyll measurements would be required to discover whether the peaks are synchronous with chlorophyll maxima, to assess whether Mn/Ca in *A. stutchburyi* is related to phytoplankton availability.

A further factor to consider is the relative amounts of organic material and mineral component in the shell. Takesue et al. (2008) found in aragonitic *C. amurensis* bivalves that the component of Mn that was non-lattice-bound (i.e. bound to organic

material) equated to 78%. Therefore variations in Mn/Ca observed in aragonitic *A. stutchburyi* might not reflect Mn substitution into $CaCO_3$, and this could have implications for the use of Mn/Ca as an environmental proxy.

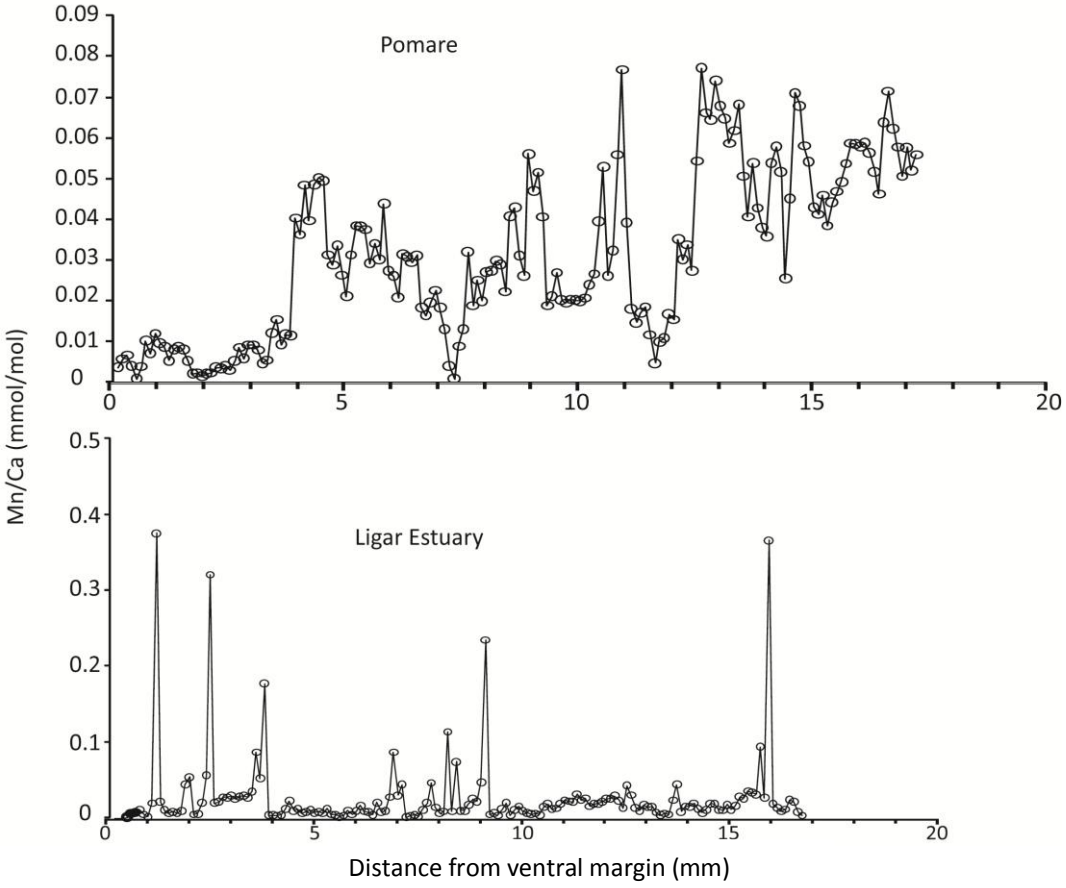

Figure 4.24 Mn/Ca records from Pomare and Ligar estuary, showing spikes in Mn/Ca.

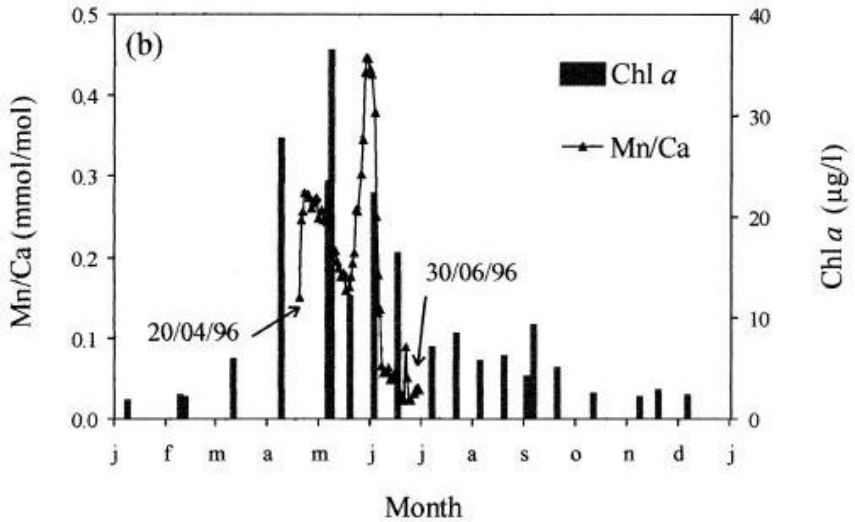

Figure 4.25 Mn/Ca profiles in the calcite shell layer of a *M. edulis* compared to measured chlorophyll *a* concentrations. The shell grew from the 20th April 1996 until the 30th June 1996; the data points correspond to shell formed during this period. Arrows indicate the moment of transplantation and the moment when the mussel was removed from the transplantation site. Figure taken from Vander Putten et al. (2000).

U/Ca ratios ranged between 0-0.0013 mmol/mol in *A. stutchburyi*. As with Mn/Ca, U/Ca was generally strongly correlated with the other TE/Ca ratios (Mn/Ca, Mg/Ca, Ba/Ca and Sr/Ca); with some exceptions for the Ligar Bay shells and Ligar Estuary shell (Chapter 3). Both growth rate and ontogenetic age were significantly correlated with U/Ca ratios in the Ligar Bay shells (r^2 = 0.63 and between 0.61-0.92, respectively). Therefore, it is thought these two effects are also the dominant control on U incorporation in *A. stutchburyi*.

As U is also a redox-sensitive element, and accumulates in anoxic, organic-rich marine sediments (Barnes and Cochran, 1991; Morford et al., 1999; Bots and Behrends, 2008) it is possible that remaining U/Ca variations could be influenced by redox conditions. Two of the same observations seen in the average Mn/Ca ratios applied to the average U/Ca ratios – the Ligar Bay shells contained the lowest U/Ca ratios, and Miranda the highest. However, the Ligar Bay U/Ca ratios are broadly the same as shells from the other sites, and intermediate to the Miranda and Ligar Bay shells, the average U/Ca ratios of the other sites do not follow the same order as for Mn/Ca (Figure 4.23 - average U/Ca ratios, above). Nevertheless, the similarities between U/Ca and Mn/Ca ratios; with Ligar Bay and Miranda; and the lower correlations with other TE/Ca ratios at the oxic Ligar Bay site, potentially suggest a redox link to the variations in these TE/Ca ratios and the possibility that their record could be a proxy for redox conditions. Further investigation is needed including constructing high-resolution chronologies for *A. stutchburyi* and measurements of redox conditions from the clams' environment, so that U/Ca records can be directly compared to them.

4.2.6 As/Ca, Zn/Ca and Cu/Ca ratios

These metals were noticeably elevated in the Ligar Bay shells and Ligar Estuary shell compared to the other shells, which may indicate more pollution at this site – potentially from a cement works in the neighbouring bay. It should be noted, however, that throughout the transects, As/Ca, Zn/Ca and Cu/Ca ratios were often 0.00, because the sample signal was relatively low for these low concentration metals (Chapter 3). It was important to assess the control growth rate and ontogenetic age had on the incorporation of these metals – as it significantly affects the potential to use these TE/Ca ratios as tracers of pollution. Growth rate appeared to have an insignificant influence on As/Ca and Cu/Ca ratios, with correlation coefficients of 0.29 and 0.20 respectively. Growth rate had a larger influence on Zn/Ca ratios, with a correlation coefficient of 0.49. Ontogenetic age differed from growth rate – with As/Ca ratios appearing to be most strongly influenced by age (r^2 = 0.51), and Zn/Ca and Cu/Ca not showing any correlation (correlation coefficients of 0.052 and 0.0024 respectively). Although the effect of ontogenetic age was not quantified for *A. stutchburyi* outside of Ligar Bay, the decreasing trend was noticeable in the Pomare and Kawhia As/Ca records (Figure 4.26). Figure 4.26 illustrates how the decrease in As/Ca of all Ligar Bay shells could be interpreted as an environmental change, but given the similar ontogenetic trend of some of the other shells from different sites (Pomare, Kaiaua), it is more likely a biological change in As/Ca incorporation.

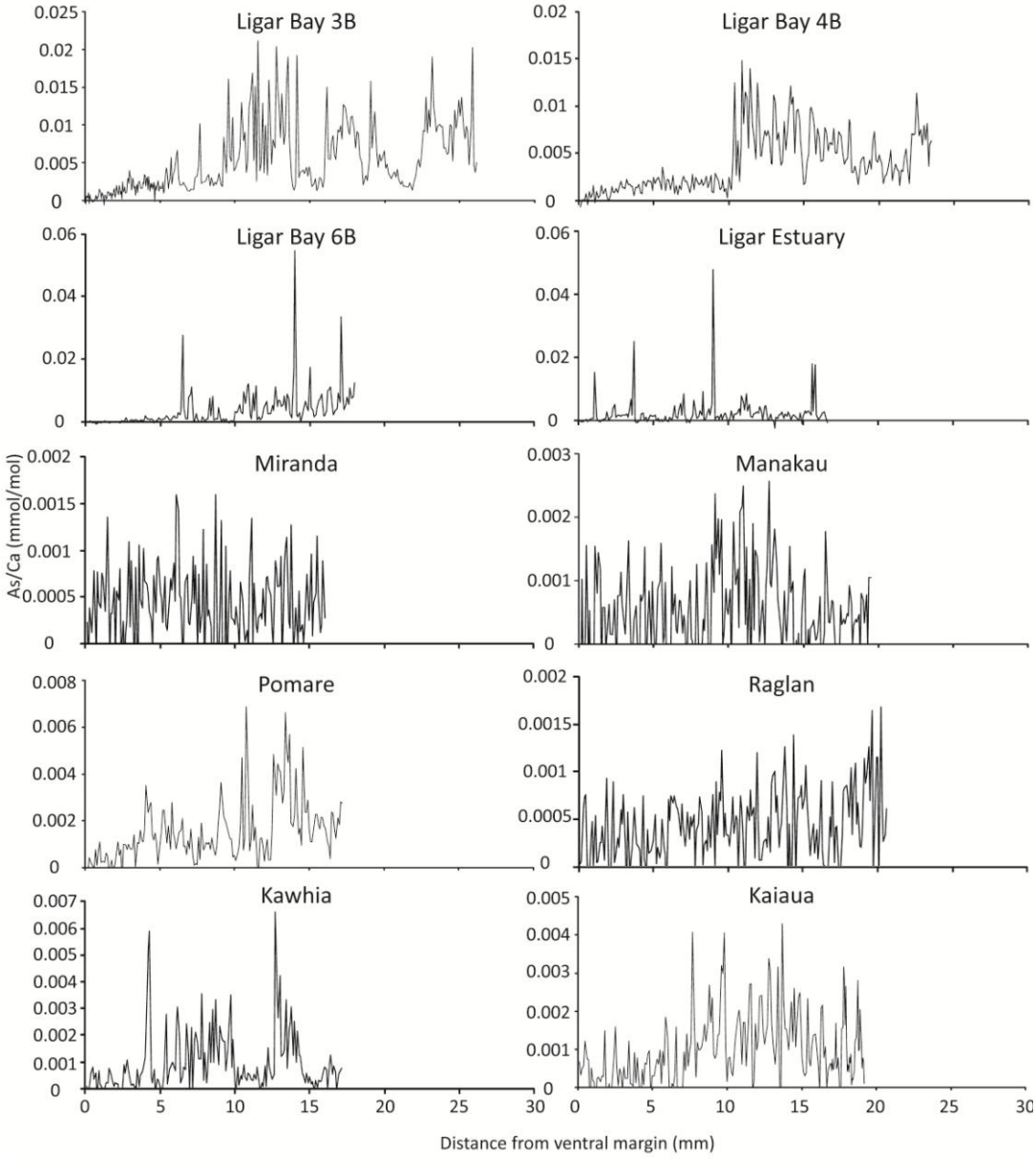

Figure 4.26 As/Ca records from all shells (except Ligar 1B where As was not measured), plotted against distance from the ventral margin.

4.3 Summary and comparison to other molluscan studies

The Mg/Ca and Sr/Ca results obtained for *A. stutchburyi* appear to be consistent with other trace element studies of molluscs produced so far that have found the incorporation of those trace elements into aragonite and calcite is not governed by thermodynamics (Table 4.3-4.4). In a few instances where Mg/Ca and Sr/Ca did appear to follow SST (e.g. coincidence of minima) this is possibly due to an indirect temperature influence through positive correlation of SST and *A. stutchburyi* growth rate. This relationship has also been postulated for *M. edulis* (Dodd, 1965) and *P. maximus* (Freitas et al., 2006). Growth rate and ontogenetic age appear to be the dominating control on Mg/Ca and Sr/Ca ratios in *A. stutchburyi*.

These biological effects also appear to be the primary control on Ba/Ca, Mn/Ca and U/Ca ratios in *A. stutchburyi*. The range in Ba/Ca ratios found in *A. stutchburyi*, fit within the range observed in other bivalves (argonitic and calcitic), which was suggested by Gillikin et al. (2008) to indicate a strong biological control on Ba^{2+} incorporation (as differences would otherwise be expected between the species and the two polymorphs of $CaCO_3$). Very low background Ba/Ca ratios (<0.0015 mmol/mol) were not typical in *A. stutchburyi* and the "background" variation in the clam, as stated, was correlated with growth rate and ontogeny. However, the characteristic peaks seen in Ba/Ca shell records were superimposed on effects driven by growth rate variation. The identical 3-point Ba/Ca peaks in the Ligar Bay 3B and Ligar Bay 4B shells are the best example of these features; and are most likely caused by an environmental process (phytoplankton blooms or elevation of dissolved Ba^{2+} from flooding) rather than being related to Ba availability during the clam's reproductive cycle (Gillikin et al., 2008). Large scale variations in Mn/Ca and U/Ca ratios seem to be associated with the redox conditions in the clams' habitat – Miranda (anoxic) and Ligar Bay (oxic). This has been

found for Mn/Ca ratios in *P. maximus* by Freitas et al. (2006), although U/Ca does not appear to have been considered in previous studies. Nonetheless, primary productivity cannot be ruled out as an influence for Mn/Ca ratios; as it has also been linked to sudden Mn/Ca peaks (Vander Putten et al., 2000), which were present in some *A. stutchburyi*.

4.3.1 Growth rate and ontogenetic trends

The strong correlations between growth rate and ontogenetic age with Mg/Ca, Sr/Ca, Mn/Ca, Ba/Ca and U/Ca ratios in *A. stutchburyi* are consistent with the increasing number of molluscan studies that have found physiological (ontogenetic age) and kinetic (growth rate) processes have a major control on trace element incorporation. However, there is no common trend between species studied as to whether growth rate and ontogeny increases or decreases trace element incorporation; nor is there a trend between aragonite and calcite mollusc shells. For example, in aragonitic *Tridacna gigas* (Elliot et al., 2009) and *Arctica islandica* (Schöne et al., 2011) and calcitic *Pinna nobilis* (Freitas et al., 2005), Mg/Ca ratios correlate negatively with growth rate and correlate positively with ontogenetic age; while in aragonitic *Protothaca staminea* (Takesue and van Geen, 2004), *Mesodesma donacium*, *Chione subrogosa* (Carré et al., 2006), *Saxidomus giganteus* (Gillikin et al., 2005), and calcitic *Mytilus edulis* (Vander Putten et al., 2000) and *Pecten maximus* (Lorrain et al., 2005) Sr/Ca ratios (and Mg/Ca, Mn/Ca and Ba/Ca ratios for *Mesodesma donacium*, *Chione subrogosa)* correlate positively with growth rate and negatively with ontogenetic age. Trace element incorporation in *A. stutchburyi* behaves similarly to the latter group of molluscs.

Heterogeneity between individuals from the same species, and within individual shells has also been reported for growth rate and ontogenetic age–TE/Ca trends (Schöne et al., 2011; Carré, 2006). For example, Carré et al. (2006) observed that the influence of

growth rate was stronger, and Sr/Ca ratios were higher in curved shell sections of *Mesodesma donacium*, *Chione subrogosa* than in flat, long sections. This formed part of Carré's (2006) reasoning for a third mechanism, driven by calcification rate, for Ca^{2+} (and Sr^{2+} and Ba^{2+}) ion transport through calcium channels, which allows different amounts of Sr^{2+} and Ba^{2+} to enter the EPF at specific locations depending on the channel density on cell membranes. Resolution of growth rate determination was not as high in the current study to observe this heterogeneity within *A. stutchburyi* and validate or negate this third mechanism of Ca^{2+} transport. However, as discussed above, the growth rate-TE/Ca ratio relationships found for Ligar Bay shells did vary between individuals, and the slow-growing Ligar Bay 6B shell having the weakest correlation with growth rate and ontogenetic age supports the suggestion by Carré et al. (2006), that slow growing individuals are not strongly affected by the calcium channel model.

Finally, Schöne et al. (2011) argued that further analyses of short-lived bivalves, including individuals from different habitats, was required to prove that environmental fluxes with a greater period than the bivalve's life (e.g. decadal) were not the cause of reported ontogenetic trends. Although ontogenetic trends were quantified only for the Ligar Bay *A. stutchburyi* in this study, these trends were also noticeable in the TE/Ca records for all other shells analysed (Chapter 3). The other sites where *A. stutchburyi* were collected from had different environmental parameters to Ligar Bay - up to 3°C higher average SST, and sheltered mud flats or estuaries rather than an open beach. This therefore indicates that the ontogenetic trends in *A. stutchburyi* are a biological effect, rather than an environmental one as Schöne et al. (2011) question.

Table 4.3 Summary of key mollscan TE/Ca studies (Mg/Ca, Sr/Ca, Mn/Ca and Ba/Ca). For each molluscan species, the range in TE/Ca ratios observed is given, and the controls on TE incorporation are summarised.

Species	Sr/Ca		Mg/Ca		Mn/Ca		Ba/Ca	
	Range	Control	Range	Control	Range	Control	Range	Control
Arctica islandica (aragonite)	0.54-5.17 mmol/mol	Strong negative correlation with growth rate, positive correlation with ontogenetic age. Age-detrended ratios inversely correlated to SST (r^2=0.41) (Schöne et al., 2011)	0.12-0.89 mmol/mol	Strong negative correlation with growth rate, positive correlation with ontogenetic age. Growth rate-detrended ratios inversely correlated to SST (r^2=0.27) (Schöne et al., 2011)				
Mytilus edulis (calcite and aragonite)	3-12 mmol/mol	Sr/Ca in calcitic sections has a positive correlation with SST during spring only. (Vander Putten et al., 2001) Sr/Ca in calcitic sections is positively correlated to SST. Sr/Ca in aragonite is negatively correlated to SST. (Dodd, 1965).	1-1.6	Positive correlation with growth rate. (Vander Putten et al., 2001) Weak positive correlation with SST - related to changes in growth rate, which is influenced by SST. (Dodd, 1965).	0-0.45	Spring phytoplankton blooms cause peaks. (Vander Putten et al., 2001)	0-0.08 mmol/mol	Spring phytoplankton blooms cause peaks. (Vander Putten et al., 2001) Background Ba/Ca is directly linked to Ba/Ca of seawater. Peaks may be caused by barite ingestion. (Gillikin et al., 2006).
Pecten maximus (calcite)	1.2-1.7 mmol/mol	Primary control is seasonal SST via influence on growth rate. Secondary control: Mg/Ca ratios. (Freitas et al., 2006) Growth rate accounts for 74% of Sr/Ca ratio variation. (Lorrain et al., 2005)	5-19.5 mmol/mol	Weak correlation with temperature: positive in spring - summer, negative from autumn-spring. (Freitas et al., 2006)	0.014-0.112 mmol/mol	Dissolved Mn^{2+} in local strait, dependent on redox conditions. (Freitas et al., 2006)	0.0007-0.005 mmol/mol	Peaks are cause by an environmental factor: close but not exact timing with chlorophyll maxima. Background ratios indicate dissolved Ba in water. (Gillikin et al., 2008)
Mesodesma donacium (aragonite) Carré et al. (2006)	Mean values: 2.2-2.8 mmol/mol	Positive correlation with growth rate (r^2 = 0.49-0.82)	0.1-1 mmol/mol	Calcification rate (r^2 = 0.36-0.61)	0-0.025 mmol/mol	Calcification rate (r^2 =0.53-0.74)	Up to 0.04 mmol/mol	Calcification rate (r^2 = 0.24-0.66)

Table 4.3 Summary of key mollscan TE/Ca studies (Mg/Ca, Sr/Ca, Mn/Ca and Ba/Ca). For each molluscan species, the range in TE/Ca ratios observed is given, and the controls on TE incorporation are summarised.

Species	Sr/Ca		Mg/Ca		Mn/Ca		Ba/Ca	
	Range	Control	Range	Control	Range	Control	Range	Control
Chione subrugosa (aragonite) Carré et al. (2006)	Mean values: 2.2-3.6 mmol/mol	Positive correlation with growth rate (r^2 = 0.67-0.85)	Mean value: 0.59 mmol/mol	Calcification rate (r^2 = 0.19-0.61)	0-0.025 mmol/mol	Calcification rate (r^2 = 0.64)	Up to 0.04 mmol/mol	Calcification rate (r^2 = 0.33)
Saxidomus giganteus (aragonite)	1-3 mmol/mol	Positive correlation with growth rate (r^2= 0.64-0.87) (Gillikin et al., 2005).					0.001 – 0.025 mmol/mol	Peaks are cause by an environmental factor (maybe primary productivity). Background ratios indicate dissolved Ba in water. (Gillikin et al., 2008)
Corbula amurensis (aragonite)	Mean values: 1.6-2.7 mmol/mol	Positive correlation with growth rate.(Takesue et al., 2008)	Mean values: 0.3-0.9 mmol/mol	Positive correlation with growth rate and amount of organic component in shell that hosts Mg. (Takesue et al., 2008)	Mean values: 0.0114-0.035 mmol/mol	Positive correlation with growth rate and amount of organic component in shell that hosts Mn. (Takesue et al., 2008)	Mean values: 0.0208-0.0495 mmol/mol	Positive correlation with growth rate.(Takesue et al., 2008)
Tridacna gigas (aragonite)	1.4-1.8 mmol/mol	SST growth rates and metabolic rates do NOT control Sr/Ca ratios. (Elliot et al., 2009)	0.3-5.4 mmol/mol	SST causes seasonal Mg/Ca variations, but ratios cannot be quantitatively linked to SST. Positive correlation with ontogenetic age. (Elliot et al., 2009)	0-0.015 mmol/mol	Timing of peaks is linked to primary production. biological processes must ultimately control Ba/Ca ratios as don't correlate quantitatively with dissolved Ba in water, or ingesting phytoplankton. (Elliot et al., 2009)		
Mytilus trossulus (aragonite and calcite)	4.68-10.78 mmol/mol	Sr/Ca ratios vary with metabolic efficiency of Ca^{2+} pumping. (Klein et al., 1996).	1-1.71 mmol/mol	Mg/Ca in calcitic sections are positively correlated to SST. (Klein et al., 1996).				
Protothaca staminea (aragonite)	1.2-3.1 mmol/mol in modern specimen, 0.9-2.4 mmol/mol in fossil.	Positive correlation with SST in one growth increment. (Takesue and van Geen, 2004)	1.4-3.8 mmol/mol in modern specimen, 0.3-2.4 mmol/mol in fossil.	Positive correlation with growth rate. (Takesue and van Geen, 2004)				

4.4 Evaluation of *A. stutchburyi* as an archive for past environmental change

The resolution of geochemical data obtained from *A. stutchburyi* in this study was annual at best due to difficulties identifying daily growth increments/bands with the time and technology available. However, the potential resolution of the clam is not necessarily limited to annual timescale - the highest resolution that could be achieved is tidal, as tidal increments were visible in some sections of the shells. There is a chance these micro-increments would be identifiable so they could be counted with more etching, and acetate peels or scanning electron microscope imaging. Alternatively, by studying the clams in culture or in situ, growth measurements could be made periodically while the individuals are still growing (McKinnon, 1996). $\delta^{18}O$ analyses from the same location as LA-ICP-MS points could also possibly refine the current chronology, and possibly improve it to a seasonal resolution.

The more problematic aspect of *A. stutchburyi* scelerochronology as far as paleoclimatic applications are considered is the continuity of the records derived. Complete growth cessation has been found to occur in *A. stutchburyi* in Dunedin – a cool environment, between 3-4 months over winter (McKinnon, 1996). These periods where micro-increments are not deposited may be shorter in warmer environments, however, further works is required to assess this possibility. Furthermore, the number of micro-increments in *A. stutchburyi* only correlates exactly to the number of low-tides for two months over summer (McKinnon, 1996; Coutts, 1974). This problem might be overcome to some extent by counting the number of fortnightly bands of micro-increments, caused by differences in spring and neap tides – if they could be identified (Carré et al., 2005; Carré et al., 2006). It should also be noted that molluscan records can never provide a truly continuous record of environmental conditions, as shell is only precipitated when the individuals are submerged (Schöne, 2008). Therefore, as the tidal

cycle progresses, the shell records information from different hours in the day. This does not preclude the usefulness of molluscan proxies, but is a limitation to be considered when interpreting climatic information derived from them. On the whole, it appears that an *A. stutchburyi* proxy (at least from a cool climate) would under represent the winter months, and would record daily environmental change for only some periods in the year. *A. stutchburyi* from warmer climates may be of more use for recording seasonal change, as winter data might not be underestimated or left out.

The results from this study suggest *A. stutchburyi* is unlikely to be a useful paleo-SST proxy using Mg/Ca or Sr/Ca ratios. However, there is promising potential for proxies for primary production (Ba/Ca and maybe Mn/Ca), or flood events/Ba influx (Ba/Ca), and redox conditions (Mn/Ca, U/Ca). The Ba/Ca proxy could potentially be very useful – as limited paleo-data is available to constrain the Ba budget in the oceans (Freitas et al., 2006).

Finally, this study did not analyse any *A. stutchburyi* fossils. This would be of prime importance if the proxies described above were subsequently found to be viable in modern specimens. The chemical composition of the shell may alter with time due to diagenesis and under or over represent certain TE/Ca ratios - as has been observed in *Protothaca staminea* fossils (Takesue and van Geen, 2004).

CHAPTER 5.0 CONCLUSIONS

The approach of this thesis was to analyse TE/Ca ratios in multiple *A. stutchburyi* individuals, including a comparison of several clams from the same site (Ligar Bay), as well as clams from a range of sites throughout NZ. The purpose of this was to assess the variation, or similarities in shell TE/Ca ratios between the individuals, which could provide information on TE incorporation and the usefulness of *A. stutchburyi* shell chemistry as a recorder of past environmental change. A secondary focus of the study was to attempt scelerochronological analysis of *A. stutchburyi* growth patterns, so TE/Ca ratios could be temporally assessed and compared to environmental parameters (such as SST); and so that the potential temporal resolution of *A. stutchburyi* geochemical records could be evaluated.

The major findings and implications of this study are:

1. Significant variability was observed in TE/Ca ratio transects measured parallel to maximum growth direction between individuals from the Ligar Bay site. There were no specific variations/patterns in the Sr/Ca, Mg/Ca or U/Ca records that could be correlated between the Ligar Bay shells. This implies that environmental factors are not *primarily* in control of TE/Ca ratios in *A. stutchburyi* shells. In particular, for Mg/Ca and Sr/Ca it appears thermodynamic-controlled substitution for Ca+ in the crystal lattice does not occur, because similar seasonal, sinusoidal trends were not observed amongst the Ligar Bay records.

2. Although a high-resolution chronology could not be constructed for *A. stutchburyi* in this study, the identification of annual bands allowed growth rate to be calculated for annual increments. Subsequent comparison with average increment TE/Ca ratios revealed growth rate is strongly positively correlated with Mg/Ca, Sr/Ca, Mn/Ca, U/Ca, Ba/Ca, and ontogenetic age is strongly negatively correlated with the same TE/Ca ratios.

Therefore, it has been suggested that these biological effects are primarily in control of trace element incorporation in *A. stutchburyi*.

3. There was a marked similarity between the Ba/Ca records of individuals from Ligar Bay. Two abrupt, yet identical 3-point peaks were found in the Ba/Ca ratio transects in the Ligar Bay 3B and 4B shells. Peaks in Ba/Ca ratios were also observed in the Ligar Bay 1B and Ligar Estuary shells, as well as in several of the shells from other sites. These findings suggest Ba/Ca peaks in *A. stutchburyi* are almost certainly linked to an environmental influence – possibly primary productivity or flooding, although more investigation of this effect is required.

4. Major inter-site differences in the range of Mn/Ca and U/Ca ratios exist between the Ligar Bay and remaining shells from other sites. These were interpreted as differences between the environment of a beach (Ligar Bay) and extensive mud flats (Miranda), which would have distinct sedimentary redox conditions, to which U and Mn are sensitive. This suggests that *A. stutchburyi* Mn/Ca and U/Ca ratios are in part an indicator of sediment redox conditions.

5.1 Suggestions for future work

This thesis study has identified several potential lines of further investigation including:

1. Directly comparing *A. stutchburyi* TE/Ca ratios with the environmental parameters that they could be related to. Such parameters would include SST, salinity, chlorophyll, rainfall (storm records), and seawater TE/Ca ratios. Real-time records from when the individuals were growing should ideally be used to allow for precise comparison. Growing the clams in culture where these parameters could be monitored while the clams grew would be one way to derive such information.

2. The first suggestion requires a higher-resolution, more accurate chronology to be constructed for *A. stutchburyi*. This could be achieved by ^{18}O analysis, as discussed in Chapter 4, and, or by closer study and measurement of *A. stutchburyi* growth, by transplanting and collecting the clams, or growing them in culture.

3. Focussing on multiple individuals from a few sites (of different latitude and with different redox conditions to Ligar Bay). Individuals could grow differently in warmer or colder conditions - providing more or less continuous geochemical records. Further, individuals from the same site but from different positions in the intertidal zone should be studied to assess tidal effects, such as the length of submergence, on shell chemistry.

6.0 REFERENCES

Appledoorn, R. S. (1983). "Variation in the growth rate of *Mya arenaria* and its relationship to the environment as analyzed through principal components analysis and the parameter of the von Bertalanffy equation." Fish. Bull. U.S. **81**: 75-84

Arbuszewski, J., P. deMenocal, et al. (2010). "On the fidelity of shell-derived δ18O seawater estimates." Earth and Planetary Science Letters **300**(3-4): 185-196.

Barnes, C. E. and J. K. Cochran (1993). "Uranium geochemistry in estuarine sediments: Controls on removal and release processes." Geochimica et Cosmochimica Acta **57**(3): 555-569.

Beentjes, M. P. and B. G. Williams (1986). "Endogenous circatidal rhythmicity in the New Zealand cockle *Chione stutchburyi* (Bivalvia, *Veneridae*)." Marine Behaviour and Physiology **12**(3): 171 - 180.

Beu, A. G. (2006). "Marine Mollusca of oxygen isotope stages of the last 2 million years in New Zealand. Part 2. Biostratigraphically useful and new Pliocene to recent bivalves." Journal of the Royal Society of New Zealand **36**(4): 151 - 338.

Bishop, J. K. B. (1988). "The barite-opal-organic carbon association in oceanic particulate matter." Nature **332**(6162): 341-343.

Bots, P. and T. Behrends (2008). "Uranium mobility in subsurface aqueous systems: the influence of redox conditions." Mineral Mag **72**(1): 381-384.

Bowen, H. J. M. (1956). "Strontium and barium in sea water and marine organisms." Journal of the Marine Biological Association of the United Kingdom **35**(03): 451-460.

Brockington, S. and A. Clarke (2001). "The relative influence of temperature and food on the metabolism of a marine invertebrate." Journal of Experimental Marine Biology and Ecology **258**(1): 87-99.

Broecker, W.S. and T.H. Peng. (1982) *Tracers in the Sea*. Eldigio Press, Palisades, New York.

Carré, M., I. Bentaleb, et al. (2005). "Stable isotopes and sclerochronology of the bivalve Mesodesma donacium: Potential application to Peruvian paleoceanographic reconstructions." Palaeogeography Palaeoclimatology Palaeoecology **228**(1-2): 4-25.

Carré, M., I. Bentaleb, et al. (2006). "Calcification rate influence on trace element concentrations in aragonitic bivalve shells: Evidences and mechanisms." Geochimica et Cosmochimica Acta **70**(19): 4906-4920.

Carter, J.G. (1980). "Guide to bivalve microstructures," in: Rhoads, D.C. and R.A. Lutz (eds.), *Skeletal growth of aquatic organisms: Biological records of environmental change.* Plenum press, New York, 1:645-651.

Chow, T. J. and E. D. Goldberg (1960). "On the marine geochemistry of barium." Geochimica et Cosmochimica Acta **20**(3-4): 192-198.

Clark, G.R., (1979). "Seasonal growth variations in the shells of recent and prehistoric specimens of *Mercenaria mercenaria* from St. Catherines Island Georgia." Anthropol. Pap. Am. Mus. Nat. Hist. **56**: 161–172

Cléroux, C., E. Cortijo, et al. (2008). "Mg/Ca and Sr/Ca ratios in planktonic foraminifera: Proxies for upper water column temperature reconstruction." Paleoceanography **23**(3): PA3214.

Coffey, M., F. Dehairs, et al. (1997). "The Behaviour of Dissolved Barium in Estuaries." Estuarine, Coastal and Shelf Science **45**(1): 113-121.

Cohen, A. L. and T. A. McConnaughey (2003). Geochemical perspectives on coral mineralization. Biomineralization. P. M. Dove, J. J. DeYoreo and S. Weiner. Washington, Mineralogical Soc America. **54:** 151-187.

Coutts, P. J. F. (1974). "Growth characteristics of the bivalve Chione stutchburyi." New Zealand Journal of Marine and Freshwater Research **8**(2): 333 - 339.

Crowley, t. J., d. A. Short, et al. (1986). "Role of Seasonality in the Evolution of Climate During the Last 100 Million Years." Science **231**(4738): 579-584.

Dalton R, Menzel W (1983) "Seasonal gonadal development of young laboratory-spawned southern (*Mercenaria campechiensis*) and northern (*Mercenaria mercenaria*) quahoqs and their reciprocal hybrids in northern Florida." J Shellfish Res **3**:11–17

Dehairs, F., R. Chesselet, et al. (1980). "Discrete suspended particles of barite and the barium cycle in the open ocean." Earth and Planetary Science Letters **49**(2): 528-550.

Dehairs, F., C. Lambert, et al. (1987). "The biological production of marine suspended barite and the barium cycle in the Western Mediterranean Sea." Biogeochemistry **4**(2): 119-140.

Deuser, W. G. and E. H. Ross (1989). "Seasonally abundant planktonic-foraminifera of the sargasso sea - succession, deep-water fluxes, isotopic compositions, and paleoceanographic implications." Journal of Foraminiferal Research **19**(4): 268-293.

Dietzel, M., N. Gussone, et al. (2004). "Co-precipitation of Sr^{2+} and Ba^{2+} with aragonite by membrane diffusion of CO2 between 10 and 50 °C." Chemical Geology **203**(1-2): 139-151.

Dobbinson SJ, Barker MF, Jillett JB (1989) “Experimental shore level transplantation of the New Zealand cockle *Chione stutchburyi*.” J. Shell Res **9**:197–212

Dodd, J. R. (1964). "Environmentally Controlled Variation in the Shell Structure of a Pelecypod Species." Journal of Paleontology **38**(6): 1065-1071.

Dodd, J. R. (1965). "Environmental control of strontium and magnesium in Mytilus." Geochimica et Cosmochimica Acta **29**(5): 385-398.

Dodd, J. R. and E. L. Crisp (1982). "Non-linear variation with salinity of sr/ca and mg/ca ratios in water and aragonitic bivalve shells and implications for paleosalinity studies." Palaeogeography Palaeoclimatology Palaeoecology **38**(1-2): 45-56.

Elderfield, H. and G. Ganssen (2000). "Past temperature and δ18O of surface ocean waters inferred from foraminiferal Mg/Ca ratios." Nature **405**(6785): 442-445.

Elderfield, H., R. Rickaby, et al. (2006). "How do marine carbonate Mg/Ca and Sr/Ca proxies constrain Cenozoic ocean history." Geochimica et Cosmochimica Acta **70**(18): A158-A158.

Elliot, M., K. Welsh, et al. (2009). "Profiles of trace elements and stable isotopes derived from giant long-lived Tridacna gigas bivalves: Potential applications in paleoclimate studies." Palaeogeography, Palaeoclimatology, Palaeoecology **280**(1-2): 132-142.

Emiliani, C. (1955). "Pleistocene temperatures." Journal of Geology **63**(6): 538-578.

Epstein,S.,R. Buchsbaum, et al. (1953). "Revised carbonate-water isotopic temperature scale." Geological Society of America Bulletin **64**(11): 1315-1326.

Erez, J. and S. Honjo (1981). "Comparison of isotopic composition of planktonic-foraminifera in plankton tows, sediment traps and sediments." Palaeogeography Palaeoclimatology Palaeoecology **33**(1-3): 129-156.

Evans, J. W. (1972). "Tidal growth increments in cockle clinocardium nuttalli." Science **176**(4033): 416-420

Ford, H. L., S. A. Schellenberg, et al. (2010). "Evaluating the skeletal chemistry of Mytilus californianus as a temperature proxy: Effects of microenvironment and ontogeny." Paleoceanography **25**(1): PA1203.

Foster, L. C., A. A. Finch, et al. (2008). "Mg in aragonitic bivalve shells: Seasonal variations and mode of incorporation in Arctica islandica." Chemical Geology **254**(1-2): 113-119.

Fox, D. L. and W. R. Coe (1943). "Biology of the California sea-mussel (Mytilus californianus). II. Nutrition, metabolism, growth and calcium deposition." Journal of Experimental Zoology **93**(2): 205-249.

Freitas, P. S., L. J. Clarke, et al. (2006). "Environmental and biological controls on elemental (Mg/Ca, Sr/Ca and Mn/Ca) ratios in shells of the king scallop Pecten maximus." Geochimica et Cosmochimica Acta **70**(20): 5119-5133.

Gaetani, G. A. and A. L. Cohen (2006). "Element partitioning during precipitation of aragonite from seawater: A framework for understanding paleoproxies." Geochimica et Cosmochimica Acta **70**(18): 4617-4634.

Gall and Zeldis (2003). "Oceanography in Tasman and Golden bays" Niwa

Gillikin, D., A. Lorrain, et al. (2008). "Synchronous barium peaks in high-resolution profiles of calcite and aragonite marine bivalve shells." Geo-Marine Letters **28**(5): 351-358.

Gillikin, D. P., F. Dehairs, et al. (2006). "Barium uptake into the shells of the common mussel (Mytilus edulis) and the potential for estuarine paleo-chemistry reconstruction." Geochimica et Cosmochimica Acta **70**(2): 395-407.

Gillikin, D. P., A. Lorrain, et al. (2005). "Strong biological controls on Sr/Ca ratios in aragonitic marine bivalve shells." Geochem. Geophys. Geosyst. **6**(5): Q05009.

Goldberg, E. D. and G. O. S. Arrhenius (1958). "Chemistry of pacific pelagic sediments." Geochimica et Cosmochimica Acta **13**(2-3): 153-212.

Goldsmith, J. R., D. L. Graf, et al. (1961). "Lattice constants of the calcium-magnesium carbonates." American Mineralogist **46**(3-4): 453-457.

Goodwin, D. H., K. W. Flessa, et al. (2001). "Cross-Calibration of Daily Growth Increments, Stable Isotope Variation, and Temperature in the Gulf of California Bivalve Mollusk Chione cortezi: Implications for Paleoenvironmental Analysis." Palaios **16**(4): 387-398.

Goodwin, D. H., B. R. Schone, et al. (2003). "Resolution and Fidelity of Oxygen Isotopes as Paleotemperature Proxies in Bivalve Mollusk Shells: Models and Observations." Palaios **18**(2): 110-125.

Green, R.H., 1973. "Growth and mortality in an arctic intertidal population of *Malcoma balthica* (Pelecypoda, Tellinidae)." Journal of the Fisheries Research Board Canada 30: 1345–1348.

Grégoire, C. (1972). "Structure of the molluscan shell," *in:* Florkin, M. and B.T. Scheer (eds.), *Chemical Zoology.* Academic press, New York, vol. VII: Mollusca: 45-102.

Heap, A. D. and S. L. Nichol (1997). "The influence of limited accommodation space on the stratigraphy of an incised-valley succession: Weiti River estuary, New Zealand." Marine Geology **144**(1-3): 229-252.

Higham, T. F. G., and A. G. Hogg. (1997) “Evidence for late Polynesian colonisation of New Zealand: University of Waikato radiocarbon measurements.” Radiocarbon **39**(2): 149–192.

Hollis, C. J., L. Handley, et al. (2009). "Tropical sea temperatures in the high-latitude South Pacific during the Eocene." Geology **37**(2): 99-102.

Horiguchi, Y., M. Miyake, et al. (1954). “Biochemical studies with radioactive isotopes on *Pteria (Pinctada) martensii* (Dunkers) and *Hyriopsis schlegelii* (v. Martens). I. Ca metabolism by Ca^{45} tracer in *Hyriopsis schlegelii* (v. Martens).” Bull. Jap. Soc. scient. Fish. **20**: 101–106.

Jones, C. C. (1979). "Anatomy of *Chione cancellata* and some other chionines (bivalvia, *veneridae*)." Malacologia **19**(1): 157-199.

Jones, D. S. (1980). "Annual Cycle of Shell Growth Increment Formation in Two Continental Shelf Bivalves and its Paleoecologic Significance." Paleobiology **6**(3): 331-340.

Jones, M.B. (1983). “Animals of the estuary shore: and illustrated guide.” University of Canterbury, Christchurch: 162.

Jodrey, L.H. (1953). “Studies on shell formation. III. Measurement of calcium deposition in shell and calcium turnover in mantle tissue using the mantle-shell preparation and Ca^{45}.” Biol. Bull. **104:** 394–397.

Kanazawa, T. and S. i. Sato (2008). "Environmental and physiological controls on shell microgrowth pattern of Ruditapes philippinarum (Bivalvia: Veneridae) from Japan." Journal of Molluscan Studies **74**(1): 89-95.

Katz, M. E., B. S. Cramer, et al. (2010). "Traditional and emerging geochemical proxies in foraminifera." Journal of Foraminiferal Research **40**(2): 165-192.

Kennedy, D. M. (2008). "Recent and future higher sea levels in New Zealand: A review." New Zealand Geographer **64**(2): 105-116.

Kinsman, D. J. J. and H. D. Holland (1969). "co-precipitation of cations with $CaCO_3$ .4. Co-precipitation of Sr^{2+} with aragonite between 16 degrees and 96 degrees c." Geochimica et Cosmochimica Acta **33**(1): 1-&.

Klein, R. T., K. C. Lohmann, et al. (1996). "Bivalve skeletons record sea-surface temperature and δ18O via Mg/Ca and 18O/16O ratios." Geology **24**(5): 415-418.

Klein, R. T., K. C. Lohmann, et al. (1996). "Sr/Ca and 13C/12C ratios in skeletal calcite of Mytilus trossulus: Covariation with metabolic rate, salinity, and carbon isotopic composition of seawater." Geochimica et Cosmochimica Acta **60**(21): 4207-4221.

Klinkhammer, G. P., A. C. Mix, et al. (2009). "Increased dissolved terrestrial input to the coastal ocean during the last deglaciation." Geochem. Geophys. Geosyst. **10**(3): Q03009.

Kobayashi, I. and T. Samata (2006). "Bivalve shell structure and organic matrix." Materials Science & Engineering C-Biomimetic and Supramolecular Systems **26**(4): 692-698.

Larcombe, M.L. (1971). "The ecology, population dynamics and energetic of some soft shore mollusks." PhD thesis, University of Auckland.

Lazareth, C. E., E. V. Putten, et al. (2003). "High-resolution trace element profiles in shells of the mangrove bivalve Isognomon ephippium: a record of environmental spatio-temporal variations?" Estuarine, Coastal and Shelf Science **57**(5-6): 1103-1114.

Lea, D. W. (2003). Elemental and Isotopic Proxies of Past Ocean Temperatures. Treatise on Geochemistry. D. H. Heinrich and K. T. Karl. Oxford, Pergamon**:** 1-26.

Lea, D. W., D. K. Pak, et al. (2000). "Climate impact of late quaternary equatorial Pacific sea surface temperature variations." Science **289**(5485): 1719-1724.

Lear, C. H., H. Elderfield, et al. (2000). "Cenozoic deep-sea temperatures and global ice volumes from Mg/Ca in benthic foraminiferal calcite." Science **287**(5451): 269-272.

Livingston, H. D. and G. Thompson (1971). "Trace Element Concentrations in Some Modern Corals." Limnology and Oceanography **16**(5): 786-796.

Lorens, R. B. (1981). "Sr, Cd, Mn and Co distribution coefficients in calcite as a function of calcite precipitation rate." Geochimica et Cosmochimica Acta **45**(4): 553-561.

Lorens, R. B. and M. L. Bender (1980). "The impact of solution chemistry on Mytilus edulis calcite and aragonite." Geochimica et Cosmochimica Acta **44**(9): 1265-1278.

Lorrain, A., D. P. Gillikin, et al. (2005). "Strong kinetic effects on Sr/Ca ratios in the calcitic bivalve Pecten maximus." Geology **33**(12): 965-968.

McCulloch, M., S. Fallon, et al. (2003). "Coral record of increased sediment flux to the inner Great Barrier Reef since European settlement." Nature **421**(6924): 727-730.

McKinnon, J.F. (1996). "Studies of the age, growth and shell increment patterns in the New Zealand Cockle (*Austrovenus stutchburyi*)." MSc thesis, University of Otago.

Miao, S., R. D. DeLaune, et al. (2006). "Influence of sediment redox conditions on release/solubility of metals and nutrients in a Louisiana Mississippi River deltaic plain freshwater lake." Science of The Total Environment **371**(1-3): 334-343.

Ministry of Fisheries, “Cockles (Coc)” <http://fs.fish.govt.nz/ > Accessed 2010

Miyaji, T., K. Tanabe, et al. (2007). "Environmental controls on daily shell growth of *Phacosoma japonicum* (Bivalvia: *Veneridae*) from Japan." Marine Ecology Progress Series **336**: 141-150.

Morford, J. L., A. D. Russell, et al. (2001). "Trace metal evidence for changes in the redox environment associated with the transition from terrigenous clay to diatomaceous sediment, Saanich Inlet, BC." Marine Geology **174**(1-4): 355-369.

Morris, A. W. (1971). "Trace Metal Variations in Sea Water of the Menai Straits caused by a Bloom of Phaeocystis." Nature **233**(5319): 427-428.

Morse, J. W. and M. L. Bender (1990). "Partition coefficients in calcite: Examination of factors influencing the validity of experimental results and their application to natural systems." Chemical Geology **82**(C): 265-277.

Morse, J. W. and A. Mucci (1984). "Composition of carbonate overgrowths produced on Iceland spar calcite crystals buried in bahamian carbonate-rich sediments." Sedimentary Geology **40**(4): 287-291.

Mortyn, P. G. and C. D. Charles (2003). "Planktonic foraminiferal depth habitat and & 18O calibrations: Plankton tow results from the Atlantic sector of the Southern Ocean." Paleoceanography **18**(2): 1037.

Mucci, A. (1987). "Influence of temperature on the composition of magnesian calcite overgrowths precipitated from seawater." Geochimica et Cosmochimica Acta **51**(7): 1977-1984.

Mucci, A. and J. W. Morse (1983). "The incorporation of Mg^{2+} and Sr^{2+} into calcite overgrowths: influences of growth rate and solution composition." Geochimica et Cosmochimica Acta **47**(2): 217-233.

Muir, R. J., S. D. Weaver, et al. (1995). "The Cretaceous Separation Point batholith, New Zealand: granitoid magmas formed by melting of mafic lithosphere." Journal of the Geological Society **152**(4): 689-701.

Palmer, J. D. (1995). "Review of the dual-clock control of tidal rhythms and the hypothesis that the same clock governs both circatidal and circadian rhythms." Chronobiology International **12**(5): 299-310.

Panella, G. (1975). “Paleontological clocks and the history of the Earth's rotation”. In: *Growth Rhythms and the History of the Earth's Rotation*, (eds. G.D. Rosenberg and S.K. Runcorn), Wiley, London: 253–284.

Paytan, A., K. Averyt, et al. (2007). "Barite accumulation, ocean productivity, and Sr/Ba in barite across the Paleocene–Eocene Thermal Maximum." Geology **35**(12): 1139-1142.

Powell, A.W.B. (1979). *New Zealand Mollusca. Marine, land and freshwater shells.* Auckland, Collins: 500.

Purchase, N. G. and J. E. Fergusson (1986). "Chione (austrovenus) stutchburyi, a New Zealand cockle, as a Bio-indicator for lead pollution." Environmental Pollution Series B, Chemical and Physical **11**(2): 137-151.

Purton, L. M. A., G. A. Shields, et al. (1999). "Metabolism controls Sr/Ca ratios in fossil aragonitic mollusks." Geology **27**(12): 1083-1086.

Putten, E. V., F. Dehairs, et al. (2000). "High resolution distribution of trace elements in the calcite shell layer of modern mytilus edulis: environmental and biological controls." Geochimica et Cosmochimica Acta **64**(6): 997-1011.

Richardson, C. A. (2001). Molluscs as archives of environmental change. Oceanography and Marine Biology, Vol 39. London, Taylor & Francis Ltd. **39:** 103-164.

Richardson, C. A., D. J. Crisp, et al. (1980). "Factors Influencing Shell Growth in Cerastoderma edule." Proceedings of the Royal Society of London. Series B, Biological Sciences **210**(1181): 513-531.

Richardson, C. A., R. Seed, et al. (1990). "Use of internal growth bands for measuring individual and population-growth rates in mytilus-edulis from offshore production platforms." Marine Ecology-Progress Series **66**(3): 259-265.

Rosenberg, G. D. and W. W. Hughes (1991). "A metabolic model for the determination of shell composition in the bivalve mollusc, Mytilus edulis." Lethaia **24**(1): 83-96.

Sadekov, A., S. M. Eggins, et al. (2009). "Surface and subsurface seawater temperature reconstruction using Mg/Ca microanalysis of planktonic Foraminifera Globigerinoides ruber, Globigerinoides sacculifer, and Pulleniatina obliquiloculata." Paleoceanography **24**(3):3201-3201.

Savenko, V. S. (2008). "Concentrating function of plankton and the residence time of dissolved species of chemical elements in the ocean." Geochemistry International **46**(2): 190-192.

Schmidt, M. W., H. J. Spero, et al. (2004). "Links between salinity variation in the Caribbean and North Atlantic thermohaline circulation." Nature **428**(6979): 160-163.

Schöne, B. (2008). "The curse of physiology—challenges and opportunities in the interpretation of geochemical data from mollusk shells." Geo-Marine Letters **28**(5): 269-285.

Schöne, B. and J. Fiebig (2009). "Seasonality in the North Sea during the Allerød and Late Medieval Climate Optimum using bivalve sclerochronology." International Journal of Earth Sciences **98**(1): 83-98.

Schöne, B., D. Rodland, et al. (2007). "Combined sclerochronologic and oxygen isotope analysis of gastropod shells (*Gibbula cineraria*; North Sea): life-history traits

and utility as a high-resolution environmental archive for kelp forests." Marine Biology **150**(6): 1237-1252.

Schone, B. R., E. Dunca, et al. (2005). "Mutvei's solution: An ideal agent for resolving microgrowth structures of biogenic carbonates." Palaeogeography Palaeoclimatology Palaeoecology **228**(1-2): 149-166.

Schöne, B. R., A. D. Freyre Castro, et al. (2004). "Sea surface water temperatures over the period 1884-1983 reconstructed from oxygen isotope ratios of a bivalve mollusk shell (Arctica islandica, southern North Sea)." Palaeogeography, Palaeoclimatology, Palaeoecology **212**(3-4): 215-232.

Schöne, B. R., S. D. Houk, et al. (2005). "Daily growth rates in shells of Arctica islandica: Assessing sub-seasonal environmental controls on a long-lived bivalve mollusk." Palaios **20**(1): 78-92.

Schöne, B. R., Z. Zhang, et al. (2011). "Sr/Ca and Mg/Ca ratios of ontogenetically old, long-lived bivalve shells (Arctica islandica) and their function as paleotemperature proxies." Palaeogeography, Palaeoclimatology, Palaeoecology **302**(1-2): 52-64.

Sinclair, D. J. and M. T. McCulloch (2004). "Corals record low mobile barium concentrations in the Burdekin River during the 1974 flood: Evidence for limited Ba supply to rivers?" Palaeogeography, Palaeoclimatology, Palaeoecology **214**(1-2): 155-174.

Skinner, H. C. W. and A. H. Jahren (2007). Biomineralization. Treatise on Geochemistry. D. H. Heinrich and K. T. Karl. Oxford, Pergamon**:** 1-69.

Stecher, H. A., D. E. Krantz, et al. (1996). "Profiles of strontium and barium in Mercenaria mercenaria and Spisula solidissima shells." Geochimica et Cosmochimica Acta **60**(18): 3445-3456.

Sunda, W. G. and S. A. Huntsman (1985). "Regulation of Cellular Manganese and Manganese Transport Rates in the Unicellular Alga Chlamydomonas." Limnology and Oceanography **30**(1): 71-80.

Takesue, R. K., C. R. Bacon, et al. (2008). "Influences of organic matter and calcification rate on trace elements in aragonitic estuarine bivalve shells." Geochimica et Cosmochimica Acta **72**(22): 5431-5445.

Takesue, R. K. and A. van Geen (2004). "Mg/Ca, Sr/Ca, and stable isotopes in modern and Holocene Protothaca staminea shells from a northern California coastal upwelling region." Geochimica et Cosmochimica Acta **68**(19): 3845-3861.

Tesoriero, A. J. and J. F. Pankow (1996). "Solid solution partitioning of $Sr^{2+,}$ $Ba^{2+,}$ and Cd^{2+} to calcite." Geochimica et Cosmochimica Acta **60**(6): 1053-1063.

Torres, M. E., J. P. Barry, et al. (2001). "Reconstructing the History of Fluid Flow at Cold Seep Sites from Ba/Ca Ratios in Vesicomyid Clam Shells." Limnology and Oceanography **46**(7): 1701-1708.

Urey, H. C. (1947). "The thermodynamic properties of isotopic substances." Journal of the Chemical Society **May**: 562-581.

Van Der Borght, O. and S. Van Puymbroeck (1966). "Calcium metabolism in a freshwater mollusc : Quantitative importance of water and food as supply for calcium during growth." Nature **210**(5038): 791-793.

Vander Putten, E., F. Dehairs, et al. (2000). "High resolution distribution of trace elements in the calcite shell layer of modern Mytilus edulis: Environmental and biological controls." Geochimica et Cosmochimica Acta **64**(6): 997-1011.

Watabe, N., and R.J Kingsley. (1989). "Extra-, inter-, and intracellular mineralization in invertebrates and algae." In *Origin, Evolution, and Modern Aspects of Biomineralization in Plants and Animals.* (ed. R.E. Crick) Plenum, New York: 209–223

Wheeler A. P. (1992). "Mechanisms of molluscan shell formation." In *Calcification in Biological systems (*ed**.** E. Bonucci). CRC Press: 179-216.

Wood, W. (1828). "A supplement to the Index Testaceologicus, or a catalogue of shells, British and foreign." London

Wilbur, K.M., and A.S.M. Saleuddin. (1983). *The Mollusca: vol 5 Physiology* (ed. Wilbur K.M.) Academic Press, New York: 237-286.